

DEFECT CLASSIFICATION IN RECIPROCATING
COMPRESSOR USING ACOUSTIC EMISSION
TECHNIQUE

SIM HOI YIN

THESIS SUBMITTED IN FULFILMENT
OF THE REQUIREMENTS FOR
THE DEGREE OF MASTER OF ENGINEERING SCIENCE

FACULTY OF ENGINEERING
UNIVERSITY OF MALAYA
KUALA LUMPUR

2013

DECLARATION BY THE CANDIDATE

UNIVERSITI MALAYA ORIGINAL LITERARY WORK DECLARATION

Name of the candidate: SIM HOI YIN (I.C/Passport No.)
Registration/Matric No: KGA 090085
Name of the Degree: MASTER OF ENGINEERING SCIENCE (M. Eng Sc)
Title of Project Paper/Research Report/Dissertation/Thesis ("this Work"):
DEFECT CLASSIFICATION IN RECIPROCATING COMPRESSOR USING
ACOUSTIC EMISSION TECHNIQUE
Field of Study: ACOUSTIC EMISSION, CONDITION MONITORING

I do solemnly and sincerely declare that:

- (1) I am the sole author/writer of this Work;
- (2) This Work is original;
- (3) Any use of any work in which copyright exists was done by way of fair dealing and for permitted purposes and any excerpt or extract from, or reference to or reproduction of any copyright work has been disclosed expressly and sufficiently and the title of the Work and its authorship have been acknowledged in this Work;
- (4) I do not have any actual knowledge nor do I ought reasonably to know that the making of this work constitutes an infringement of any copyright work;
- (5) I hereby assign all and every rights in the copyright to this Work to the University of Malaya ("UM"), who henceforth shall be owner of the copyright in this Work and that any reproduction or use in any form or by any means whatsoever is prohibited without the written consent of UM having been first had and obtained;
- (6) I am fully aware that if in the course of making this Work I have infringed any copyright whether intentionally or otherwise, I may be subject to legal action or any other action as may be determined by UM.

Candidate's Signature

Date

Subscribed and solemnly declared before,

Witness's Signature

Date

Name:

Designation:

ABSTRACT

Performance of reciprocating machines relies heavily on health condition of its moving components, most importantly the valve. Non-intrusive methods such as vibration or acoustic emission (AE) technique are preferable in valve failure diagnosis as they can provide earlier fault detection. In this study, a valve failure detection methodology is proposed by using the AE technique. Wavelet packet transform (WPT) is chosen as the signal processing method over continuous wavelet transform (CWT) and discrete wavelet transform (DWT). This is because WPT can overcome high computational time and high redundancy problem in CWT and capable of providing detailed analysis of high frequency components which is found feeble in DWT. The features of AE signal can be extracted by computing normalized WPT coefficients under different valve conditions and machine operating conditions through statistical method. Finally, a classifying strategy is proposed to discriminate the signal under different valve conditions. Vibration signal will serve as a reference in comparing the effectiveness of AE signal in valve failure detection.

ABSTRAK

Prestasi pemampat salingan banyak bergantung kepada keadaan komponen yang bergerak, terutamanya injap. Kaedah pengesanan yang tidak intrusif seperti getaran atau acoustic emission (AE) adalah lebih digemari dalam diagnosis kegagalan injap sebab ia boleh memberikan pengesanan kegagalan injap yang lebih awal. Dalam kajian ini, satu metodologi pengesanan kegagalan injap dicadangkan dengan menggunakan teknik AE. Wavelet packet transform (WPT) dipilih sebagai kaedah pemprosesan isyarat berbanding dengan continuous wavelet transform (CWT) dan discrete wavelet transform (DWT). Ini adalah kerana WPT boleh mengatasi masalah seperti masa pengiraan yang panjang dan pengiraan lebihan yang tinggi dalam CWT. Selain itu, WPT boleh memberikan analysis terperinci ke atas komponen frekuensi yang tinggi berbanding dengan DWT. Ciri-ciri isyarat AE boleh diekstrak dengan menilai pekali WPT yang dinormalisasi di bawah keadaan injap dan keadaan operasi mesin yang berbeza melalui kaedah statistik. Akhirnya, satu klasifikasi strategi dicadangkan untuk mendiskriminasi isyarat di bawah keadaan injap yang berbeza. Isyarat getaran akan menjadi rujukan dalam perbandingan keberkesanan isyarat AE untuk mengesan kegagalan injap.

ACKNOWLEDGEMENTS

I am indebted to many people for helping me throughout the entire period of this research. Therefore, upon completion of this research, I would like to express my sincerest gratitude to the following people who have assisted me throughout the entire research.

First of all, I would like to show my sincere appreciation and gratitude to my thesis supervisor, Dr. Rahizar Ramli for his guidance towards a better understanding of this work, and his invaluable advice and continuous support during the hard time of the research. I wished to thank Dr. Ir. Hj. Mohd Abdul Karim Abdullah and Mr. Anbalagan from Serba Dinamik Sdn. Bhd. for the advice and experience contributed throughout the research period. Besides, I would like to express my greatest appreciation to Dr. Ahmad Saifizul for his precious advice in statistical analysis.

A special thanks to my colleagues, Mr. K. S. Chin and Mr. J. Y. Tey for their help, cooperation, and motivation for the continuation of this research. An acknowledgement is also made to our technical staff, Mr. Kandasamy and Mr. Amir for the utility and laboratory supports.

Lastly, sincere thanks are due to my family and friends for their endless supports and encouragements throughout the entire period of the research.

TABLE OF CONTENTS

DECLARATION BY THE CANDIDATE.....	ii
ABSTRACT.....	iii
ABSTRAK.....	iv
ACKNOWLEDGEMENTS	v
TABLE OF CONTENTS	vi
LIST OF FIGURES.....	ix
LIST OF TABLES	xiii
LIST OF APPENDICES	xv
LIST OF ABBREVIATIONS	xvi
CHAPTER 1 INTRODUCTION	1
1.1 Introduction.....	1
1.2 Background of problem	2
1.3 Objectives	6
1.4 Scope of the study.....	6
1.5 Outline of thesis	7
CHAPTER 2 LITERATURE REVIEW	9
2.1 Overview.....	9
2.2 Reciprocating Compressor Valves.....	9
2.3 Characteristics of Acoustic Emission (AE)	17
2.4 Acoustic Emission (AE) in Condition Monitoring.....	22
2.4.1 AE in Bearing Monitoring	23
2.4.2 AE in Gear Monitoring	25
2.4.3 AE in Valve Monitoring.....	27
2.5 Time-Frequency Analysis.....	31
2.5.1 Fourier Transform	32
2.5.2 Short Time Fourier Transform (STFT)	33
2.5.3 Wavelet Transform.....	35
2.5.4 Review of different time-frequency analysis in condition monitoring	48
2.6 Artificial Intelligence (AI) techniques in fault identification	52
2.7 Summary	55
CHAPTER 3 METHODOLOGY	57

3.1	Overview.....	57
3.2	Experiment set-up.....	58
3.2.1	Test bed setup.....	58
3.2.2	Instrumentation	61
3.3	Synchronous time averaging.....	63
3.4	Mother wavelet selection for WPT.....	67
3.5	Signal segregation.....	70
3.6	Parameter Comparison.....	72
3.6.1	Root-mean-square (RMS)	72
3.6.2	Crest factor.....	73
3.6.3	Skewness	73
3.6.4	Kurtosis	74
3.6.5	Normalized energy	75
3.7	Summary	75
CHAPTER 4	SIGNAL ANALYSIS.....	77
4.1	Overview.....	77
4.2	Visual inspection of signal.....	77
4.2.1	Validation of AE and vibration signals with valve motion.....	77
4.2.2	Comparison of signals under different valve conditions.....	79
4.2.3	Comparison of signals at different speed	83
4.3	Methodology for signal analysis.....	84
4.3.1	One way analysis of variance (ANOVA).....	84
4.3.2	Tukey comparison test	87
4.4	Parameter selection	88
4.4.1	Results	89
4.4.2	Discussions.....	102
4.5	Signal Analysis	104
4.5.1	Results	105
4.5.2	Discussions.....	119
4.5.3	Conclusions	123
4.6	Test data study	124
4.7	Summary	133
CHAPTER 5	SIGNAL CLASSIFICATION	135
5.1	Overview.....	135

5.2	Theoretical background	135
5.2.1	Risk minimization	135
5.2.2	Support vector machine (SVM)	138
5.3	Methodology for SVM signal classification	143
5.3.1	Non-linear classification kernel	143
5.3.2	Multiclass classification	146
5.3.3	Process flow for SVM classification.....	149
5.4	Cross validation	151
5.4.1	Cross validation results	152
5.4.2	Discussions on cross validation results	160
5.5	Multiclass classification.....	166
5.5.1	Classification results of each testing class	167
5.5.2	Overall classification results	173
5.6	Summary	177
CHAPTER 6	CONCLUSIONS AND RECOMMENDATIONS	178
6.1	Conclusions.....	178
6.2	Recommendations for future works.....	181
REFERENCES	183
APPENDICES	191

LIST OF FIGURES

Figure 2.1: Typical horizontal balanced reciprocating compressor (Courtesy Sulzer-Burckhardt, Winterthur, Switzerland).....	10
Figure 2.2: Structure of a typical reciprocating compressor	12
Figure 2.3: Pressure-Volume (PV) diagram and valve event of a reciprocating compressor	13
Figure 2.4: Structure of typical plate valve (Courtesy Dresser Rand Company).....	14
Figure 2.5: Sealing element movement in suction and discharge valve (Hoerbiger, 2007)	15
Figure 2.6: (a) Valve fluttering (b) Valve delayed closure (Hoerbiger, 2007)	16
Figure 2.7: (a) Clogged valve (b) Broken valve ring (Courtesy of Hoerbiger Company)	17
Figure 2.8: Types of Acoustic Emission Waves (Muravin, 2009).....	18
Figure 2.9: Spectrum of vibration and sound used for inspection and testing (Williams, 1980)	19
Figure 2.10: Types of AE Signals (a) Burst (b) Continuous (c) Mixed mode (Sikorska and Mba, 2006)	20
Figure 2.11: Traditional features of an AE Signal (Sikorska and Mba, 2006)	21
Figure 2.12: Classification of signals (Shin and Hammond, 2008)	31
Figure 2.13: Time frequency plane of STFT for (a) Narrow window (b) Wide window	34
Figure 2.14: Time-scale plane of wavelet transform	36
Figure 2.15: Mother wavelet with scale 0.5 and scale 1.5	38
Figure 2.16: Two-scale relations for (a)Primal space (b) Dual space.....	42
Figure 2.17: Sub-band coding algorithm (Valens, 1999).....	44
Figure 2.18: Splitting the signal spectrum with an iterated filter bank (Valens, 1999) ..	45
Figure 2.19: WPT under three level decomposition (Yen and Lin, 2000).....	47
Figure 3.1: Entire flow chart of the study	58

Figure 3.2: Test compressor for valve failure simulation	59
Figure 3.3: Structural diagram of cylinder indicating location of (a) Suction valve (b) Discharge valve	60
Figure 3.4: Physical condition of valve plate (a) Normal (b) Grease (c) Leakage	60
Figure 3.5: A schematic diagram of data acquisition system.....	61
Figure 3.6: Block diagram of configuration setting of sensors in LabVIEW	65
Figure 3.7: Block diagram of linear averaging in LabVIEW.....	66
Figure 3.8: Comparison of AE signal between different numbers of averages	67
Figure 3.9: Segregation of signal at different time segments and frequency ranges	72
Figure 4.1: Valve displacements and pressure difference at its corresponding crank angle (MacLaren and Kerr, 1969)	78
Figure 4.2: Comparison of (a) Vibration (b) AE signal at 450 rpm under normal condition.....	79
Figure 4.3: AE (a) – (c) and vibration (d) – (f) signal acquired at F1(0 – 3200 Hz) under different conditions and speeds.....	80
Figure 4.4: AE signal at 450 rpm and F16 (48 – 51.2 kHz) under (a) Normal (b) Grease (c) Leakage condition.....	82
Figure 4.5: Tukey test result for kurtosis at F2 and time segment 1 (F2T1).....	92
Figure 4.6: Tukey test result for RMS at F3 and time segment 3 (F3T3).....	93
Figure 4.7: Tukey test result for normalized energy at F1 and time segment 1 (F1T1) .	93
Figure 4.8: Comparison of AE signal at F12 (35.2 – 38.4 kHz) and 450 rpm under (a) normal (b) grease (c) leakage condition.....	108
Figure 4.9: Comparison of vibration signal at F1 (0 – 3.2 kHz) and 450 rpm under (a) normal (b) grease (c) leakage condition.....	109
Figure 4.10: Comparison of vibration signal at F7 (19.2 – 22.4 kHz) and 450 rpm under (a) normal (b) grease (c) leakage condition	109
Figure 4.11: Comparison of vibration signal at F4 (9.6 – 12.8 kHz) and 450 rpm under (a) normal (b) grease (c) leakage condition	112
Figure 4.12: Comparison of AE signal at F2 (a) – (c), F14 (d) – (f), and F16 (g) – (i) under different valve conditions at 800 rpm	116

Figure 4.13: Comparison of vibration signal at F1 and 800 rpm under (a) normal (b) grease (c) leakage condition.....	118
Figure 4.14: Plan view of test compressor JGJ/2	125
Figure 4.15: Test compressor JGJ/2	125
Figure 4.16: Comparison of AE signal (a) Raw signal (b) WPT decomposed signal ..	127
Figure 4.17: Comparison of vibration signal (a) Raw signal (b) WPT decomposed signal	127
Figure 4.18: Comparison of vibration and AE signal at 800 rpm under normal (a)-(b) and grease (c)-(d) condition	128
Figure 4.19: Comparison of AE signal during different months (a) August (b) September (c) December.....	129
Figure 4.20: Comparison of vibration signal during different months (a) August (b) September (c) December.....	130
Figure 4.21: Comparison of normalized energy over three measurements for (a) AE signal (b) Vibration signal.....	132
Figure 5.1: Nested subset of functions (Burges, 1998)	137
Figure 5.2: Possible hyper-planes to separate two classes	138
Figure 5.3: Classification of two classes using SVM	140
Figure 5.4: (a) Data in original input space X (b) Data in transformed feature space F	144
Figure 5.5: One-against-all (OAA) strategy.....	147
Figure 5.6: One-against-one (OAO) strategy.....	148
Figure 5.7: Optimal separating hyper-plane with features from (a) Time segment 1 and 2 (b) Time segment 3 and 4.....	150
Figure 5.8: Flow chart for signal classification.....	151
Figure 5.9: Classification success rate for AE signal, Class 1-2 classifier on (a) Loose grid (b) Fine grid at F1 and 450 rpm.....	153
Figure 5.10: Classification success rate for AE signal, Class 1-3 classifier on (a) Loose grid (b) Fine grid at F1 and 450 rpm.....	154
Figure 5.11: Classification success rate for AE signal, Class 2-3 classifier at F1 and 450 rpm	154

Figure 5.12: Classification success rate for vibration signal, Class 1-2 classifier on (a) Loose grid (b) Fine grid at F1 and 450 rpm	155
Figure 5.13: Classification success rate for vibration signal, Class 1-3 classifier on (a) Loose grid (b) Fine grid at F1 and 450 rpm	156
Figure 5.14: Classification success rate for vibration signal, Class 2-3 classifier on (a) Loose grid (b) Fine grid at F1 and 450 rpm	157
Figure 5.15: Classification success rate for AE signal, Class 1-2 classifier on (a) Loose grid (b) Fine grid at F1 and 800 rpm.....	158
Figure 5.16: Classification success rate for vibration signal, Class 1-2 classifier on (a) Loose grid (b) Fine grid at F1 and 800 rpm	159
Figure 5.17: Classification success rate for vibration signal, Class 2-3 classifier at F1 and 800 rpm.....	159
Figure 5.18: Effect of gamma values at $C=2$ on (a) Classification success rate (b) Number of support vectors in Class 2-3 classifier of AE signal at F4 and 450 rpm.....	162
Figure 5.19: Total classification results of AE and vibration signals at (a) 450 rpm (b) 800 rpm	174
Figure 5.20: Total classification results of (a) AE (b) Vibration signal at different speed	176

LIST OF TABLES

Table 2.1: Components of reciprocating compressor shutdown (Foreman, 2002)	11
Table 2.2: Distribution of reciprocating compressor failures (Smith et al., 1997)	11
Table 2.3: Breakdown of maintenance costs of reciprocating compressor (Smith et al., 1997)	12
Table 2.4: Characteristics of orthogonal and biorthogonal wavelets	43
Table 2.5: Some reviews of time-frequency analysis technique in condition monitoring	50
Table 2.6: Comparison of the performances of different time-frequency analysis.....	51
Table 3.1: Specifications of test compressor.....	59
Table 3.2: List of equipments.....	62
Table 3.3: Hölder exponent $\alpha(L)$ estimates for the Daubechies scaling function $\phi(t)$ of order L and regularity of B-spline scaling function of the same order L (Daubechies, 1992)	68
Table 3.4: Summary of properties of commonly used finite support wavelets (Ahuja et al., 2005).....	69
Table 4.1: One way ANOVA.....	87
Table 4.2: One way ANOVA result for kurtosis at F2 and time segment 1 (F2T1)	89
Table 4.3: p value for all parameters at 450 rpm (AE signal).....	91
Table 4.4: Characteristic segments for all parameters at 450 rpm (AE signal)	94
Table 4.5: p value for all parameters at 450 rpm (Vibration signal).....	96
Table 4.6: Characteristic segments for all parameters at 450 rpm	97
Table 4.7: p value for all parameters at 800 rpm (AE signal).....	99
Table 4.8: Characteristic segments for all parameters at 800 rpm	100
Table 4.9: p value for all parameters at 800 rpm (Vibration signal).....	101
Table 4.10: Characteristic segments for all parameters at 800 rpm	102
Table 4.11: Characteristic segments of AE and vibration signal at 450 rpm.....	105
Table 4.12: 95% confidence interval (C.I) of AE signal at 450 rpm in the best frequency range	106
Table 4.13: Sequence of confidence interval (C.I) of AE signal at 450 rpm in ascending order (1: lowest mean value and 3: highest mean value)	107
Table 4.14: 95% confidence interval (C.I) of vibration signal at 450 rpm in the best frequency range	111
Table 4.15: Sequence of confidence interval (C.I) of vibration signal at 450 rpm in ascending order (1: lowest mean value and 3: highest mean value)	111

Table 4.16: Characteristic segments of AE and vibration signal at 800 rpm.....	113
Table 4.17: 95% confidence interval (C.I) of AE signal at 800 rpm in the best frequency range.....	114
Table 4.18: Sequence of confidence interval (C.I) of AE signal at 800 rpm in ascending order (1: lowest mean value and 3: highest mean value)	115
Table 4.19: 95% confidence interval (C.I) of vibration signal at 800 rpm in the best frequency range	117
Table 4.20: Sequence of confidence interval (C.I) of vibration signal at 800 rpm in ascending order (1: lowest mean value and 3: highest mean value)	118
Table 4.21: Joint confidence interval (C.I) of AE and vibration signal at T3 under different speed and valve conditions.....	123
Table 4.22: Joint confidence interval (C.I) of AE and vibration signal at T4 under different speed and valve conditions.....	123
Table 4.23: Specification of test compressor JGJ/2	126
Table 5.1: Best parameters of Gaussian radial basis kernel classifier for AE and vibration signal at 450 rpm	163
Table 5.2: Best parameters of Gaussian radial basis kernel classifier for AE and vibration signal at 800 rpm	165
Table 5.3: Classification success rate of multiclass system trained with data at 450 rpm	167
Table 5.4: Classification success rate of multiclass system trained with data at 800 rpm	170

LIST OF APPENDICES

APPENDIX A	Tukey test for all parameters.....	191
APPENDIX B	Tukey test result of normalized energy under 450 rpm.....	211
APPENDIX C	Sample AE and vibration signals at 450 rpm under different valve conditions.....	227
APPENDIX D	Specification of accelerometer.....	233
APPENDIX E	Tukey test result of normalized energy under 800 rpm.....	234
APPENDIX F	Sample AE and vibration signals at 800 rpm under different valve conditions.....	250

LIST OF ABBREVIATIONS

AE	Acoustic emissions
AI	Artificial intelligence
ANOVA	Analysis of variance
BDC	Bottom dead centre
C.I	Confidence interval
d.o.f.	Degree of freedom
DAQ	Data acquisition device
ERM	Empirical risk minimization
HSD	Honest and significance difference
MRA	Multi-resolution analysis
NDT	Non-destructive testing
NN	Neural network
OAA	One-against-all
OAo	One-against-one
P	Dilatational wave
PV	Pressure-Volume
RMS	Root-mean-square
RSPWVD	Reassigned Smoothed Pseudo WVD
S	Transverse wave
S/N	Signal-to-noise ratio
SPWVD	Smoothed Pseudo Wigner-Ville Distribution
SRM	Structural risk minimization
STFT	Short Time Fourier Transform
SVM	Support vector machine
TDC	Top dead centre
VC	Vapnik Chervonenkis
WPT	Wavelet Packet Transform
WT	Wavelet transform
WVD	Wigner-Ville Distribution

CHAPTER 1 INTRODUCTION

1.1 Introduction

The competitiveness in industry nowadays has urged plant personnel to reduce operating cost without sacrificing plant efficiency. In fact, the industry environment has evolved to the extent that requires the process plants to improve plant efficiency and maintain optimal operating condition while reducing cost and wastage at the same time. One of the cost-effective approaches is by implementing predictive or condition based maintenance as it can monitor current and future condition of plant equipments (Sikorska and Mba, 2008). Non-destructive testing (NDT) techniques such as vibration, wear particle analysis, oil analysis, infrared thermograph, and the newer technique, acoustic emission (AE) analysis prevailed over destructive method as they can save both time and money. This is because the destructive methods such as pressure and temperature analysis often require proper installation of transducer. Poor installation of probe will lead to leakage or changes in the operating condition of machinery, thus increasing the risk of introducing faults to the system. In this research, the acoustic emission (AE) technique is utilized as the diagnostic tool as it can provide early fault detection in reciprocating machines (Sikorska and Mba, 2008).

Reciprocating compressor is one of the rotating machinery widely found in oil and gas industry such as in refinery and gas transmission line. In reciprocating compressor, the greatest concern is those parts with a finite life, such as bearings, seals, and valves, or parts that are highly stressed. This research focuses on the failure detection of valve as it is the major moving component in reciprocating compressor. It has higher probability of contributing to most of the failures as there are always more than two valves in a reciprocating compressor. Moreover, the large number of valves in

a reciprocating compressor often makes task difficult for identifying faulty valve, resulting in a longer repairing time for the machine. The faulty valve can eventually cause secondary damage to the compressor especially when the chips from valve enter the rotating crankshaft area. To avoid further breakdown, changing all the valves in a reciprocating compressor is the normal practice in industry despite there maybe just one defective valve. This practice has led to enormous wastage and high operating cost.

Therefore, AE technique is applied in this study to identify and detect common valve failures such as valve leakage, contaminated lubrication in valve, and valve plate deformation, enabling the machine to be repaired timely and efficiently. By developing the condition monitoring system, condition of valves in a reciprocating compressor can be monitored and assessed easily. This will ultimately help in reducing maintenance cost of the machines. As the system can detect valve failures, early replacement of valves can be done before it causes any breakdown to the machines, thus reducing unplanned shutdown and production losses in a plant. Besides, plant maintenance can be better planned and it can be carried out in co-ordination with the operation and maintenance departments. Thus both the production and maintenance requirements can be fulfilled at the same time.

1.2 Background of problem

Condition monitoring has been proposed by many researchers as one of the predictive maintenance in the plant. In contrast to the breakdown maintenance where the machine is run until failure or the preventive maintenance where the maintenance is performed at a fixed time schedule irrespective of machine's health condition, the

predictive maintenance is more flexible as the parts are only changed when needed and maintenance is only performed when convenient. Thus, it helps in saving time as the number of overhauls reduces to a minimum besides decreasing costly inventories for machine parts replacement. Moreover, production loss is reduced tremendously as unexpected catastrophic breakdowns are avoided in addition to eliminating unnecessary interventions to the machine (Courrech, 1996).

Condition monitoring is especially needed in detecting valve failures in the reciprocating compressor. According to the technical note by Dresser-Rand (Foreman, 2002), 36% of the unscheduled shutdowns of reciprocating compressor was attributed to the valve failure. There are a number of reasons which contributed to the valve failures, and they can be categorized into two broad categories; failures caused by environmental effects or abnormal mechanical action. Valve plate corrosion and crack are some of the examples of failures caused by environmental effects as these valves are mostly deformed by the corrosive contaminants or foreign particles carried by the gas. Meanwhile, valve failures due to abnormal mechanical action normally happen when the valves are operated beyond designed range of conditions or under pressure pulsations.

Condition of a machine can be determined by observing various parameters related to mechanical condition of the machine. A few measurement techniques have been utilized for the past decade to monitor the condition of reciprocating compressors, namely vibration monitoring, rod-drop monitoring, pressure-volume analysis, and temperature measurement (Schultheis et al., 2007). Vibration analysis is the measure of physical movement of machine relative to a reference point over a frequency range. The type of transducer for vibration analysis is dependent on the frequency range intended to measure by the personnel. The accelerometer is utilized for high frequency

measurements (above 1000 Hz) while the velocity transducer and displacement transducer is applied for medium (10 to 1000Hz) and low (below 10 Hz) frequency measurement respectively (Girdhar, 2004). The measured vibration level will be plotted against time. Abnormal condition of the machine will be detected if the vibration level exceeds pre-set threshold.

Meanwhile, rod-drop monitoring is especially useful in monitoring reciprocating compressors with horizontal cylinders and piston. The gravity force experienced by the horizontal cylinders causes more friction at the bottom than the top, which results in more wear at the bottom part of the piston. To avoid damage the cylinder wall is usually covered with rider band as a protective measure. Nevertheless, excessive wear of the rider band will eventually damage the cylinder lining in the long run. Thus, rod-drop monitoring which utilizes a proximity probe located under the piston rods to monitor the vertical position of the piston rod from time to time is a preferred monitoring technique in detecting the rider band wear.

Pressure-volume analysis and temperature measurement are conducted traditionally to monitor condition of reciprocating compressors with respect to piston position (Schultheis et al., 2007). The condition of valves, rings, and packing can be monitored closely by installing the pressure and temperature transducer in the cylinder. Thus, the valve leakage, bearing damage and packing leakage can be identified clearly by tracing the pressure and temperature measurement for a period of time. The API 618 (1995) has recommended cylinder discharge temperature as one of the protection parameter as ring and valve leakages are often reflected in the discharge temperature due to the recompression of gas. For valve monitoring, pressure and temperature transducer are installed through the valve cover and the measurements are trended with its corresponding crank angle position for comparison. However, these measurement

techniques often reflect significant changes when the machinery condition becomes too critical, with the possibility of causing sudden shutdown and imposing secondary damage to the machine itself.

In this study, the AE technique was chosen to monitor condition of valve in reciprocating compressors. This technique measures transient elastic waves generated when a material undergoes deformation or fracture development. Besides, this technique is also sensitive to leakages and friction between two surfaces. As the measurement itself is non-destructive, it will not disturb the existing system, thereby reducing the possibility of introducing unwanted disturbances to the machines. Hence, it is a prevailing measurement technique compared to other intrusive techniques such as the pressure and temperature measurement. Most importantly, this technique ensures earlier fault to be detected before it can cause any major damage to the machine. The superiority of AE in early fault detection mainly attributes to its ability to measure material deformation, as opposed to vibration measurement technique where it measures the response of the structure to the developing fault (Sikorska and Mba, 2008). Therefore, it becomes supplementary to conventional vibration technique. Current work aims to develop a methodology in detecting valve failures through analysis of AE signals. Vibration signals will serve as the reference to AE signals to compare the effectiveness of the AE technique in identifying valve failures.

1.3 Objectives

Objectives of the study are shown as follows:

- i) To correlate acoustic emission (AE) and vibration signatures with valve timing at three different valve conditions and two compressor speeds under no load condition.
- ii) To identify and compare the acoustic emission (AE) and vibration signatures at different valve conditions for different compressor speeds and determine the frequency ranges at various valve timing and conditions.
- iii) To enable automated classification of valve signature at different conditions.

1.4 Scope of the study

This study is proposed with the intention of increasing efficiency of reciprocating compressor and reducing possibility of machine shutdowns. It examines the effectiveness of acoustic emission (AE) as a reliable measurement technique in detecting valve failures in reciprocating compressors. The output of AE analysis will be compared with the conventional non-intrusive condition monitoring technique, the vibration measurement for reference.

The scopes of study are listed as follows:

- a) The valve of the reciprocating compressor is chosen for the study.
- b) Three valve conditions will be simulated experimentally based on the actual valve problems in industry. This includes the normal, grease, and leakage valve condition.
- c) Acoustic emission technique is chosen as the measurement technique and the results will be compared with that from vibration technique.

- d) The signals are analyzed based on simulated valve problems, without monitoring the initiation and propagation of defects continuously.
- e) The methodology developed can distinguish the normal and abnormal valve condition automatically.

1.5 Outline of thesis

The thesis consists of 6 chapters. It begins by providing information about background and objectives of the study in Chapter 1. Chapter 2 includes a comprehensive review regarding valves of reciprocating compressor, AE measurement technique in machine condition monitoring and characteristics of AE signal. Besides, different time-frequency analysis methods will be discussed in Chapter 2, together with the strengths and weaknesses for each analysis method. Moreover, details about machine learning technique for automated classification of signal will also be included in this chapter.

Chapter 3 describes work flow of the study. This includes hardware setup and data acquisition, signal conditioning and synchronous time-averaging, and parameter comparison. Different parameters will be introduced in this chapter and the parameter best describing different conditions of valve will be discussed in following chapter. Additionally, the time-frequency analysis technique employed in the current study will be discussed and justified in detail.

Chapter 4 presents signal analysis of AE and vibration signal, which includes visual inspection and time-frequency analysis of signals. In addition, this chapter evaluates different parameters indicating the health condition of valve through statistical hypothesis testing. Besides, time segments and frequency range which discriminate the

normal valve condition from the abnormal valve condition will be identified. Comparison will be made between each rotating speed for both signals under three different valve conditions.

Chapter 5 involves implementing machine learning technique for automated valve failure classification. It includes training the input data and fine tuning the parameters of classifier before testing the classifier with the test data. The performance of classifier at each frequency range is assessed and compared under different rotating speed.

Finally, Chapter 6 provides a summary of the current work, achievement of the study and recommendations for future study.

CHAPTER 2 LITERATURE REVIEW

2.1 Overview

This chapter begins with introduction of valves in reciprocating compressors. It explains the need for valve monitoring and further discusses the valve mechanism and some examples of valve failures in the plant. Characteristics of AE signal and application of AE technique in condition monitoring will be discussed in the later section of the chapter. The chapter continues with the review of time-frequency analysis in condition monitoring. The strengths and weaknesses of each time-frequency analysis method are discussed and reasons of selecting wavelet packet transform (WPT) for signal analysis in the current study is justified.

This chapter ended with comparison of 2 supervised learning technique, namely the neural network (NN) and support vector machine (SVM). The SVM technique is found to be more suitable for the current study due to its small sample size requirement, attainment of global minimum, fast training time and robustness towards larger number of features/ fault conditions.

2.2 Reciprocating Compressor Valves

Reciprocating compressors are one of the oldest yet widely used compressors in the gas-transmission, refinery and petrochemical industry. They provide a broad range of capacity control and high compression-ratio regardless of molecular weight, which are properties very much needed in the gas-transmission line (Ramesh, 2007). Figure 2.1 shows a typical horizontal balanced reciprocating compressor.

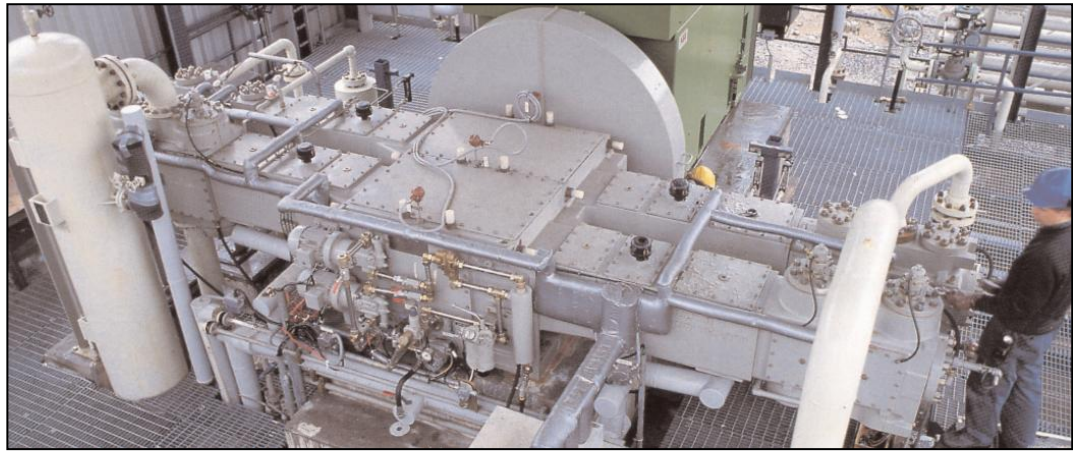


Figure 2.1: Typical horizontal balanced reciprocating compressor (Courtesy Sulzer-Burckhardt, Winterthur, Switzerland)

However, the maintenance cost of the reciprocating compressors is relatively higher compared to the others, such as the centrifugal compressor. It can be increased to the extent that the ratio of maintenance cost of reciprocating compressor to centrifugal compressor become 5:1 (Diab and Howard, 2004). In fact, the cost of unscheduled shutdown for reciprocating compressor can be as high as USD 100, 000.00 per day (Leonard, 1997). Therefore, condition monitoring is essential to reduce the possibility of sudden shutdown in the plant.

Some investigations were conducted to study the causes of sudden shutdown of reciprocating compressor. According to a survey conducted by the Dresser-Land company (Foreman, 2002), the compressor valves ranked the top among the components causing compressor shutdown, followed by pressure packing and process problems, as summarized in Table 2.1.

Table 2.1: Components of reciprocating compressor shutdown (Foreman, 2002)

Component	Percentage (%)
Compressor valves	36
Pressure packing	17.8
Process problems	8.8
Piston rings	7.1
Rider bands	6.8
Unloaders	6.8
Cylinder lube systems	5.1
Instrumentation	5.1
Others	3.4
Piping	1.3
Frame and running gear	0.7
Frame lube systems	0.4
Foundation	0.3
Cylinder coolant system	0.2
Partition packings	0.2

Indeed, valve failures such as the valve leakage alone may not be sufficient to cause a compressor shutdown. It is the effect of valve failures which imposes additional dynamic forces to the compressor and eventually causes secondary damage to other parts of the compressor (Griffith and Flanagan, 2001), such as overloading and lubrication problem as displayed in Table 2.2. Hence, it can be deduced that valve failure is the source for most of the problems in reciprocating compressor.

Table 2.2: Distribution of reciprocating compressor failures (Smith et al., 1997)

Cause	Percentage (%)
Overload	28
Liquid or foreign object ingestion	18
Lubrication	12
Fatigue	9
Freezing	6
Other or undetermined causes	27

Therefore, the cost of valves accounted for 50% of the total maintenance costs of reciprocating compressor is not something coming out of the blue, as displayed in the

cost breakdown in Table 2.3. This is followed by the cost of packing and piston rings, which has a percentage of 20% each.

Table 2.3: Breakdown of maintenance costs of reciprocating compressor (Smith et al., 1997)

Component	Cost Percentage (%)
Valves	50
Packing	20
Piston rings	20
Rider bands	7
Piston rods	2
Cylinder liners	0.5
Bearings	0.5

As valve is the major concern for the rising cost of maintenance, it is necessary to understand both the valve design and valve dynamics within the reciprocating compressor. Figure 2.2 shows the structure of a typical reciprocating compressor.

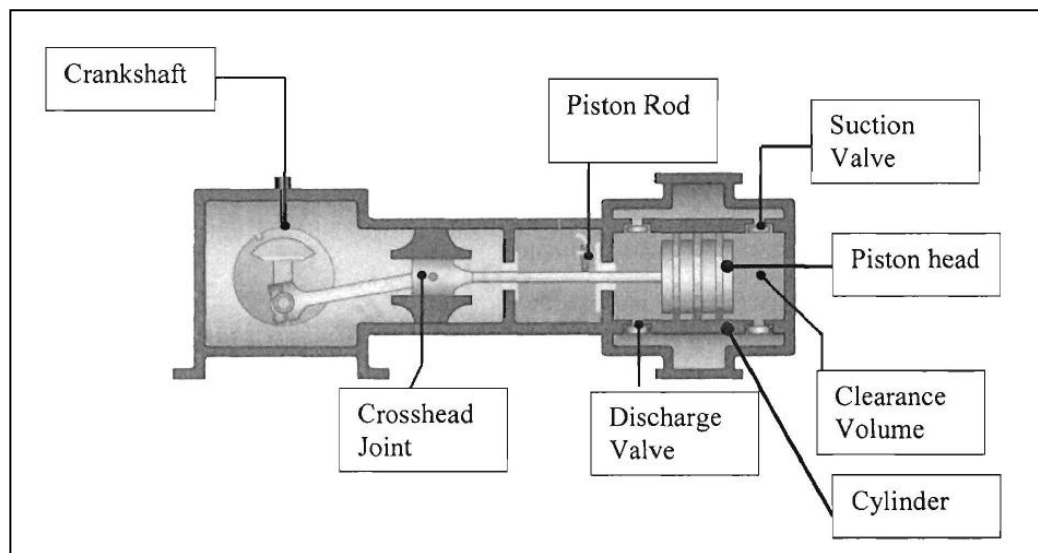


Figure 2.2: Structure of a typical reciprocating compressor

The crankshaft is usually driven by a prime mover to compress the fluid through reciprocating motion of a piston. As the piston moves downwards from the top-dead-

centre (TDC), as indicated by Point 1 in Figure 2.3, volume occupied by the cylinder head and the piston head is increased. Volume expansion will reduce the pressure within the space, to a certain extent that the pressure within the cylinder is equal to the pressure in the suction line, as indicated by Point 2 in Figure 2.3. As the piston moving further downwards from Point 2 to Point 3 in Figure 2.3, pressure difference between the suction line and cylinder causes the suction valve to open. Hence, the suction valve lift can be observed at Point 2 in Figure 2.3. The pressure difference between the suction line and cylinder become smaller as the fluid flows into the cylinder through suction valve. When the piston reaches the bottom dead centre (BDC), as shown in Point 3, there is almost no pressure difference. Thus, the suction valve starts to close, as displayed by the valve movement from the valve guard/ stop plate to valve seat in Figure 2.3.

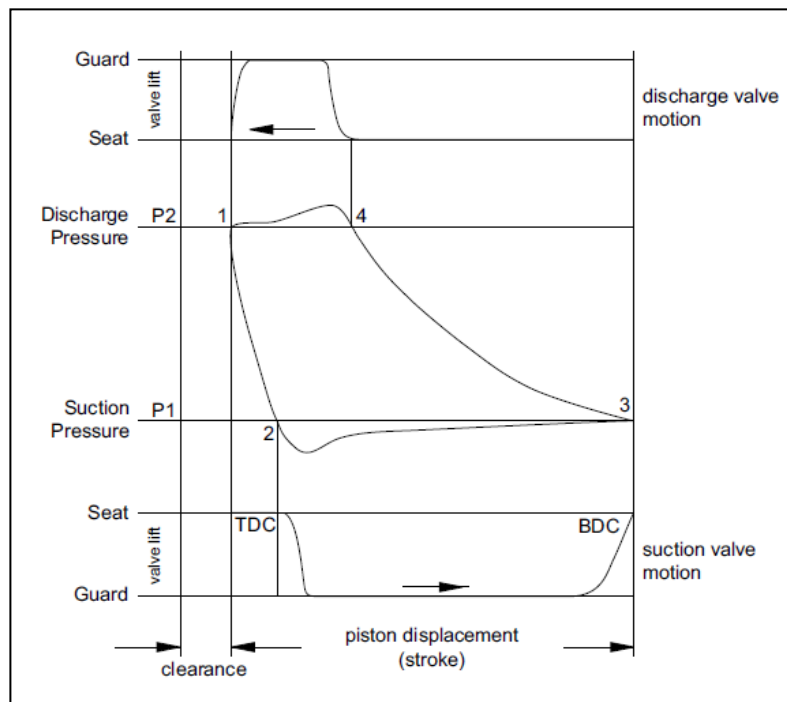


Figure 2.3: Pressure-Volume (PV) diagram and valve event of a reciprocating compressor

During the compression cycle, piston starts to move from BDC to TDC. As the volume decreases, the pressure within the cylinder increases, as displayed by Point 3 to Point 4 in Figure 2.3. At Point 4, pressure within the cylinder is equal to the pressure at the discharge line. Any further compression will force the discharge valve to open as the pressure within the cylinder is greater than the pressure at the discharge line. Thus, a discharge valve opening as displayed by the movement of valve from valve seat to valve guard can be clearly seen at Point 4 in Figure 2.3. As the fluid discharges from cylinder through the discharge valve, the pressure difference between the cylinder and the discharge line becomes smaller and eventually the discharge valve closes at Point 1.

In fact, the opening and closing event of the valves are activated by the pressure difference between the cylinder and the suction/ discharge line. To understand the valve dynamics, it is vital to study structure of the valve. Figure 2.4 shows the cross-section of a typical plate valve.

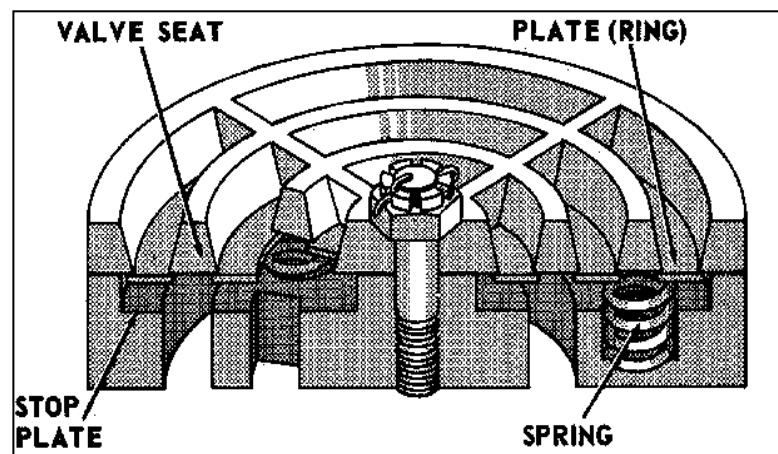


Figure 2.4: Structure of typical plate valve (Courtesy Dresser Rand Company)

When the valve is closed, the sealing element namely the valve plate/ ring is set firmly against the valve seat. As the pressure difference is sufficient to overcome pressure within the cylinder, spring load force, and sticking effect of lubrication

(Hoerbiger, 2007), the sealing element lifts off the suction valve seat and accelerates towards the valve guard/ stop plate, thus producing an impact on the valve guard/stop plate. The lifting of sealing element against the spring enables fluid to flow into the cylinder through the valve. When the pressure difference is insufficient to support the suction valve opening event, the spring bounces off and pushes the sealing element to return back to the valve seat, thus blocking fluid from entering the cylinder. This suction valve closing event occurs when the piston is at the BDC.

Further illustration on the valve dynamics is lucidly shown in Figure 2.5. Similarly, discharge valve opens and closes with the same principle as suction valve. The only difference between the suction and discharge valve is the position of valve mounted at the cylinder wall. In fact, discharge valve is mounted in the inverse position of suction valve, as illustrated in Figure 2.5.

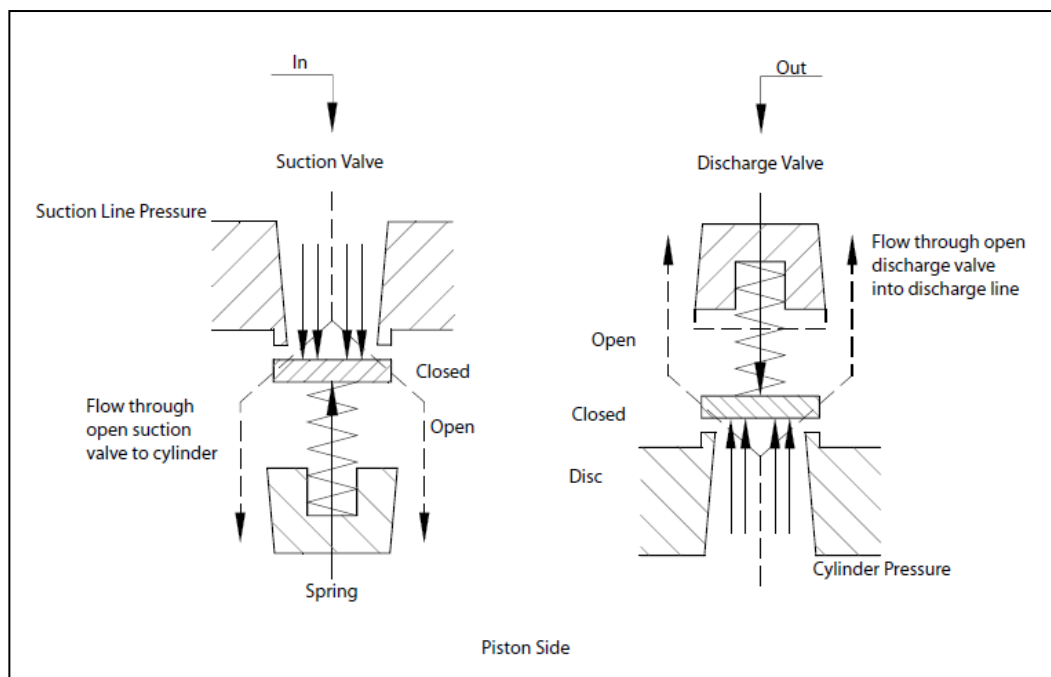


Figure 2.5: Sealing element movement in suction and discharge valve (Hoerbiger, 2007)

As valve opens and closes with each revolution of crankshaft, the possibility of valve failure is always higher compared to other components of reciprocating compressor. A compressor with a rotational speed of 800 rpm can easily have more than a million of valve opening and closing event throughout one day of operation. Therefore, establishing a valve failure monitoring system is paramount to the plant maintenance team. Valve problems such as the valve fluttering can reduce the compressor efficiency. This is because when the sealing element flutters between the valve seat and valve guard, as shown in Figure 2.6(a), the effective suction/discharge volumetric efficiency decreases. Meanwhile, valve delayed closure displayed in Figure 2.6 (b) can ultimately reduce the valve life as it is often associated with deterioration of spring.

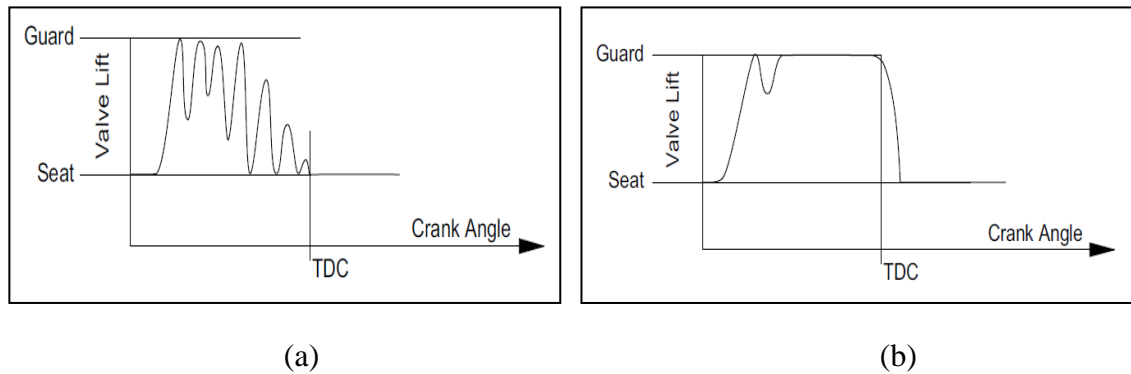


Figure 2.6: (a) Valve fluttering (b) Valve delayed closure (Hoerbiger, 2007)

There are a number of reasons contributed to the valve failure. Environmental factors such as contaminated fluid or improper lubrication can lead to clogged valve problem, as depicted in Figure 2.7(a). Moreover, foreign materials or impurities carried by the fluid through the valve and the valve delay closing can bring damage to the sealing element, as shown in Figure 2.7(b). These problems can be detected earlier through condition monitoring before they cause any additional damage to the machine. Current study investigates the problem of valve failures by using acoustic emission

(AE) technique. A broad review of the AE technique and its characteristics in condition monitoring will be explained in the following section.



(a) (b)
Figure 2.7: (a) Clogged valve (b) Broken valve ring (Courtesy of Hoerbiger Company)

2.3 Characteristics of Acoustic Emission (AE)

Acoustic emission (AE) is defined as the generation of transient elastic waves due to the release of rapid and localized energy as a result of deformation or dislocation within or on the surface of a material (Scruby, 1987; Mba and Rao, 2006). This technology began with Kaiser's (1950) research on the characteristics of AE in engineering materials by using the tensile test. His discovery is then termed the Kaiser effect, which is the immediate irreversible characteristics of AE phenomenon where there is little or no AE signals generated in a material until the stress levels exceed its previous value (McElroy, 1975).

In rotating machinery, AE signals are usually generated during asperities contact, cyclic fatigue, friction, turbulence, material loss, cavitations, and leakage. The type of AE waves generated depends on material properties, its mechanical behaviour and level of stresses at the source. Elastic waves such as longitudinal (dilatational, P) wave, shear (transverse, S) wave, Rayleigh (surface) wave, and Lamb (plate) wave are commonly detected and analyzed in AE testing (Muravin, 2009). AE signal is usually measured by AE transducer made from piezoelectric materials. The transducer mostly

captures Rayleigh wave as it has relatively higher amplitude compared to P and S wave amplitude (Hill et al., 1996), as shown in Figure 2.8.

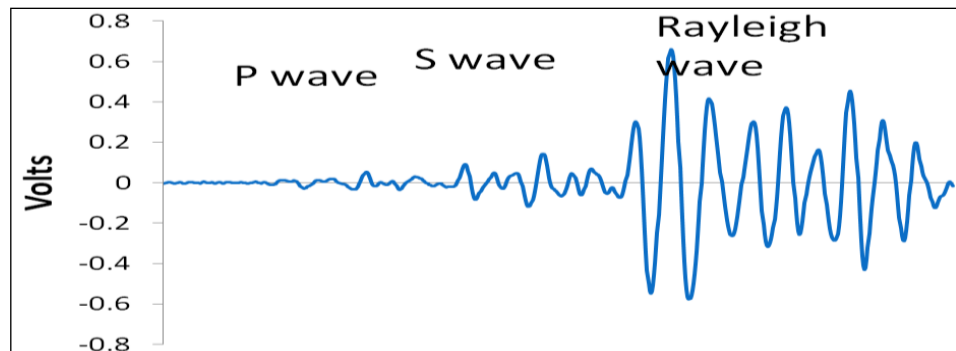


Figure 2.8: Types of Acoustic Emission Waves (Muravin, 2009)

This is due to the nature of Rayleigh wave in which it attenuates lesser as it spreads two-dimensionally rather than three-dimension. Thus, most of the waves acquired at the surface of structure are comprised of Rayleigh wave especially when the distance of AE transducer from the source is large (Scruby, 1987).

Unlike the vibration transducer which is direction dependent, AE transducer can receive signals from all directions (omnidirectional). Therefore, the AE transducer is not necessary to be attached near to the source of emissions. Once attached to a large structure, AE transducer can scan the entire structure by placing the transducer at 1-10 m intervals. It offers advantages over other non-destructive tools such as the ultrasonic where the later requires more transducers to scan through every part of the examined structure. One of the limitations of AE technique is on its generation of low energy pulses, which is mostly near the lower level of detection of piezoelectric transducers. Thus, complicated and expensive electronic apparatus is required to amplify the signals acquired (Williams, 1980). However, this issue is resolved nowadays with cheaper transducer produced as a result of a great improvement in instrumentation technology.

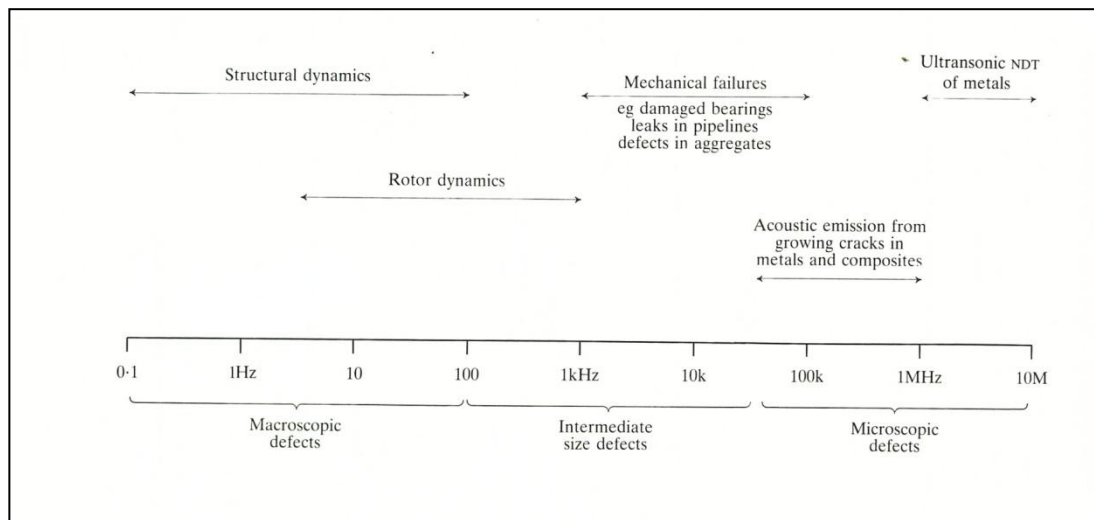


Figure 2.9: Spectrum of vibration and sound used for inspection and testing (Williams, 1980)

AE waves are typically in the frequency range of 100 kHz to 1 MHz (Leahy et al., 2006). Figure 2.9 shows the spectrum of vibration and sound used for inspection and testing. In contrast to vibration technique which focused on frequency range less than 100 kHz, AE technique is focused on the higher frequency range, where most of the microscopic defects within a material can be detected. Therefore, AE technique can provide superior early fault detection capabilities over vibration analysis (Sikorska and Mba, 2006). In high frequency range, signals from other machine components and its environment are attenuated easily, thus enabling AE signal to have a higher signal-to-noise ratio compared to signals acquired by accelerometer. However, the high frequency nature of AE also causes the signals captured to be much smaller, in the unit of milli or micro Volt (Sikorska and Pan, 2003). Low noise signal conditioning hardware and amplifiers are normally used to enlarge the AE signals. To have a better signal acquisition, AE sensors are normally placed as close as possible to the AE source and suitable couplant is applied between the sensor and its mounting surface to enable better signal transmission.

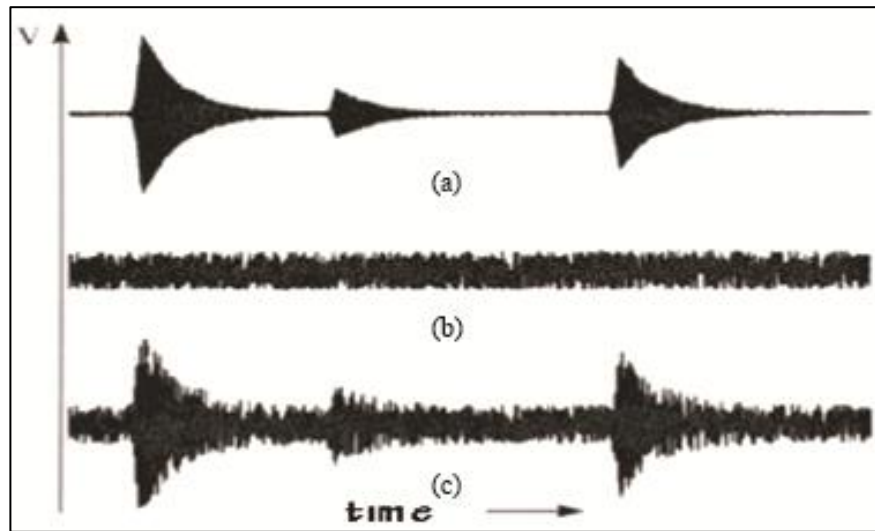


Figure 2.10: Types of AE Signals (a) Burst (b) Continuous (c) Mixed mode (Sikorska and Mba, 2006)

There are generally three types of AE signals, namely burst, continuous, and mixed mode type as shown in Figure 2.10. The burst types are associated with discrete transient signals with short decay time and rise time. Continuous types are bursts that occur too close to each other, thus appear as background signal level. The mixed mode type is a combination of both burst type and continuous type signal (Sikorska and Mba, 2006). The opening and closing mechanisms of valve in the compressor is usually represented by the burst signals in the time domain (Gill et al., 1998), along with the background noise. Due to the broadband nature of acoustic emission, AE signals are usually analyzed in the time domain (Sikorska and Mba, 2006). There are a few features which can be extracted from the AE signals plotted in time domain, namely peak amplitude, AE hits or counts, and burst duration as shown in Figure 2.11.

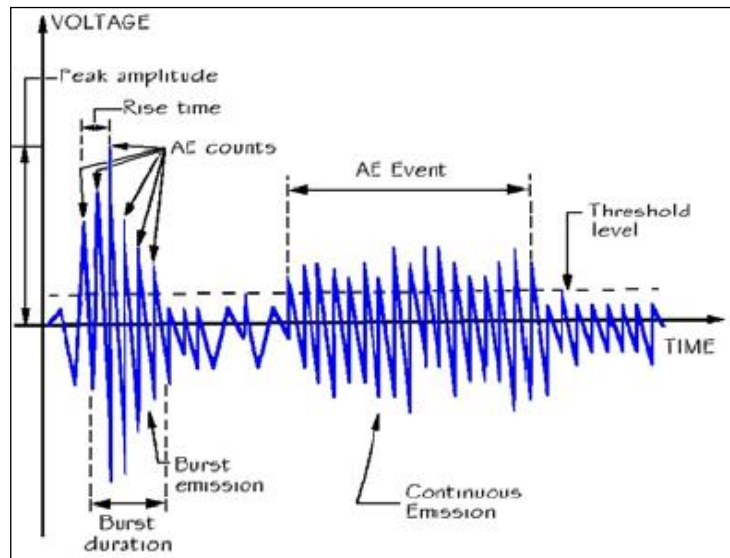


Figure 2.11: Traditional features of an AE Signal (Sikorska and Mba, 2006)

Peak amplitude is the highest amplitude of the signals while AE hits or counts are the number of AE bursts which exceeds certain threshold (Sikorska and Mba, 2006). A consecutive of AE hits or counts is termed AE event. The threshold level shown in Figure 2.11 is usually determined according to background noise and applications. There are two types of threshold, namely fixed threshold and floating threshold. Fixed threshold is a constant value set for the whole duration of test while floating threshold is the threshold level set as a fix amount above the background level. Generally, floating threshold will be utilized to avoid overloading of the data acquisition hardware when there is any increment of the background level due to the fluctuations in operating conditions (Sikorska and Mba, 2006).

Nevertheless, both thresholds are not employed in the current study. Instead of acquiring the AE hits/ counts, this study emphasizes on capturing the whole AE signal in the time domain as it can give more information about the valve condition. The following section provides a broad review regarding application of AE technique in condition monitoring of rotating machineries.

2.4 Acoustic Emission (AE) in Condition Monitoring

Condition monitoring plays a major role in predictive maintenance where it helps predicting the time of failure of a machine. It allows remedial action to be taken before significant permanent damage occurs. In recent years, industries are more inclined to adopt condition monitoring method as it allows machines to work more efficiently while reducing the cost of damage. The process involves monitoring certain parameters of machine condition without disturbing the operation. The parameters are typically byproducts generated when converting potential energy to kinetic energy, in the form of wear and tear, heat, vibration, and noise. There are few methods available to measure these byproducts such as vibration analysis, infrared thermograph, wear particles analysis, oil analysis or acoustic emission approach. In this research, condition monitoring system based on acoustic emission (AE) technique is chosen to provide a timely detection for valve failures in reciprocating machine.

Acoustic emission (AE) is a phenomenon of transient elastic waves generation by rapid release of energy from localized sources within or on the surface of a material (Leahy et al., 2006). It usually occurs when a small surface displacement of a material is produced. There are many sources of acoustic emission which include plastic deformation, micro fracture, wear, bubble collapse, friction, and impacts. It is measured and detected by the acoustic emission sensors (typically piezoelectric devices) when it propagates to the surface of the material (Sikorska and Mba, 2006).

In general, the application of acoustic emission has been largely neglected by the scientific and engineering communities, until the great advancement in modern instruments and transducer in the past fifty years, which eventually enables researchers to detect dislocation phenomena in metals (Liptai et al., 1972). Recently, acoustic emission technique has been used as a nondestructive testing (NDT) technique for

condition monitoring to examine either structural integrity or incipient fault in rotating equipment. The application of AE technique in fault detection of rotating equipment such as rolling element bearings, mechanical seals and journal bearings, gearboxes, pump and reciprocating machinery has been investigated by many researchers. The following section shows reviews on some of the common equipment of rotating machinery.

2.4.1 AE in Bearing Monitoring

Balerston (1969) is one of the earlier researchers who applied AE technology to identify artificially seeded defects in rolling element bearings. The defects simulated include outer and inner race defects, ball defects, and lack of lubrication. About a decade after Balerston, researchers found that AE offer better incipient fault detection of rolling element bearings over vibration. Roger (1979) commented that

“because of the slow rotational speed of the crane, application of conventional vibration analysis (0-20 kHz) was of limited value for on-line condition monitoring”.

He suggested using 100 to 300 kHz AE resonant transducer for on-line monitoring of bearings. Additionally, McFadden and Smith (1983) found that by using a AE transducer with frequency response beyond 300 kHz, minute strains (local distortions) of bearing housing can be detected at slow speed bearings (10 rpm) which could not be detected by accelerometer as the vibration energy is small and easily overlapped with other machine rotational speed. However, vibration analysis is better in detecting bearing fault in higher rotational speed range (850 rpm) (McFadden and Smith, 1983) as AE signals appear to be low frequency noise under higher rotating speed.

Al-Ghamd and Mba (2006) supported this finding when examining AE and vibration analysis for bearing defect identification and estimation of defect size. They found that over a range of speed (10-4000 rpm) and load conditions (up to 16 kN), AE technique can provide earlier detection of bearing defects compared to vibration technique. Furthermore, the AE burst duration and amplitude can indicate defect size, which is not achievable through vibration analysis. Thus, the propagation of defect and severity of fault can be monitored closely through AE technique, enabling defective bearings to be changed in time. The AE technique is capable of detecting the growth of subsurface cracks, whereas the vibration technique can only detect defects when they appear at the surface. In addition, the high frequency range of AE signals generated also offers an extra advantage compared to vibration signals as the former will not be masked by other machinery noise which is usually present in lower frequency range (up to 50 kHz) (Tandon and Choudhury, 1999).

The AE technique is particularly good in detecting defects of rolling element bearings with rotational speed below 16 rpm. Jamaludin et al. (2001) commented that vibration technique has difficulty in detecting bearing failures at low rotational speed due to limitations of the instrument itself, besides the fact that vibration energy is usually weak and occurs over a longer period (Kuboyama, 1997). He showed that AE technique is capable of detecting early stages of bearing damage at rotational speed as low as 1.12 rpm, although complicated signal processing and clustering techniques are needed in the analysis. In fact, advanced signal processing technique such as adaptive line enhancer and peak-hold down sampling are employed in industries nowadays for online monitoring of slow rotating machinery as the former can improve the signal-to-noise ratio while the later can reduce the burden of handling huge amount of data (Kim et al., 2009).

The development of AE monitoring in bearing diagnosis is in fact the most established application of AE in rotating machinery monitoring (Mba and Rao, 2006). This is proved by the ubiquitous commercial software in the current market for AE monitoring of rolling element bearing. Nevertheless, there are still rooms to enhance the current diagnosis and prognosis techniques.

2.4.2 AE in Gear Monitoring

For the gear fault diagnosis, Miyachika et al. (1995) examined AE waves by conducting the bending fatigue test on spur gear. He found that crack initiation can be predicted by using AE technique for case hardened gear. Besides, cumulative event count of AE increased with the crack growth until a specific depth of hardness. However, the same observation is difficult in the case of normalized gear.

Detection of gear pitting can be seen clearly in the research done by Singh et al. (1996). Gear pitting is the result of a combination of Hertzian fatigue forces and surface tension. It occurs when loads applied on the gear far exceeding the designed load or due to some metallurgical problems. Eventually, tooth breakage can happen after gear pitting as the remaining core of gear is weakened when the hard outer layer is penetrated. According to Singh et al. (1996), both the AE and vibration technique can detect the gear pitting. Nevertheless, AE signals have a greater signal-to-noise ratio compared to vibration signals. He stated that gear pitting cannot be detected at a very high speed or unloaded conditions for both the AE and vibration techniques. This is because under such circumstances the background noise level increases while the amplitude of AE or vibration signals due to pitting decreases. Singh et al. (1999) later investigated on the capability of AE in detecting gear tooth breakage. When compared to the vibration analysis technique, AE shows a better performance as it can detect the

initial stage of crack propagation while there is no significant change in the vibration level. This once again shows that AE technique offers an advantage over vibration monitoring techniques.

The superiority of AE maybe attributed to the mechanism of AE generation. Tan et al. (2007) mentioned that the major source of AE activity at gear mesh is the asperity contact during sliding or rolling of gear teeth. The AE activity is more sensitive to the rotational speed than applied load under the same operating temperature (Tan and Mba, 2005a). On the other hand, a change in the stiffness of gear as a result of gear damage will alter the vibration signals collected from the gears (Tan et al., 2007). However, the change of gear stiffness needs to be large enough for a change in the vibration level. This is supported by the finding that the vibration level only started to rise after a minimum gear pitting area of 25%. Nonetheless, AE is more sensitive than vibration and spectrometric oil analysis in detecting the natural life degradation of spur gear. In fact, AE level increases linearly with increasing pitted area, which is not the case for vibration and spectrometric oil analysis. Hence, it can be concluded that AE performs better in pit growth monitoring of gear while vibration technique can only detect the gear defect at a later stage, when the pit development was advanced.

Although AE is sensitive in detecting natural pitting of spur gear, it seems to be challenging in identifying defects of artificially seeded spur gear (Tan and Mba, 2005b). Besides having non-consistent of AE burst with gear defect location, it was found that the lubricant temperature has an influence on the AE level, in addition to other variables such as the load and rotational speed which had been discovered by other researchers (Tandon and Mata, 1999; Toutountzakis and Mba, 2003). Thus, the timing of data acquisition, in effect the lubricant temperature, will affect the AE level, which causes the problem of inconsistencies of data. In contrast, the seeded defects of helical gear can

contribute to an obvious burst of AE signal. In fact, Eftekharijad and Mba (2009) stated that the burst occurred at the exact location of the seeded defect, which is not possible for the similar test with spur gear (Tountzakis et al., 2005; Tan and Mba, 2005b). Further finding on the direct relation between AE level and the volume of removed material of helical gear demonstrate potential of AE technique as a diagnostic tool in future.

Despite the fact that the application of AE in gear diagnosis is still in its infancy, this technique has started to display its potential as a promising diagnostic tool in gear monitoring. It is expected to become a complementary tool for vibration technique in gear diagnostics in the near future, after more investigations performed to ensure robustness and reliability of the technique, which include understanding the effect of operational variables on the generation of AE activity (Mba and Rao, 2006).

2.4.3 AE in Valve Monitoring

Conventionally, condition of valves in reciprocating compressor is monitored through pressure-volume (PV) and temperature measurement. These techniques have been proven to be successful and applied widely in the industry (Afimiwala and Woollatt, 1984; Davis, 2004). Indeed, software for monitoring reciprocating compressor through pressure and temperature measurements is prevalent in the current market. By superimposing current PV diagram and temperature data to the baseline data from time to time, condition of the valves can be monitored closely. In addition, the suction and discharge volumetric efficiency and flow balance acquired from the PV measurement can give important information about the health condition of valve (Schirmer et al., 2004). Although these measurement techniques can effectively detect valve leakage before causing any secondary damage to other parts of the compressor namely the

crosshead pin bushing or piston rod, these intrusive measurement techniques always require proper installation of transducer. Besides, these techniques may not be able to detect early changes of valve condition such as degradation of spring or initiation of cracks in the valve plate. Recently, other non-intrusive technique such as the instantaneous angular speed (IAS) was introduced due to the ease of installation and flexibility in giving minimum interference to the operating conditions (Elhaj et al., 2008; Elhaj et al., 2010). Nevertheless, this technique can only prove to be capable of detecting valve leakage based on previous research. No further studies are conducted to examine other valve failure conditions by using IAS to date.

Due to the mechanism of AE signal generation as discussed in the previous section, this non-intrusive technique can be a better measurement technique for valve failure detection. Although AE monitoring has been applied to the detection of valve leakage in reciprocating compressors, there are still limited resources in this field. Gill et al. (1998) proposed to use AE technique as a non-destructive testing tool (NDT) in monitoring a large reciprocating compressor. The poppet valves of a two stage, horizontally opposed reciprocating compressor with working pressure from 260 to 3200 Barg had been investigated on site. Gill et al. (1998) found that majority of the poppet valve failures were due to degradation of impact valve faces and springs. There were also other possible causes such as the sticking of valves due to uneven loading, excessive wear of the valve guides or broken springs. The AE root-mean-square (RMS) signal corresponding to the angular position of crankshaft was acquired and compared between normal and faulty compressor. The opening and closing of the suction and discharge valve can be detected clearly both by the accelerometer and the AE sensor, thus the timing of all valves can be monitored. These events were displayed as signals with a sudden rise followed by a gradual decay. However, whilst AE technique can

detect fluid-mechanical motion in the valve due to its wide frequency range, the fluid movement around the valve cannot be detected by using the vibration technique as it is not sensitive to the high frequency noise emitted by the fluid motion.

Gill's work was mainly focused on the fault diagnosis of valve through visual inspection of AE and vibration time signal. With the advance of technology, there are some researchers introduce the idea of automated pattern recognition techniques where the fault of reciprocating compressors can be identified automatically by applying some feature extraction algorithms. El-Ghamry et al. (2003) proposed pattern recognition and statistical feature isolation techniques to identify problems in reciprocating machines. The authors intended to develop a generic algorithm for diagnosing problems in any reciprocating machines by relating the mechanical events with signals recorded. By employing suitable filters to locate the features of AE signal, faulty conditions were detected automatically when the statistical parameters exceed certain threshold value. They further concluded that this diagnostic method can reduce intense computation of AE signals while obtaining an accurate result of fault diagnosis. Meanwhile, the mean value of AE RMS signal was selected as the best parameter in valve monitoring. However, detailed comparison such as the time-frequency analysis between vibration and AE technique in valve diagnosis of reciprocating machine is yet to be conducted.

As AE and vibration signals exhibit non-stationary behaviour such as having different pulse timing and amplitude under different valve conditions, it is believed that time-frequency analysis can provide better diagnosis on the valve condition. Elhaj et al. (2001) used time-frequency analysis technique namely continuous wavelet transform (CWT) to analyze vibration and airborne sound signals for valve diagnosis. Yang et al. (2004) further demonstrated the use of discrete wavelet transform (DWT) in combination with higher order statistics and neural networks for automated quality

examination in the production line of small reciprocating compressors through vibration signals. It was found that features of the vibration signals revealing the condition of compressors can be extracted through DWT and served as the inputs for neural networks.

Lin, et al. (2006, 2009) later proposed on using some time-frequency analysis techniques and classification strategy to examine the valve condition in a reciprocating machine. A single stage, two cylinder reciprocating compressor is used as a test bed for simulating seeded valve faults and the signals generated are acquired by using an accelerometer with the resonant frequency of more than 50 kHz. Three time-frequency analysis techniques, namely the Short Time Fourier Transform (STFT), smoothed pseudo Wigner-Ville distribution (SPWVD), and reassigned smoothed pseudo WVD (RSPWVD) are used as the basis for classification strategy. Data reduction algorithm such as the mean variation method, min/max method, and the unit standard deviation method are used to reduce the large number of data sets for practical system classification. The authors concluded that though better resolution of time-frequency images can be obtained through SPWVD and RSPWVD, they do not produce better classification results by using the current extraction mechanism. In fact, STFT can provide similar classification results with less computation time. This is indicated by the full success of classification (with zero percent of misclassification) by using the mean variation method and the STFT datasets.

Despite several attempts to examine the effectiveness of time-frequency analysis by other researchers in detecting valve failures, most of the studies were focused on analyzing vibration signals under different valve conditions. There is limited study conducted in analyzing AE signal through time-frequency analysis method. Moreover, most of the valve diagnoses through AE signal are emphasized on detecting the valve

leakage, when there are possibilities for other valve failures such as spring deterioration, valve misplacement, cracked valve plate, and over/inadequate tightening of valve cover/seat which occur much earlier before they cause serious leakage in the valve. This study is intended to fill up the gap by analyzing the AE signal under different valve conditions by using the time-frequency analysis method. Details of different time-frequency analysis technique will be discussed and the decision of selecting a particular time-frequency technique will be justified in the following section.

2.5 Time-Frequency Analysis

Signal generally represents physical phenomenon such as temperature fluctuations in a room, pressure changes in a chamber or displacement changes in a structure. A signal captured is usually displayed as a time history. To study and classify a signal, one has to know the type or behaviour of the signal. Signals are generally classified as deterministic and random, as shown in Figure 2.12 .

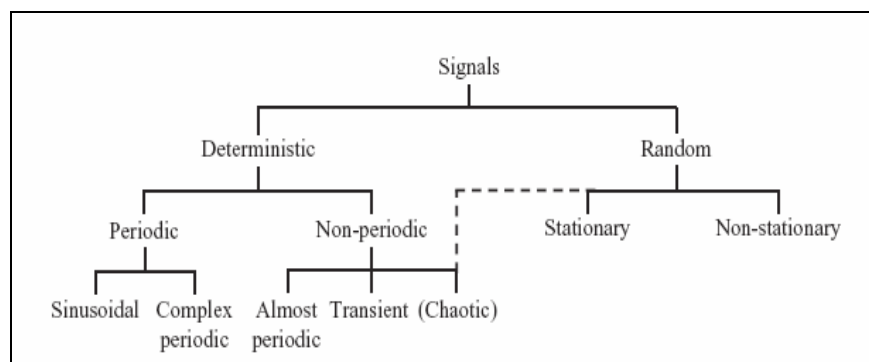


Figure 2.12: Classification of signals (Shin and Hammond, 2008)

Behaviour of a deterministic signal can be predicted exactly while in turn for a non-deterministic or random signal, it could not be forecasted accurately. However, in

practical applications, this classification can only serve as a reference because most of the signals are mixtures of different types of signal.

Most of the information embedded in signal could not be displayed in the time domain. This is especially true when the signal is a combination of different frequency content. If one of the components is of smaller amplitude compared to the others, it will be hidden under the signal of larger amplitude and will not be differentiated in the time domain. This phenomenon often causes difficulty in extracting important information from a signal. Thus, signal transformation is needed to extract the frequency components of the signal. One of the popular ways is by the Fourier transformation.

2.5.1 Fourier Transform

Fourier transform (FT) enables a periodic or stationary signal to be decomposed to its constituent frequency components, which is a combination of sine and cosine waves. The coefficients of Fourier transform indicates how closely the signal is related to a particular frequency component. The higher the value of coefficient $X(f)$, the more dominant is the frequency component f in the signal being analyzed. Fourier transform is shown in Equation 2.1, where $x(t)$ denotes the time domain signal and f represents frequency of the signal.

$$X(f) = \int_{-\infty}^{\infty} x(t)e^{-j2\pi ft} dt \quad (2.1)$$

These sine and cosine waves can be summed up to form the original signal through the inverse Fourier transform, as shown in Equation 2.2.

$$x(t) = \int_{-\infty}^{\infty} X(f) e^{j2\pi ft} df \quad (2.2)$$

Fourier transform is very useful in solving linear partial differential equations in heat conduction, magnetic, wave propagation to name a few. In engineering application, it is utilized widely in signal processing, image processing, and vibration analysis.

However, as Fourier transform is the integration of inner product of the signal $x(t)$ with sine and cosine functions, $e^{j2\pi ft}$ where these two functions are global functions, the Fourier transform exhibit global information of the signal. In other words, a small perturbation of signal in the time domain will spread through the entire frequency domain. Therefore, one can only observe the frequency components of the signal without knowing the time properties of these frequency components. This made Fourier transform unsuitable in analyzing non-stationary signals as the local property of the signal could not be extracted. Hence, other methods such as the short time Fourier transform (STFT) and wavelet transform are introduced to enable time-frequency analysis in the same platform.

2.5.2 Short Time Fourier Transform (STFT)

Short Time Fourier Transform (STFT) is introduced by Gabor (1946) to overcome the inadequacy of Fourier transform. In STFT, the signal is divided into small segments, where each segments is assumed to be stationary. This is achieved when the signal $x(t)$ is multiplied with a window function $g(t)$ centered at certain time location τ , as shown in Equation 2.3, where $*$ denotes the complex conjugate of the function and $S(\tau, f)$ represents the coefficient at time τ and frequency f .

$$S(\tau, f) = \int_{-\infty}^{+\infty} x(t) g^*(t - \tau) e^{-j2\pi ft} dt \quad (2.3)$$

Indeed, the time and frequency resolution of signal are dependent on the width of window. A wide window will result in better frequency resolution but poor time resolution while a narrow window will result in better time resolution but poor frequency resolution, as shown in Figure 2.13.

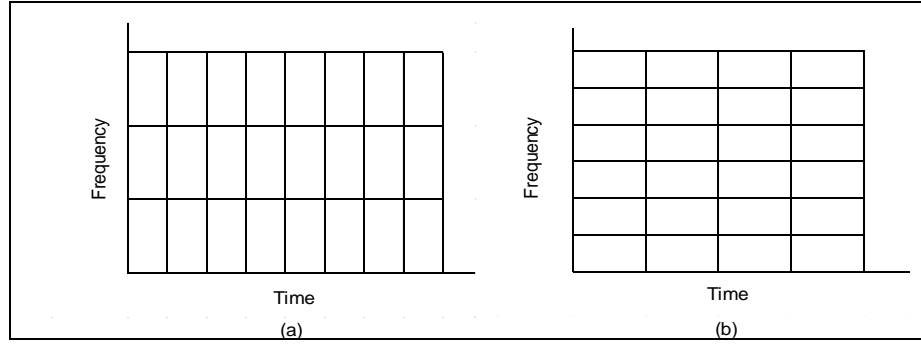


Figure 2.13: Time frequency plane of STFT for (a) Narrow window (b) Wide window

Since the width of windowing function is fixed, the resolution of STFT is fixed. Therefore, better frequency resolution is achieved with the compromise on time resolution and vice versa for the entire time-frequency plane. This is due to the fact that the windowing function is lower-bounded by the Heisenberg uncertainty principle, as displayed in Equation 2.4.

$$\Delta f \Delta t \geq \frac{1}{4\pi} \quad (2.4)$$

This principle states that the exact time frequency representation of a signal cannot be achieved. One can only know the time intervals within certain frequency band, but not

the exact point in the time-frequency plane. Therefore, the time and frequency resolution, Δf and Δt cannot be arbitrarily small as they have a lower bound.

Due to the limitation of fixed resolution, STFT is not favourable in the analysis of non-stationary signal, especially when the signal is a combination of extremely high and low frequency components. Although one can vary the windowing function at certain time instant to change the time-frequency resolution, this method is not preferable as knowledge of windowing function is needed for analysis and comparison is difficult to be made as the whole signal is analyzed with different windowing function.

2.5.3 Wavelet Transform

2.5.3.1 Continuous Wavelet Transform (CWT)

The wavelet transform had been a subject of study since 1930s, where several studies were performed on developing the representation of functions through scale-varying basis functions (Graps, 1995). The multi-resolution analysis proposed by Mallat (1989) had accelerated the wavelet theory as he managed to develop the link between quadrature mirror filters, pyramid algorithms and orthonormal wavelet bases.

Similar to STFT, the wavelet coefficient is obtained by multiplying the time signal with a basis function. However, the wavelet basis function is utilized instead of the windowing function in STFT. In addition, no Fourier transform is performed on the multiplied signal. In other words, the wavelet transformed signal is not a time-frequency representation. In fact, it is a time-scale representation. This is because, as opposed to a fixed window width in STFT, the wavelet basis has variable width of window. This property enables the signal to be analyzed under different scale or resolution. Higher

scale corresponds to a dilated signal while lower scale corresponds to a compressed signal. Heisenberg uncertainty principle is still satisfied under wavelet transform and the wavelet basis inherited the property of having good time resolution and poor frequency resolution at smaller scale and good frequency resolution and poor time resolution at larger scale, as shown in Figure 2.14.

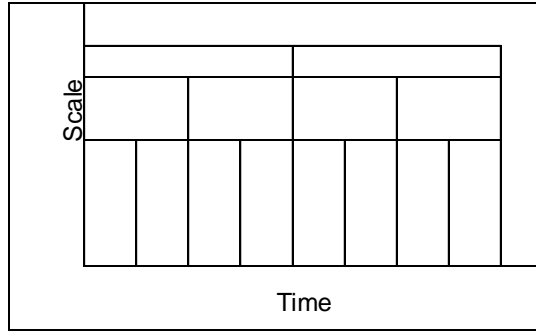


Figure 2.14: Time-scale plane of wavelet transform

Fortunately, most of the signals in real world application are of this property. Therefore the wavelet transform is good in representing real world signal and excellent in detecting signal discontinuity.

The wavelet coefficients are computed by shifting a given scaled wavelet through the whole time signal. The operation is repeated over a number of scales until the wavelet covered the whole frequency range of signal. The wavelet coefficients computed represent a level of correlation between the signal and the scaled wavelet basis at a certain time instant. A higher value of coefficient will be obtained if the signal has the same scale as the wavelet basis and vice versa.

For wavelet analysis, the signal being analyzed must contain finite energy. In other words, the signal must be square integrable, as shown in Equation 2.5. The continuous wavelet transform (CWT) is shown in Equation 2.6. $\gamma(s, \tau)$ denotes the

wavelet coefficient at scale factor s and translation parameter τ . $\psi_{s,\tau}^*(t)$ is the conjugate of mother wavelet. It is given in Equation 2.7, where the normalization factor $\frac{1}{\sqrt{s}}$ ensures that energy remain the same at different scales.

$$\int_0^{\infty} |x(t)|^2 dt < \infty \quad (2.5)$$

$$\gamma(s, \tau) = \int_{-\infty}^{+\infty} x(t) \psi_{s,\tau}^*(t) dt \quad (2.6)$$

$$\psi_{s,\tau}(t) = \frac{1}{\sqrt{s}} \psi\left(\frac{t-\tau}{s}\right) \quad (2.7)$$

Mother wavelet is a prototype function generating wavelets at different scales. All other wavelets at different scales are derived from the mother wavelet. Compressed, high-frequency (low scale) of the mother wavelet enables temporal analysis while dilated, low frequency (high scale) of the same wavelet enables frequency analysis. This is because the former has higher time resolution while the later has higher frequency resolution. Figure 2.15 shows the compressed and dilated function of a Morlet wavelet.

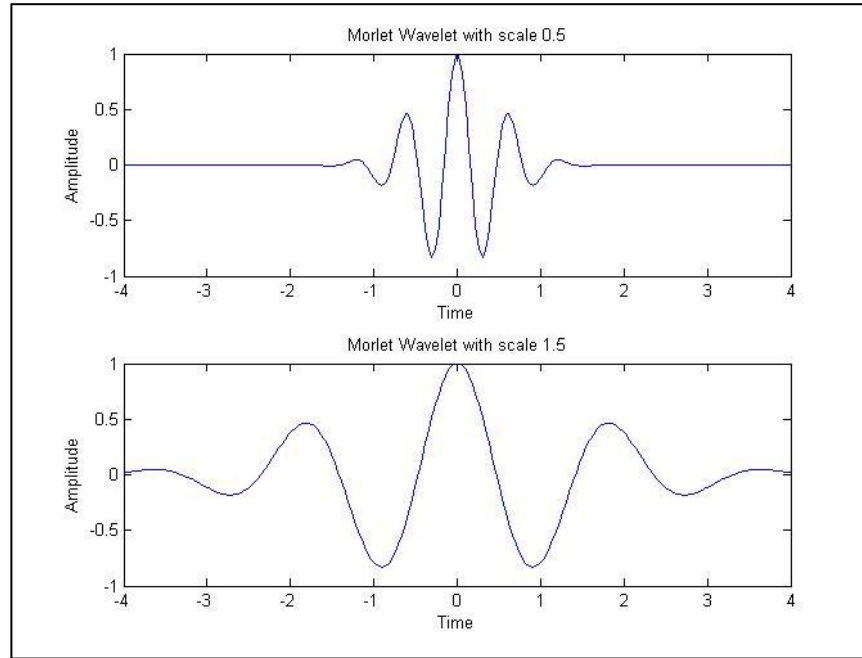


Figure 2.15: Mother wavelet with scale 0.5 and scale 1.5

In fact, certain mathematical requirements are needed to be satisfied before a function can be chosen as a mother wavelet. These mathematical requirements will determine the properties of a mother wavelet. Firstly, to ensure that a signal is analyzed and reconstructed without any loss of information, the admissibility condition must be satisfied, as displayed in Equation 2.8.

$$C_\psi = \int_{-\infty}^{+\infty} \frac{|\hat{\psi}(\omega)|^2}{|\omega|} d\omega < \infty \quad (2.8)$$

This condition restricts the class of functions that can be wavelets. It implies that the Fourier transform of wavelet $\psi(\omega)$ is zero at zero frequency, given in Equation 2.9.

$$\hat{\psi}(0) = 0 \quad (2.9)$$

This property enables wavelet to have a band-pass spectrum characteristic (Valens, 1999), which is very useful in discrete wavelet transform. Equation 2.9 also implies that average value of wavelet is zero in the time domain, given in Equation 2.10.

$$\int_{-\infty}^{\infty} \psi(t) dt = 0 \quad (2.10)$$

Hence, the wavelet is oscillatory and behaves like a wave. In fact, the term wavelet signifies “small wave”. The admissibility condition provides the requirement for a function to behave like a wave while the regularity condition ensures that the function to be small. In other words, the wavelet should have some degree of smoothness and concentration which enable it to have a fast decay. This also suggested that the wavelet have to be compactly supported (with finite width of length).

The regularity condition depends on the number of vanishing moments in a wavelet function. The vanishing moments is given in Equation 2.11.

$$\gamma(s,0) = \frac{1}{\sqrt{s}} \left[\sum_{p=0}^n f^{(p)}(0) \int \frac{t^p}{p!} \psi\left(\frac{t}{s}\right) dt + O(n+1) \right] \quad (2.11)$$

$$\gamma(s,0) = \frac{1}{\sqrt{s}} \left[f(0)M_0s + \frac{f^{(1)}(0)}{1!}M_1s^2 + \frac{f^{(2)}(0)}{2!}M_2s^3 + \dots + \frac{f^{(n)}(0)}{n!}M_ns^{n+1} + O(s^{n+2}) \right] \quad (2.12)$$

$$M_p = \int_{-\infty}^{\infty} t^p \psi(t) dt = 0 \quad (2.13)$$

$f^{(p)}$ denotes the p^{th} derivative of function f while $O(n+1)$ denotes the rest of the Taylor series expansion at zero time instant (Valens, 1999). Equation 2.11 can be further rewritten as Equation 2.12. From Equation 2.12, the vanishing moment M_p can

be expressed as Equation 2.13. The higher the number of vanishing moments M_p , the faster is the decay of wavelet coefficients. Hence, if a scaling function or wavelet has p vanishing moments, the scaling function can represent the signal up to a polynomial degree of $p-1$.

One of the important features of wavelet basis is its orthogonality, which ensures the signal to be non-overlapped in the wavelet space. Therefore the signal can be transformed to the wavelet space back and forth without any loss of energy. The orthogonality condition is satisfied in the Fourier transform as its basis function, the sine and cosine function are orthogonal to each other.

$$\int_a^b \phi_k(t) \phi_l^*(t) dt = \delta_{kl} \quad (2.14)$$

$$\delta_{kl} = \{1, k=1; 0, k \neq 1\}$$

In wavelet transform, Equation 2.14 must be satisfied for orthogonality. Equation 2.14 implies that the scaling function, $\phi(t)$, which is a basis for wavelet function construction, must be orthogonal to its translation. Further information on orthogonality will be discussed in the section of discrete wavelet transform (DWT).

In CWT, the scale varies indefinitely until it covers the entire spectrum. However, the possible number of resolution or scale levels is dependent on the signal length. A signal with length of 2^j will have a maximum resolution of j level. Due to the high computational time and high redundancy of CWT, discrete wavelet transform (DWT) is introduced as a preferable method in signal analysis.

2.5.3.2 Discrete Wavelet Transform (DWT)

Discrete wavelet transform (DWT) can reduce the number of scaled wavelets required for covering the entire spectrum, thus reducing the computational time. This provides an extra advantage compared to CWT especially when the signal length is very long. Besides, DWT can overcome the redundancy problem in CWT. As opposed to CWT where the wavelets are continuously scalable and translatable, discrete wavelets are scaled and translated in discrete steps, as shown in Equation 2.15, where j and k denotes the scale factor and translation parameter respectively.

$$\psi_{j,k}(t) = \frac{1}{\sqrt{2^j}} \psi\left(\frac{t - 2^j k}{2^j}\right) \quad (2.15)$$

DWT is performed based on the two-scale relations. It relates the scaling function and wavelet at a given scale with the scaling function at the next-higher scale. This can be expressed in Equation 2.16.

$$A_1 = A_0 + W_0 \quad (2.16)$$

The scaling function at the higher scale, A_1 is composed of the scaling function, A_0 and wavelet W_0 at the next lower scale, as shown in Figure 2.16(a).

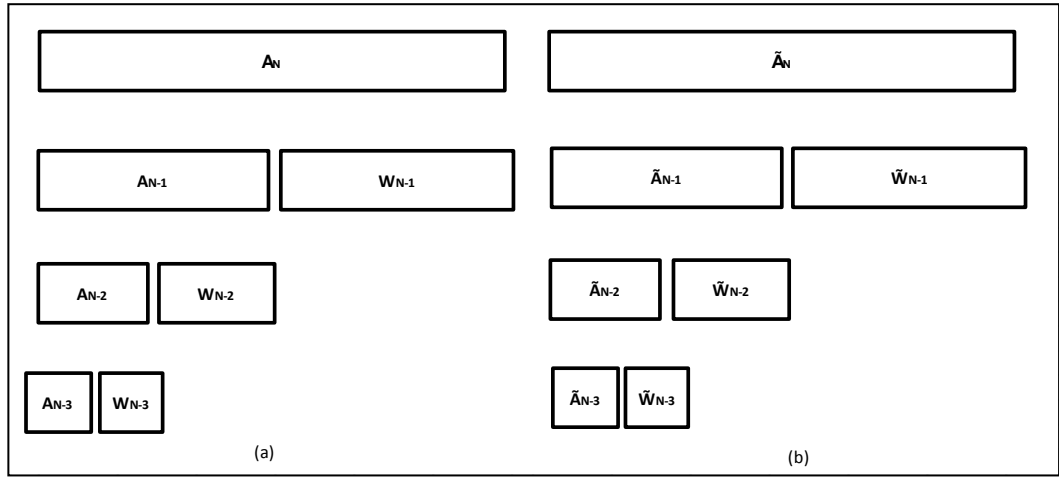


Figure 2.16: Two-scale relations for (a) Primal space (b) Dual space

This relation enables multi-resolution analysis (MRA) to be performed on a signal as the signal can be decomposed under different scales. As shown in Equation 2.17 and 2.18, where $\phi(2^j t) \in A_0 \subset A_I$ and $\psi(2^j t) \in W_0 \subset A_I$, the coarser resolution of the scaling function, $\phi(2^j t)$ and wavelet, $\psi(2^j t)$ at lower space can be represented as the finer resolution scaling function, $\phi(2^{j+1} t)$ at the next higher space by the two-scale relations.

$$\phi(2^j t) = \sum_k h_0[k] \phi(2^{j+1} t - k) \quad (2.17)$$

$$\psi(2^j t) = \sum_k g_0[k] \phi(2^{j+1} t - k) \quad (2.18)$$

To perform two-scale relations, the orthogonality of subspaces must be satisfied first. The scaling function must be orthogonal with respect to its translation in a given scale, as given in Equation 2.14 while the wavelet must be orthogonal with respect to its scale and translation. This implies that $A_0 \perp W_0$ such that $A_0 \oplus W_0 = A_1$. However, the orthogonality and linear phase (symmetry) property of wavelets cannot be satisfied at the same time, except the Haar wavelet family (Vetterli et al., 1995). The non-linear phase property of orthogonal wavelets such as Daubechies, Symlet, and Coiflet will result in phase distortions. Thus, biorthogonal wavelets are introduced to overcome the

limitations of orthogonal wavelets. The characteristics of orthogonal and biorthogonal wavelets are shown in Table 2.4.

Table 2.4: Characteristics of orthogonal and biorthogonal wavelets

Orthogonal wavelets	Biorthogonal wavelets
<ul style="list-style-type: none"> • Analysis and synthesis filter are of the same function. • Generally do not have closed-form expressions. • Usually not symmetric (linear phase), except Haar wavelet. • Higher-order filters (with more coefficients) have poor time-frequency localization. 	<ul style="list-style-type: none"> • Analysis and synthesis filter are of two different functions. • Normally have explicit expression. • Symmetric (linear phase). • Good time-frequency localization even at higher-order.

Biorthogonal wavelet has a dual space, as shown in Figure 2.16 (b). The duality in biorthogonal wavelet ensures that $W_0 \perp \tilde{A}_0$ and $A_0 \perp \tilde{W}_0$. In other words, the biorthogonal wavelet is not orthogonal to its primal space, but to its dual space. This ensures the linear phase property of biorthogonal wavelets. Besides, more freedoms are achieved in designing biorthogonal wavelets as the analysis and synthesis filters are composed of different functions.

The two-scale relations enable signal decomposition by passing the signal through a series of filter bank. The whole signal can be represented as a combination of scaling function $\phi(t)$ and wavelet $\psi(t)$, as shown in Equation 2.19 and 2.20,

$$\phi(2t) = \sum_k \{h_1[2k]\phi(t-k) + g_1[2k]\psi(t-k)\} \quad (2.19)$$

$$\phi(2t-1) = \sum_k \{h_1[2k-1]\phi(t-k) + g_1[2k-1]\psi(t-k)\} \quad (2.20)$$

where $\phi(2t), \phi(2t-1) \in A_1$ and $(\{h_1[k]\}, \{g_1[k]\})$ are the low pass and high pass filter in the square integrable space ℓ^2 . Both equations can be combined to form the decomposition equation, Equation 2.21 at a given scale j .

$$\phi(2^{j+1}t - \ell) = \sum_k \{h_1[2k - \ell]\phi(2^j t - k) + g_1[2k - \ell]\psi(2^j t - k)\} \quad (2.21)$$

From Equation 2.21, the signal is passed through a low pass filter (scaling filter) and high pass filter (wavelet filter) simultaneously, where the detailed wavelet coefficients at the higher frequency range are extracted through the high pass filter while the remaining portion, which forms the approximation coefficients are extracted from the low pass filter. The approximation coefficients will then split into its detailed and approximation portion again and the process is iterated until the number of samples is smaller than the length of the high pass or low pass filter (Valens, 1999). This process is termed sub-band coding, as shown in Figure 2.17, where $G[n]$ and $H[n]$ denote high pass and low pass filter respectively.

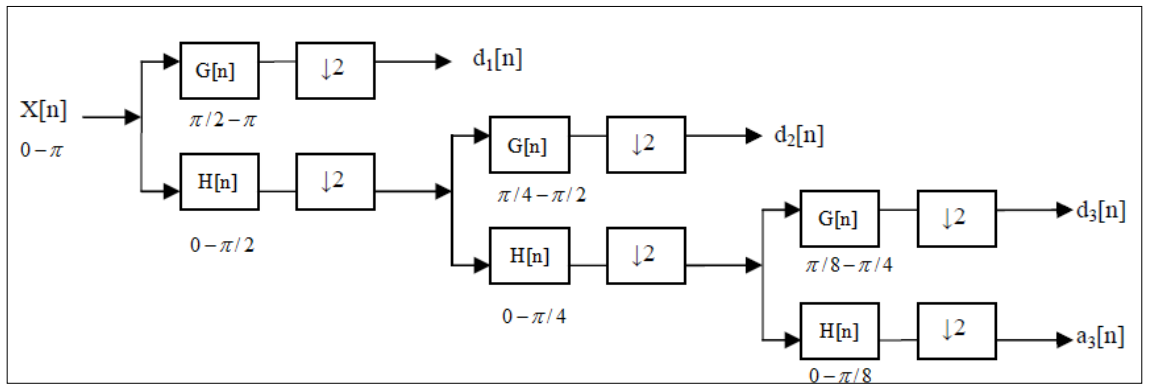


Figure 2.17: Sub-band coding algorithm (Valens, 1999)

When the signal is passed through the high pass or wavelet filter, its spectrum is doubled as the compression of wavelet by a factor of 2 in time domain will result in an upward frequency shift by a factor of 2. The same principle applies to the scaling function, thus producing a low pass spectrum. This enables the wavelet to cover the higher frequency portion and the scaling function to cover the lower frequency portion. Eventually, the scaling function and wavelet will cover the entire spectrum of the signal, where the detailed components are extracted every iteration, as shown in Figure 2.18. Since the frequency range of scaling function and wavelet spectrum is halved every iteration, the signal is decimated by a factor of 2 with every iteration, causing the number of samples reduced by a factor of 2 with every iteration.

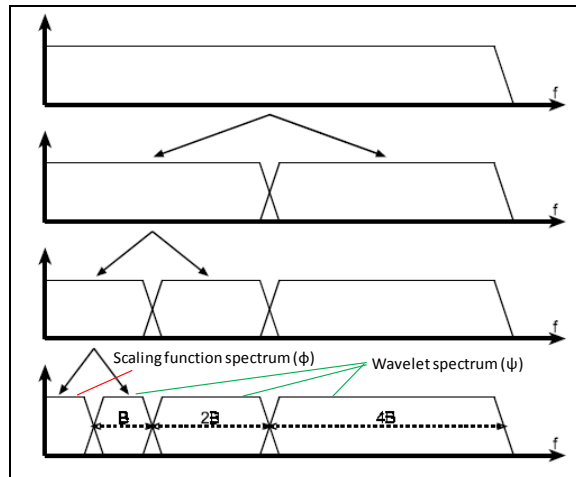


Figure 2.18: Splitting the signal spectrum with an iterated filter bank (Valens, 1999)

2.5.3.3 Wavelet Packet Transform (WPT)

In DWT, signal is further decomposed in the low pass result (approximation coefficient) only. No further analysis is performed on the high pass results, which is the detailed coefficients. Therefore, DWT is not suitable for analyzing signal with high

frequency band (Wu and Liu, 2009), or in applications where detailed features of every frequency band are needed such as in signal compression. Wavelet packet transform (WPT) is introduced to address the limitations of DWT.

The working principle of WPT is similar to DWT. However, instead of further analyzing the approximation coefficients, both the detailed and approximation coefficients are further analyzed in WPT. The wavelet packet function is similar to DWT, with additional index n as the modulation parameter or the oscillation parameter (Yen and Lin, 2000), as shown in Equation 2.22,

$$W_{j,k}^n(t) = 2^{j/2} W^n(2^j t - k) \quad (2.22)$$

where j and k represent scale factor and translation parameter respectively. To initiate the decomposition, the scaling function $\phi(t)$ and the mother wavelet $\psi(t)$ are utilized, as shown in Equation 2.23 and 2.24.

$$W_{0,0}^0(t) = \phi(t) \quad (2.23)$$

$$W_{0,0}^1(t) = \psi(t) \quad (2.24)$$

When $n = 2, 3, \dots$, further decomposition is achieved by using the recursive relationships shown in Equation 2.25 and 2.26,

$$W_{0,0}^{2n}(t) = \sqrt{2} \sum_k h(k) W_{1,k}^n(2t - k) \quad (2.25)$$

$$W_{0,0}^{2n+1}(t) = \sqrt{2} \sum_k g(k) W_{1,k}^n(2t - k) \quad (2.26)$$

where $h(k)$ and $g(k)$ are the quadrature mirror filter (QMF) associated with the predefined scaling function and mother wavelet function. Eventually, the wavelet packet coefficient, $w_{j,k}^n$ is computed as in Equation 2.27.

$$w_{j,k}^n = \langle f(t), W_{j,k}^n \rangle = \int f(t) W_{j,k}^n(t) dt \quad (2.27)$$

Indeed, the wavelet packet coefficient is a measure of how closely related the signal is to certain frequency range, determined by the scale factor, j , at certain time instant $2^j t$, shifted by translation parameter k . The concept of WPT is shown in Figure 2.19.

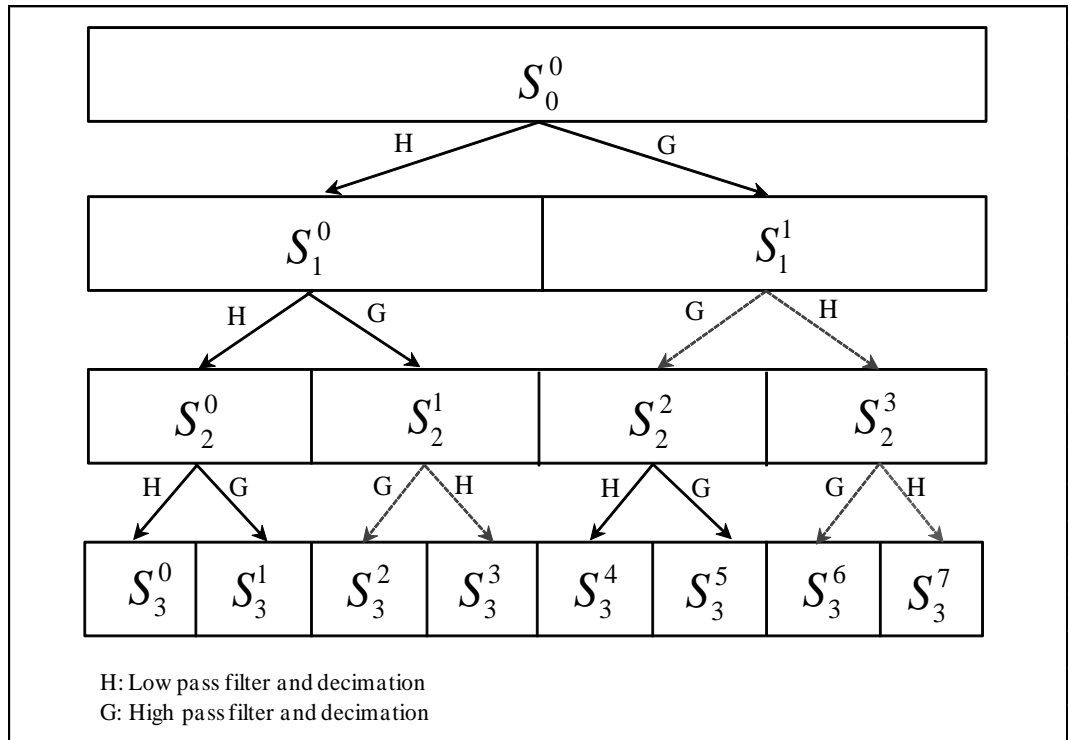


Figure 2.19: WPT under three level decomposition (Yen and Lin, 2000)

The dashed lines indicate swapping between subspaces after high pass filter, to overcome the effect of aliasing which exchanges frequency ordering of subspaces. Thus, subspaces in Figure 2.19 are displayed in increasing frequency order, which are also referred as the Paley ordering (Wickerhauser, 1994). In Figure 2.19, the original

signal S_0^0 is decomposed into three resolution levels. S_3^0 represents the first subspace at third resolution level. In the present study, the AE and vibration signals are decomposed into four resolution levels, producing a total of 16 subspaces. The frequency intervals of each subspace can be computed as in Equation 2.28, where m denotes the subspace number, j denotes the resolution level and f_s denotes the sampling rate (Hu et al., 2005).

$$\left[(m-1)2^{-j-1}f_s, m2^{-j-1}f_s \right] \quad (2.28)$$

For instance, in the present study, $f_s = 102.4$ kHz, the frequency interval of the original signal S_0^0 is (0, 51200]. Similarly, the frequency interval of the third subspace of fourth level S_4^2 is (6400, 9600].

2.5.4 Review of different time-frequency analysis in condition monitoring

Conventionally, Fourier transform (FT) is most widely used for spectral analysis of signals in fault diagnosis of machinery. As Fourier analysis is confined to stationary signals, the time-frequency analysis techniques are introduced for the analysis of transient signals. The Short Time Fourier transform (STFT), Wigner-Ville distribution (WVD), continuous wavelet transform (CWT), discrete wavelet transform (DWT) and wavelet packet transform (WPT) are examples of time-frequency analysis technique. Table 2.5 displayed some of the reviews regarding time-frequency analysis technique in condition monitoring. It can be seen that the aforementioned techniques were applied in monitoring of machine components such as pump, bearing, gear, internal combustion engine and valve of compressors. Besides, the wavelet transform was found useful in monitoring the propagation of crack width of structure (Gabbanini et al., 2004). In fact, these time-frequency analysis techniques can be a reliable tool in processing

contaminated and weak signals. This is proven by the implementation of discrete wavelet transform (DWT) in de-noising and extraction of electromyography (EMG) signals from the human muscle (Phinyomark et al., 2011).

Table 2.5: Some reviews of time-frequency analysis technique in condition monitoring

Components	Measurement Technique	References	Time-frequency analysis	Remarks
Reactor coolant pump	Vibration	Koo and Kim (2000)	FT, WVD	Monitor abnormalities and extract features for neural network
Bearing	Motor stator current	Zarei and Poshtan (2007)	WPT	Incipient bearing failure detection
Gear	Vibration and acoustics	Baydar and Ball (2003)	CWT	Early detection of gear failures
Gear	Vibration and acoustics	Baydar and Ball (2001)	SPWVD	Early detection of failures and its propagation
Gear and bearing	Vibration	Lin and Qu (2000)	CWT	To denoise signal and increase signal-to-noise ratio
Gear and bearing of model driveline	Vibration	Paya and Esat (1997)	Wavelet Transform (WT)	WT as a preprocessor of signal before neural network
Gear and bearing of model driveline	Vibration	Rafiee et al. (2010)	CWT	Proposed selection of best mother wavelet through similarity of shape between mother wavelet and vibration signal. CWT was utilised to extract features of bearing and gear problems.
Valve of reciprocating compressor	Vibration	Lin et al. (2009)	STFT, SPWVD, RSPWVD	To obtain time-frequency characteristics for fault classification
Valve of reciprocating compressor	Pressure and temperature	Ramesh (2007)	WPT	To extract features for fault classification
Valve of reciprocating compressor	Vibration and acoustics	Elhaj et al. (2001)	CWT	Leakage detection of compressor valves
Compressor	Vibration	Yang et al. (2004)	DWT	Quality examination in production line of compressors
Washing machine	Laser vibration velocity	Goumas et al. (2002)	DWT	Employed DWT for feature extraction
Structure	Displacement	Gabbanini et al. (2004)	WPT	Crack width monitoring on dome of cathedral.
Internal combustion engine	Acoustics/ Sound	Wu and Liu (2009)	WPT	WPT as signal processing technique for feature extraction of fault condition before neural network
Human body	Electromyography (EMG)	Phinyomark et al. (2011)	DWT	To denoise signal and extract useful information

There are always strengths and weaknesses for a particular time-frequency analysis technique. Thus, it is necessary to compare the performance of each time-frequency analysis technique and select the most suitable technique for the study. Table 2.6 shows the details of WVD, STFT, CWT, DWT, and WPT in increasing order of speed. As STFT can only be limited to a fixed time or frequency resolution, it is not flexible in analyzing non-stationary signals. Indeed, STFT is more suitable in the analysis of quasistationary signals (Peng and Chu, 2004). Meanwhile, WVD is better in analyzing time varying signal as it is good in its time and frequency resolution. Nevertheless, WVD suffers from severe interference terms due to the overlapping of different components of signals. Although the performance of WVD can be improved through smoothed pseudo Wigner-Ville distribution (SPWVD) and reassigned smoothed pseudo WVD (RSPWVD), these techniques require much computational time compared to the other techniques.

Table 2.6: Comparison of the performances of different time-frequency analysis

Methods	Resolution	Interference term	Speed
FT	Frequency resolution only	No	Fast
WVD	Good time and frequency resolution	Severe interference terms	Slower than STFT
STFT	Dependent on windowing function, good time or frequency resolution	No	Slower than CWT
CWT	Good frequency resolution and low time resolution for low-frequency components; low frequency resolution and good time resolution for high-frequency components	No	Slower than DWT
DWT	Good time and frequency resolution in lower frequency band	No	Faster than CWT
WPT	Good time and frequency resolution in lower and higher frequency band	No	Faster than CWT

Therefore, the wavelet transform (WT) is a preferable time-frequency analysis technique for the current study as it is more flexible than STFT and performs faster than SPWVD and RSPWVD. Though CWT can give thorough time-frequency analysis, its redundancy problem due to overlapping may lead to the smearing of spectra features (Yang, 2004), in addition to the long computational time required compared to DWT and WPT. In fact, discretized wavelet transform such as DWT and WPT are employed widely in condition monitoring as the discretized features extracted can combine easily with other artificial intelligence techniques for automated fault classification. Since WPT can provide good time and frequency resolution in both lower and higher frequency band as displayed in Table 2.6, it is chosen over DWT for the current study.

2.6 Artificial Intelligence (AI) techniques in fault identification

The time-frequency analysis technique enables extraction of signal features for machine monitoring. These features are usually monitored by the plant personnel with broad knowledge and experiences. With the advance of computational technology, it is now feasible for the implementation of artificial intelligence (AI) techniques in fault identification. Indeed, the demand for automated fault identification is growing as it provides a fast and reliable diagnosis due to removal of human subjectivity and reduction of interpretation time during the diagnostic process.

It is always desirable for the plant personnel to monitor the machine without any prior knowledge regarding the operating condition and working principle of the machine. Therefore supervised learning techniques such as the neural networks (NN) and support vector machine (SVM) are preferable for fault identification. Both techniques are based on the concept of learning from examples. They involve training a

set of samples and producing a target function which predicts the output correctly for any input inserted into the learning algorithm. Absolutely, it is important for the learning algorithm to have good generalization ability to avoid over-fitting or under-fitting problem. Over-fitting problem occurs when the learning algorithm fails to generalize the problem by memorizing the training data and exaggerating minor variation of data. Meanwhile, the failure of algorithm in learning pattern of the training data will lead to the under-fitting problem. Both problems are not desirable in NN and SVM.

NN is inspired by the biological learning process of the human brain (Anderson, 1972). The development of NN follows a heuristic approach where extensive experimentation comes before proper theory development. The objective of NN is to obtain a set of coefficient values (weight) which minimize the training error. This is termed empirical risk minimization (ERM). In contrast, the SVM starts from a sound theory and enters into implementation gradually. It is developed from the principle of structural risk minimization (ERM), which controls the capacity of algorithm by maximizing the margin between the two classes being classified. Burges (1998) stated that the capacity is the ability of the learning algorithm to learn any training set without error. Large capacity will result in the over-fitting problem while small capacity will lead to the under-fitting problem. He highlighted that the right balance between training error and capacity is the key towards best generalization performance.

As the learning algorithm of NN is developed based on the principle of minimizing the training errors, it requires large number of samples to reduce the errors. On the other hand, only a small number of samples are required by SVM to achieve good classification performance as the learning algorithm minimizes the upper bound of expected risk which controls the capacity while simultaneously minimizing the training

errors. Therefore, SVM is a favourable machine learning technique in the fault diagnosis of valves of reciprocating compressors as it is not practical to collect adequate samples in every failure modes (Ren et al., 2005 ; Cui et al., 2009; Chen and Lian, 2010; Qin et al., 2012). More importantly, unlike conventional NN which suffers from local minimum, SVM attempts to obtain global minimum of the problem. Thus the generalization ability of SVM is always higher than conventional NN.

In condition monitoring, robustness of the learning algorithm towards large number of features is always one of the sought-after properties. This property ensures little limitation on the number of features inputted into the algorithm and thus causing the algorithm to be more practical and efficient in fault diagnostics. Conventional NN often suffers from the curse of dimensionality, where the amount of training data needed increases exponentially with the number of features/dimension. Thus, pre-processing of input data is often needed in NN to reduce the dimensional space and training data required for a complex problem, with the aim of reducing long computational time and avoiding over-fitting problem. On the contrary, SVM can accommodate larger feature space as it involves separating the two classes through a linear function. In the case of non-linearly separable data, the linear classification can be achieved by transforming data from the original space into higher dimensional space through kernel functions which satisfy Mercer's condition. In fact, Ahmed et al. (2011) stated that SVM performed better than NN in the time domain for larger number of features, where multiple fault conditions are inputted into the algorithm for classification. Details of the kernel function will be further discussed in Chapter 5.

A number of comparisons between NN and SVM were conducted in various fields such as in the biomedical science for eye events classification from electroencephalographic (EEG) signal (Singla et al., 2011) and in the chemical industry

for drug classification (Byvatov et al., 2003). The former found that overall performance of SVM is better than feed forward back propagation neural network while the later concluded that SVM classifier is more robust with smaller error compared to standard NN. In fault diagnostics, Yang et al. (2005) employed NN and SVM in the classification of small reciprocating compressors in the production line. He later concluded that SVM and learning vector quantisation (LVQ) are the best techniques in small compressor fault classification. Besides, Tyagi (2008) compared the effectiveness of NN and SVM in the diagnosis of rolling element bearing. He commented that SVM performed better than NN in most cases and proposed the possibility of SVM in on-line monitoring due to fast training time of the classifier. This is further supported by Saravanan et al. (2010) who highlighted that NN has longer training and classifying time compared to SVM in the monitoring of spur bevel gearbox. More reviews regarding the implementation of SVM in the monitoring of pumps, induction motors, engine, machine tools and the list goes on can be found in Widodo and Yang (2007). With regard to the advantages of SVM discussed above, it is chosen as the machine learning technique for automated fault classification in the diagnosis of valve failure.

2.7 Summary

Past researches showed the potential of AE technique as a promising tool in condition monitoring. This technique can serve as a complementary tool to vibration technique as it is sensitive to both mechanical and fluid motion. Moreover, various studies revealed that AE technique is superior in providing earlier fault detection of rotating machinery components. Since this study requires inspection of valve dynamics and fluid flow within the cylinder, AE technique appears to be a suitable measurement technique for valve failure detection. Nevertheless, due to the broad frequency range

and omnidirectional property of AE sensor, AE signal requires advanced signal processing technique to ascertain signal at different time and frequency domain. This chapter compares different time-frequency analysis method namely FT, STFT, CWT, DWT, and WPT and justifies the reason of selecting WPT as the post-processing method for AE signal. Features computed from WPT decomposed AE signal will serve as the input vectors for automated classification. The last section of this chapter compares 2 artificial intelligence (AI) techniques in fault identification and highlights that SVM is more suitable for automated signal classification in this study due to its small sample size requirement.

The next chapter proposes methodology of the study, starting from data acquisition, parameter selection, and signal analysis to fault classification. Features of valve under different condition will be examined through combination of WPT and statistical analysis. This is followed by classifying the features into its corresponding valve conditions through SVM technique.

CHAPTER 3 METHODOLOGY

3.1 Overview

This chapter presents instrumentation and work flow of the study. First of all, raw AE and vibration signals will be obtained from experimental test bed simulated with different valve problems. These signals will be processed through a synchronous time averaging algorithm with the purpose of reducing noise which is non-synchronous with the piston movement before they are saved for further analysis. The saved signals will be post-processed by passing the signal through a WPT algorithm to decompose signals into 16 frequency ranges. To enable extraction of features corresponding to different valve movements, signals in each frequency ranges will be further segregated to 4 time segments, resulting in 64 time frequency segments. Different parameters will be computed next from the WPT decomposed signals in these time frequency segments. Finally, parameter best indicating valve conditions will be selected as the best parameter for signal analysis and signal classification. Figure 3.1 displays entire flow chart of the study.

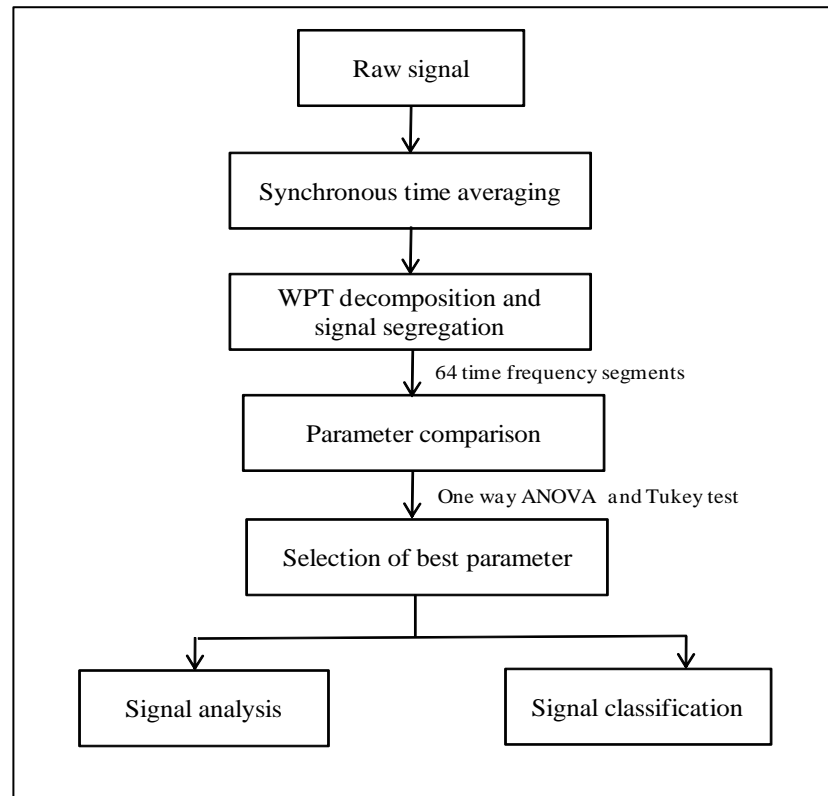


Figure 3.1: Entire flow chart of the study

3.2 Experiment set-up

3.2.1 Test bed setup

Figure 3.2 shows experimental test rig of the current study which consists of a single stage, 2 cylinder and air cooled reciprocating compressor. The AE sensor and accelerometer are mounted on the suction valve cover, as shown in Figure 3.2 (a). A laser tachometer is incorporated into the data acquisition system to trigger the acquisition of AE and vibration signal whenever it receives a pulse from the reflective tape attached on the flywheel, as displayed in Figure 3.2 (b). Details on the specifications of the test compressor can be seen in Table 3.1.

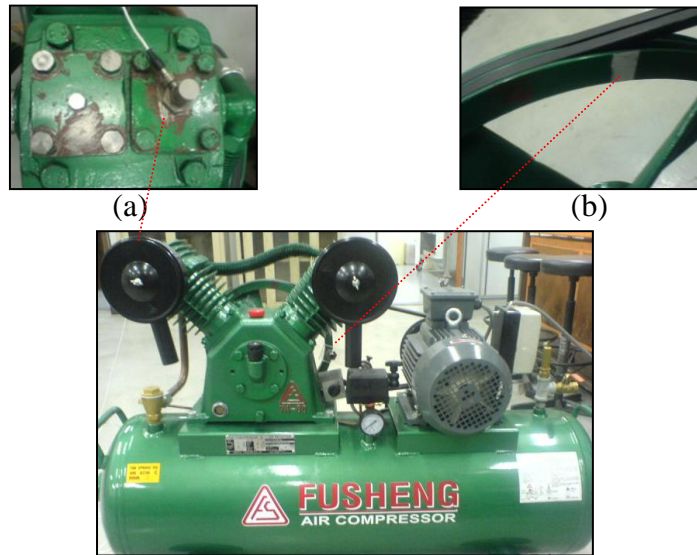


Figure 3.2: Test compressor for valve failure simulation
(a) Accelerometer mounted on the valve cover. (b) Reflective tape for tachometer.

Table 3.1: Specifications of test compressor

Model	VA-80
Motor power	2.2 kW
Cylinder number	2
Cylinder bore (mm)	80
Cylinder stroke (mm)	60
Rotational speed (rpm)	800
Piston displacement	462 L/ min (16.32 CFM)
Actual air delivery (at 7 kg/cm²G or 100 PSIG)	346.5 L/min (12.24 CFM)
Working pressure	7 kg/cm ² G
Air receiver dimension	ϕ 350x1160 mm
Air receiver capacity	105 L
Net weight	145 kg

The experiment had been conducted when the compressor was running under the free load condition, by simulating three suction valve conditions at two compressor speed of 450 and 800 rpm. Figure 3.3 shows the suction and discharge valve and its mounting location in the cylinder of the test compressor.

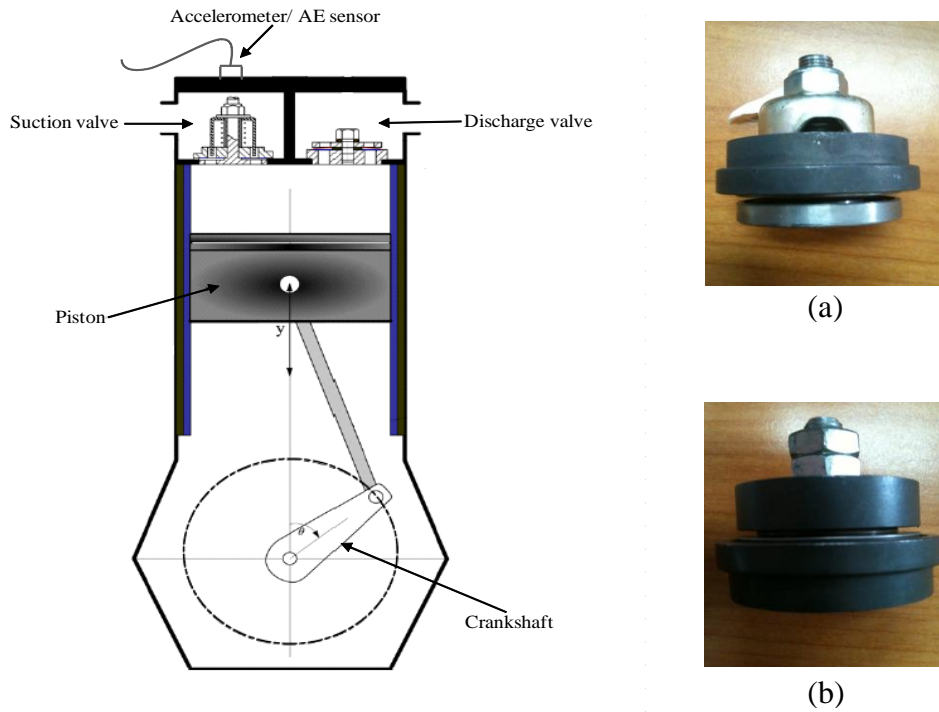


Figure 3.3: Structural diagram of cylinder indicating location of (a) Suction valve (b) Discharge valve

Three valve conditions namely the normal, grease and leakage condition had been simulated for the current study. The greased condition of the suction valve had been simulated by applying a layer of grease onto the valve plate to emulate the condition of valve stickiness due to excessive oil distribution. On the other hand, the leakage condition had been simulated by grinding a small passage of 3 mm width on the valve plate to emulate the condition of valve degradation. Physical condition of the valve plate is displayed in Figure 3.4.

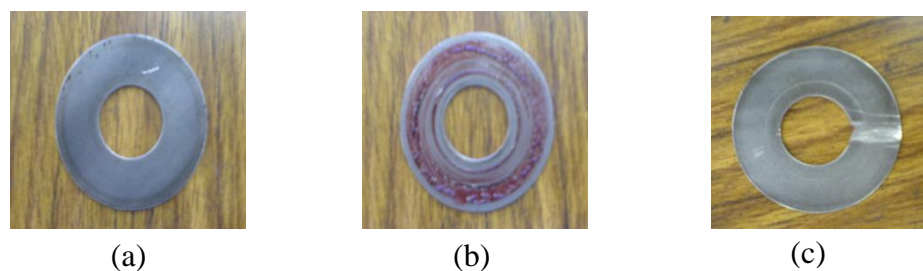


Figure 3.4: Physical condition of valve plate (a) Normal (b) Grease (c) Leakage

3.2.2 Instrumentation

The acquisition process of AE and vibration signals is displayed in Figure 3.5. Firstly, the AE signal is acquired by the AE sensor while the vibration signal is obtained through the uniaxial Integrated Electronic Piezoelectric (IEPE) accelerometer. Both sensors are connected to the data acquisition device (DAQ) NI USB 4431 for signal conditioning before the signals are saved and displayed by the in-house developed LabVIEW software installed in a laptop. The acquisition of both signals commences whenever the DAQ receives a reference signal from a laser tachometer. Each reference signal sent corresponded to the position of piston at the top dead centre (TDC). Thus, both signals can be acquired for one period of time with regard to its piston position. Details of the equipments utilized during the data acquisition process are shown in Table 3.2.

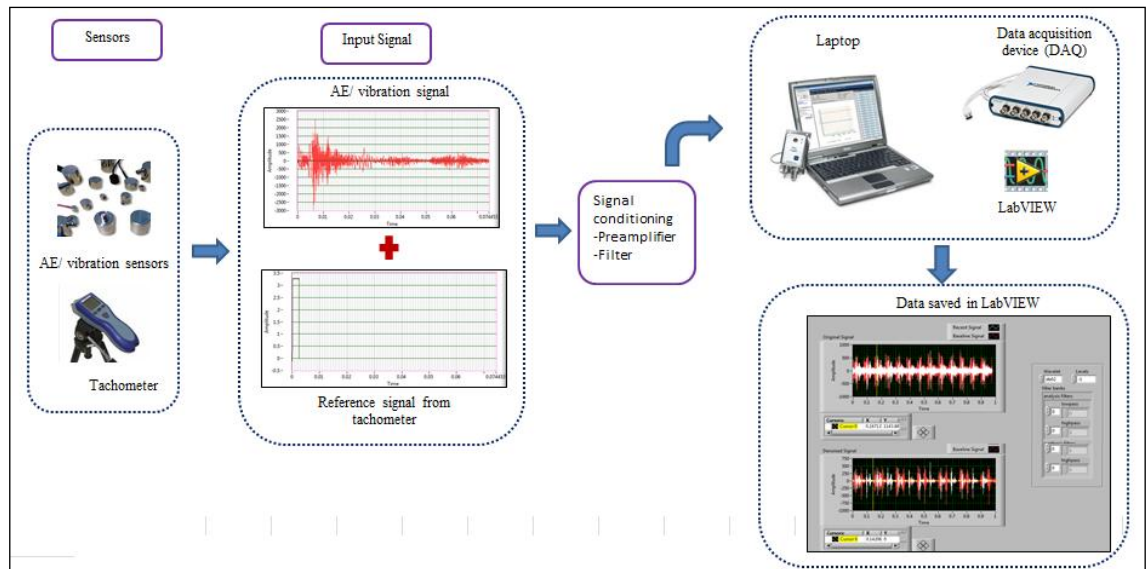






Figure 3.5: A schematic diagram of data acquisition system

Table 3.2: List of equipments

Equipment	Description
AE sensor and preamplifier 	<p>Operating specifications:</p> <p>Physical: Dimensions: 35(H) x 60(W) x 65(L) mm Weight: 270g</p> <p>Performance: Frequency range: 100-450 kHz Resonant frequency: 150 kHz Temperature range: -50-100 °C Capacity: 350pF Peak sensitivity: -63 dB re 1V/ μ bar</p> <p>Electrical: Pre-amplifier gain: 34dB Power supply: 28V_{DC} Output connector: BNC Magnet hold-down force: 3 x 60N Sensor hold-down force: 10N (spring loaded)</p>
Accelerometer PCB C320 	<p>Operating specifications:</p> <p>Physical: Dimensions: 20.6(Height)x12.7(Hex) mm Weight: 10.5g</p> <p>Performance: Frequency range: 1-6 kHz Resonant frequency: ≥ 35 kHz Temperature range: -73-163 °C Sensitivity: 1.02 mV/ms⁻²</p> <p>Electrical: Excitation voltage: 18-30 V_{DC} Constant current excitation: 2-20mA Electrical connector: 10-32 Coaxial Jack Mounting Torque: 113-225 Ncm</p>
Data acquisition device NI 4431 	<p>Operating specifications:</p> <p>Physical: Dimensions: 142x180x38 mm Weight: 675g Analog input channels: 4 Analog output channels: 1 Connection: BNC</p> <p>Analog input: Sampling rate: 1-102.4 kS/s Input range: $\pm 10V_{pk}$</p>

	<p>ADC resolution: 24 bits Input coupling: AC or DC (software selectable) IEPE current excitation: 0 or 2.1mA (software selectable)</p> <p>Analog Output: Frequency range: DC to 43.5 kHz DAC resolution: 24 bits Output signal range: $\pm 3.5 V_{pk}$ Output coupling: DC Operating temperature: -30-70°C</p>
<p>Laser tachometer PLT 200</p> 	<p>Operating specifications:</p> <p>Physical: Dimensions: 17.58(H) x 6.10(W) x 4.06(D) cm Weight: 210g</p> <p>Performance: Display: 5 digits, Alphanumeric LCD Range(s): Optical: 5 to 200000 rpm Contact: 0.5 to 20000 rpm Accuracy: Optical: $\pm 0.01\%$ of reading Contact: $\pm 0.05\%$ of reading Resolution: 0.001 to 10 rpm (range dependent) Operating distance: 5cm to 7.62m, $\pm 70^{\circ}\text{C}$ from perpendicular Power: (2) "AA" 1.5 V_{DC} batteries (30 hours) Environmental: 5° to 40°C (40° to 105°F) 80% RH up to 31°C (88°F)</p>

3.3 Synchronous time averaging

Prior to saving the signal, synchronous time averaging with linear weighting had been performed to improve signal-to-noise ratio (S/N) of the signal acquired. By using this method, signals which are synchronous to the TTL pulse from the tachometer will be reinforced while non-synchronous components will be averaged to zero, thus producing a cleaner signal in the time domain (Rahman et al., 2010).

For a time domain signal $x(t)$ with period P and N number of averages, the synchronous average with linear weighting $y(t)$ is computed via Equation 3.1.

$$y(t) = \frac{1}{N} \sum_{r=0}^{N-1} x(t + rP) \quad (3.1)$$

This method helps in reducing unwanted noise effectively. In fact, the signal-to-noise ratio (S/N) is proportional to the square root of number of averages. Thus, a sufficient number of averages are needed to produce the desired result.

The software architecture of data acquisition process is illustrated by Figure 3.6 and Figure 3.7. Figure 3.6 shows the block diagram of configuration setting of sensors in LabVIEW. Specifications of sensors such as the maximum and minimum value, sensitivity value, units, and input terminal configuration had been set in the block diagram. Besides, the sampling rate and sample mode had been configured through the front panel of the software. The laser tachometer had been connected to channel 0 while the AE sensor and accelerometer had been connected to channel 1 and 2 of the DAQ device respectively. The VI started to acquire signal when it received a rising pulse from the tachometer at channel 0. The signal was then transmitted into a “for loop” to perform linear time averaging before it was being saved and displayed. The number of averages for the linear time averaging can be configured by changing the number of iterations in the “for loop”. Figure 3.7 shows the linear time averaging program in LabVIEW.

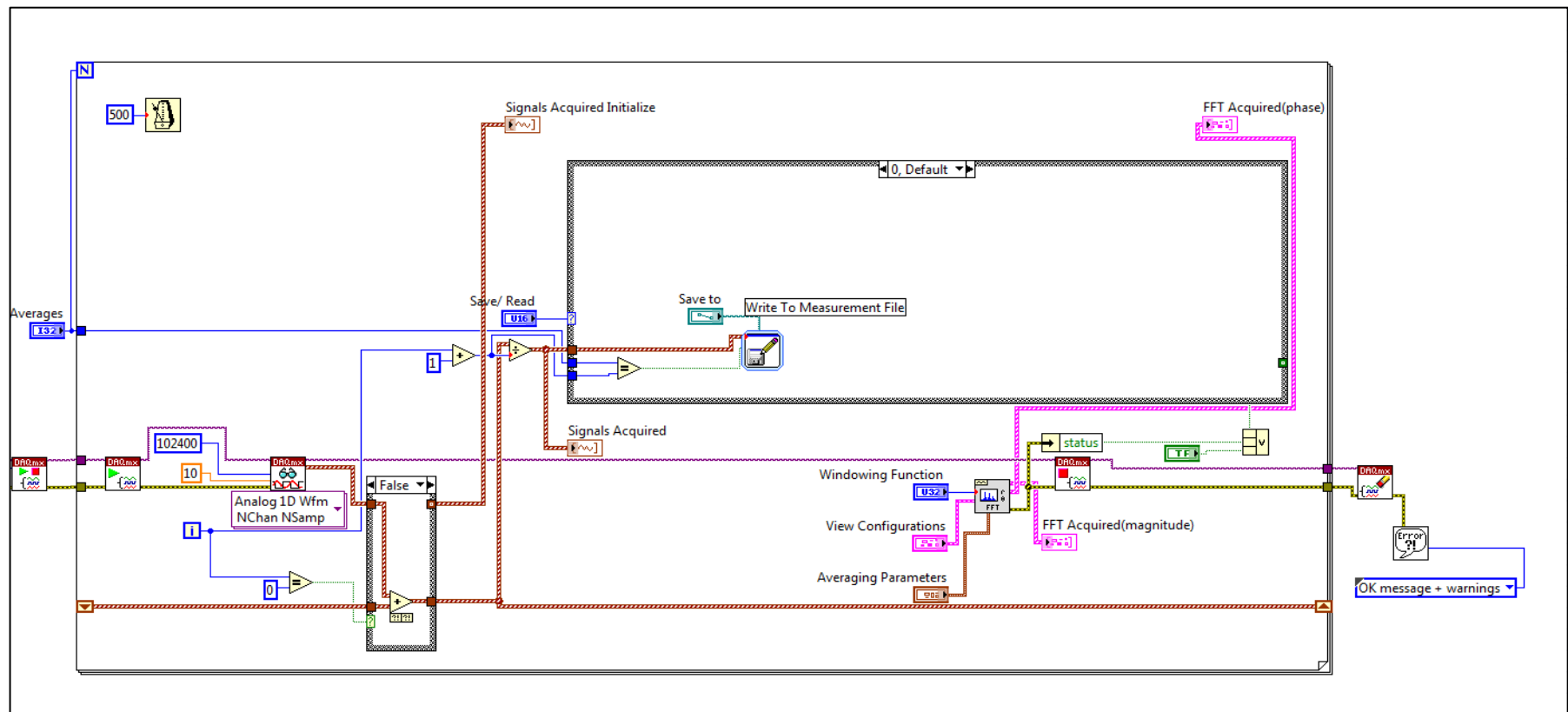


Figure 3.7: Block diagram of linear averaging in LabVIEW

Figure 3.8 shows the comparison of AE signal between different number of averages for a suction valve under normal condition. A crank angle of 0° corresponds to the piston position at the top dead centre (TDC) while a crank angle of 180° corresponds to the piston position at the bottom dead centre (BDC). From Figure 3.8, it can be observed that the transient signal becomes clearer when the number of averages increased from 10, 30, 50, to 100, as parts of the non-synchronous components are averaged out during the averaging process. In this study, all signals acquired are averaged over a number of 50 averages as this number is sufficient enough to remove the background noise.

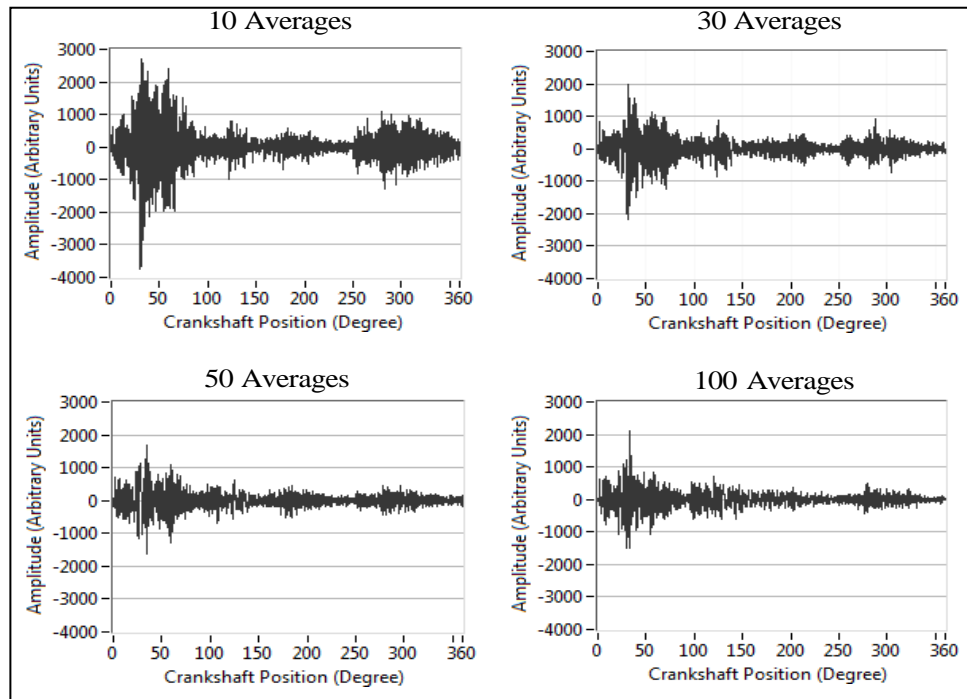


Figure 3.8: Comparison of AE signal between different numbers of averages

3.4 Mother wavelet selection for WPT

Though some non-synchronous background noises can be removed through synchronous time averaging, there is always possibility for synchronous noise to mask

the signals and causes them insensitive to minor changes of valve condition. Therefore, post-processing of AE and vibration signal through wavelet packet transform (WPT) had been proposed to extract the features of the signal under different valve conditions.

The wavelet analysis was performed by shifting the wavelet function across the time domain at different scales. The wavelet function is originated from a mother wavelet. Therefore, selection of mother wavelet is of utmost important as the right mother wavelet will give the best time-frequency representation of the signal analyzed. In fact, selection of mother wavelet is dependent on the characteristics of signal being analyzed.

One property of determining the mother wavelet selection lies on its regularity, which is related to the degree of smoothness of the function. Unser (1999) states that regularity of the scaling function must be smaller than the approximation order L . From Table 3.3, it can be seen that B-spline scaling function has the maximum regularity compared to Daubechies scaling function at a given approximation order L . By comparing the regularity between different wavelets such as Haar, Daubechies, Symlet, Coiflet, and B-spline in Table 3.4, it can be concluded that the B-spline function has the highest regularity; therefore it is more suitable to be the mother wavelet.

Table 3.3: Hölder exponent $\alpha(L)$ estimates for the Daubechies scaling function $\phi(t)$ of order L and regularity of B-spline scaling function of the same order L (Daubechies, 1992)

L	2	3	4	5	6	7	8	9	10
Db L regularity: $\alpha(L)$	0.500	0.92	1.28	1.60	1.89	2.16	2.42	2.66	2.90
B-spline (L, \tilde{L}) : $L-2$	0	1	2	3	4	5	6	7	8

As this study is focused on detecting abnormalities such as sudden changes in a signal, scaling function with small finite support is desirable. From Table 3.4, it can be observed that the B-spline scaling function has the smallest support size compared to the others. Additionally, unlike the Daubechies, Symlet, and Coiflet function which are generated implicitly from an iterative filter bank, the B-spline scaling function can be expressed explicitly, thus enabling faster computation of the wavelet analysis.

Table 3.4: Summary of properties of commonly used finite support wavelets (Ahuja et al., 2005)

Name	Haar(B-spline 1)	Daub L	Symlet L	Coiflet L	B-spline L, \tilde{L}
Explicit expression	yes	no	no	no	yes
$\phi(x)$ support	1	$2L-1$	$2L-1$	$3L-1$	L
$\psi(x)$ support	1	$2L-1$	$2L-1$	$3L-1$	$L+\tilde{L}-1$
Frequency decay	$1/ \omega $	$1/ \omega ^{\alpha(L)}$	N/A	N/A	$L-2$
Regularity	not regular	$\approx 0.2L$	N/A	N/A	$L-2$
Vanishing moments	1	L	L	L	\tilde{L}
Orthogonal/biorthogonal	orth	orth	orth	orth	biorth
Time-bandwidth product	∞	asyp. ∞	asyp. ∞	asyp. ∞	approaches $1/4$ as $L \rightarrow \infty$
Linear phase	yes	no	no	no	yes

¹N/A= not available but similar to that of the Daubechies wavelet

² L = order of the wavelet, which is the number of zeros at $z=-1$ in the filter $G(z)$ corresponding to the scaling function; specifically, in the B-spline case, the box function is denoted as the first order B-spline

³Asyp ∞ indicates that the time-bandwidth product approaches ∞ as $L \rightarrow \infty$

⁴ $\alpha(L)$ is the Hölder exponent given in Table 3.3

As discussed previously in the prior chapter, the linear phase (symmetry) property of a scaling function is more desirable as it enables filter designed to retain the phase information without distortion. However, most of the orthogonal scaling functions such as the Daubechies, Symlet and Coiflet functions are not symmetric as the orthogonality and linearity of finitely supported functions are mutually exclusive. Therefore, biorthogonal scaling functions such as the B-spline functions are introduced to achieve its linearity by sacrificing its orthogonality in its primal space. Hence, the biorthogonal scaling functions are more suitable in the wavelet analysis.

It is known from the Heisenberg uncertainty principle that good time resolution and good frequency resolution cannot be achieved simultaneously. In selecting mother wavelet, it is desirable to select the wavelet functions with the lowest time-bandwidth product. From Table 3.4, it can be observed that the time-bandwidth product of most wavelet functions approaches infinity when the order of wavelet, L approaches infinity, except the B-spline wavelet. The B-spline wavelet approaches $\frac{1}{4}$ as L approaches infinity, indicating the good time-frequency localization of the function.

Due to the high regularity, small finite support, good linearity, and good time-frequency localization of the B-spline function, the biorthogonal function was chosen as the mother wavelet for signal analysis.

3.5 Signal segregation

In the current study, 40 samples of AE and vibration signals had been acquired under the normal, grease and leakage conditions at the speed of 450 and 800 rpm. They were further decomposed into 16 smaller frequency ranges by using the wavelet packet

transform (WPT) algorithm with a B-spline mother wavelet function and fourth level of resolution in MATLAB.

To correlate the signal with the major valve events in each frequency range, signals after WPT were further segregated into 4 time segments, with the first, second, third, and fourth time segments corresponded to a crankshaft movement of approximately 0° - 18.8° , 18.8° - 131.4° , 131.4° - 244° , and 244° - 360° respectively. The valve failure can then be identified by comparing the parameters in Section 3.6 for each time segments under different frequency ranges and valve conditions by using statistical method. Equation 3.2 expressed the parameter Z , where w_i denotes the parameter in Section 3.6, and u and t shows the beginning and ending time of a particular time segment.

$$Z = \sum_{i=u}^t w_i \quad (3.2)$$

The concept of signal segregation is further illustrated in Figure 3.9 for a third level WPT decomposition. In fact, for the current study, the raw AE/ vibration signals acquired had been segregated into 64 time frequency segments. Different parameters were computed and compared between these time frequency segments. These parameters will be introduced in the next section.

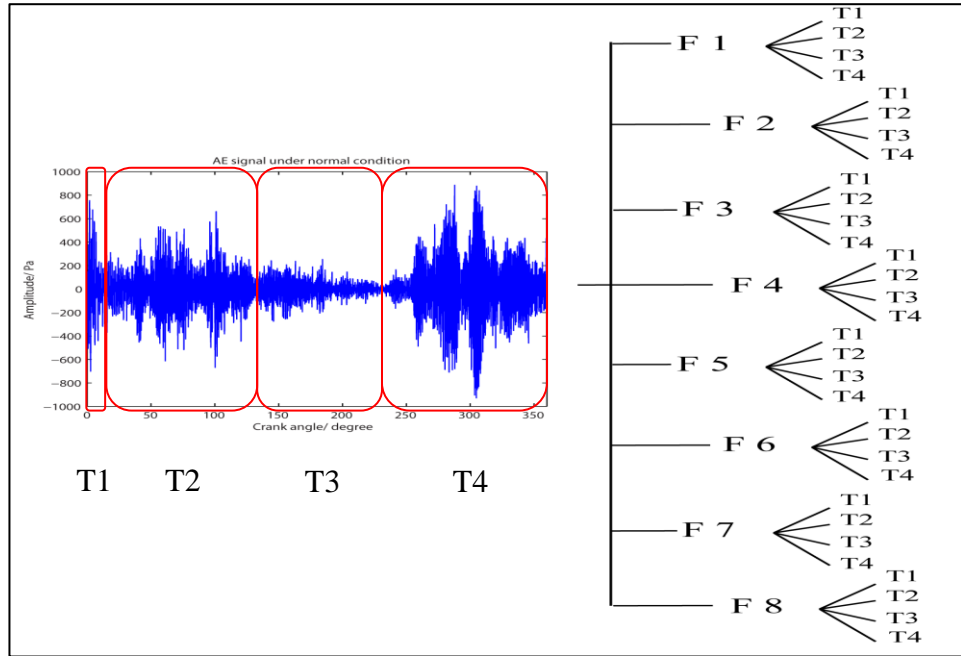


Figure 3.9: Segregation of signal at different time segments and frequency ranges

3.6 Parameter Comparison

Previous research had been conducted on comparing the AE and vibration signals visually under normal and abnormal condition (Gill et al., 1998). However, visual inspection is not a good method in examining the health condition of valve as most of the judgments are bound to be subjective. Therefore, a few statistical parameters such as the root-mean-square (RMS) value, crest factor, skewness, kurtosis, and normalized energy were studied to analyze contributing parameter to the valve condition.

3.6.1 Root-mean-square (RMS)

The root-mean-square (RMS) value, m of a time signal x_i is derived mathematically as in Equation 3.3,

$$m = \sqrt{\frac{1}{n} \sum_{i=0}^{n-1} x_i^2} \quad (3.3)$$

where n is the total number of samples within the time series. It measures the magnitude of the time signal.

3.6.2 Crest factor

The crest factor is the ratio of peak, A to the average of the signal, μ . It is computed as in Equation 3.4,

$$C = \frac{A}{\mu} \quad (3.4)$$

$$\mu = \frac{1}{n} \sum_{i=0}^{n-1} x_i \quad (3.5)$$

where μ can be computed from Equation 3.5. It measures the amount of impacts in a signal. This parameter is frequently used in detecting bearing faults (Williams et al., 2001).

3.6.3 Skewness

Skewness S is a measure of the degree of asymmetry of a signal about its mean. Generally, a symmetric signal has zero skewness. Meanwhile, a negatively skewed signal has a longer tail to the left of the mean value and a positively skewed signal is represented by a long tail towards the right of the mean value. Skewness is mathematically expressed as Equation 3.6,

$$S = \frac{\frac{1}{n} \sum_{i=0}^{n-1} (x_i - \mu)^3}{\sigma^3} \quad (3.6)$$

$$\sigma = \sqrt{\frac{1}{n} \sum_{i=0}^{n-1} (x_i - \mu)^2} \quad (3.7)$$

where n is the number of samples for a time series x_i , μ is given in Equation 3.5 and the standard deviation σ is computed as in Equation 3.7. This parameter is commonly used in monitoring machinery components such as bearing (Kim et al., 2007) and induction motor (Günel et al, 2009).

3.6.4 Kurtosis

Kurtosis, K is the ratio of fourth moment about the mean to the square of variance. It measures the flattening of a probability function near its mean and shows the contributing portion of the high amplitude signal in time (Sikorska, 2006). It is computed as in Equation 3.8,

$$K = \frac{\frac{1}{n} \sum_{i=0}^{n-1} (x_i - \mu)^4}{\sigma^4} \quad (3.8)$$

where n is the number of samples for a time series x_i , μ is shown in Equation 3.4 and σ is given in Equation 3.7. This parameter is served to differentiate the continuous and the burst signal. The burst or impulsive signal spends lesser time at higher amplitudes and thus producing higher kurtosis value (Sikorska, 2006). On the other hand, continuous signal is generally a Gaussian distribution, and has a kurtosis value of 3. Therefore, a significant increase of kurtosis value from 3 to a higher value could suggest a change from continuous to burst signal.

3.6.5 Normalized energy

The normalized energy, W of a time signal x_i is shown mathematically in Equation 3.9,

$$W = \frac{\sum_{i=u}^t x_i}{\sum_{i=1}^T x_i} \quad (3.9)$$

where u and t denote the beginning and ending time of a particular time segment, and T denotes period of the signal. This parameter represents the ratio of energy in a particular time segment with regard to its overall energy.

3.7 Summary

This chapter includes experiment test bed, hardware utilized, and signal conditioning process (synchronous time averaging) for acquisition of AE and vibration signals. These signals had been post-processed through WPT decomposition and signal segregation before different parameters were computed from the resulted time frequency segments.

The significant difference of each parameter Z namely the RMS, crest factor, skewness, kurtosis, and normalized energy value between three simulated valve conditions will be investigated through one way analysis of variance (ANOVA) and Tukey test in Chapter 4. By comparing the results of Tukey test, the best parameter representing valve conditions can be selected. This parameter will be further analyzed through one way ANOVA and Tukey test at each time segment and frequency range,

with the aim of retrieving the time frequency segments which can distinguish each valve condition clearly from the parameter. The parameter selection and signal analysis section will be discussed thoroughly in Chapter 4. Meanwhile, the parameter computed can be served as the input feature vector for automated signal classification through a multiclass support vector machine. Comparisons of success rate between each frequency range at different speed will be performed and discussed in Chapter 5.

CHAPTER 4 SIGNAL ANALYSIS

4.1 Overview

The analysis of AE and vibration signal acquired at two different speeds under different valve conditions is presented in this chapter. The first section of the chapter presents visual inspection of AE and vibration signal at its corresponding crank angle. It is followed by methodology involved in the analysis of these signals. Comparison of a few parameters was performed as to obtain the best parameter representing condition of valves. By using the best parameter, time-frequency segments which are significantly different between valve conditions were identified. The results were compared between AE and vibration signals at both speeds. The chapter ends with a case study of an actual reciprocating compressor where the proposed technique was applied to assess the valve condition.

4.2 Visual inspection of signal

4.2.1 Validation of AE and vibration signals with valve motion

To validate the relationship of AE and vibration signals with valve motion, both signals acquired at 450 rpm were compared with the experimental and analytical results of suction and discharge valve displacement obtained from a study conducted by MacLaren and Kerr (1969). Figure 4.1 shows the valve displacement and pressure difference at its corresponding crank angle obtained from a compressor at 400 rpm and pressure ratio 7.7. It can be seen that the suction valve plate achieves its maximum displacement at crank angle approximately 50° and flutters between the valve seat and valve guard before it starts to close at crank angle approximately 170° . Meanwhile, the discharge valve starts to open at crank angle approximately 320° and closes at 360° .

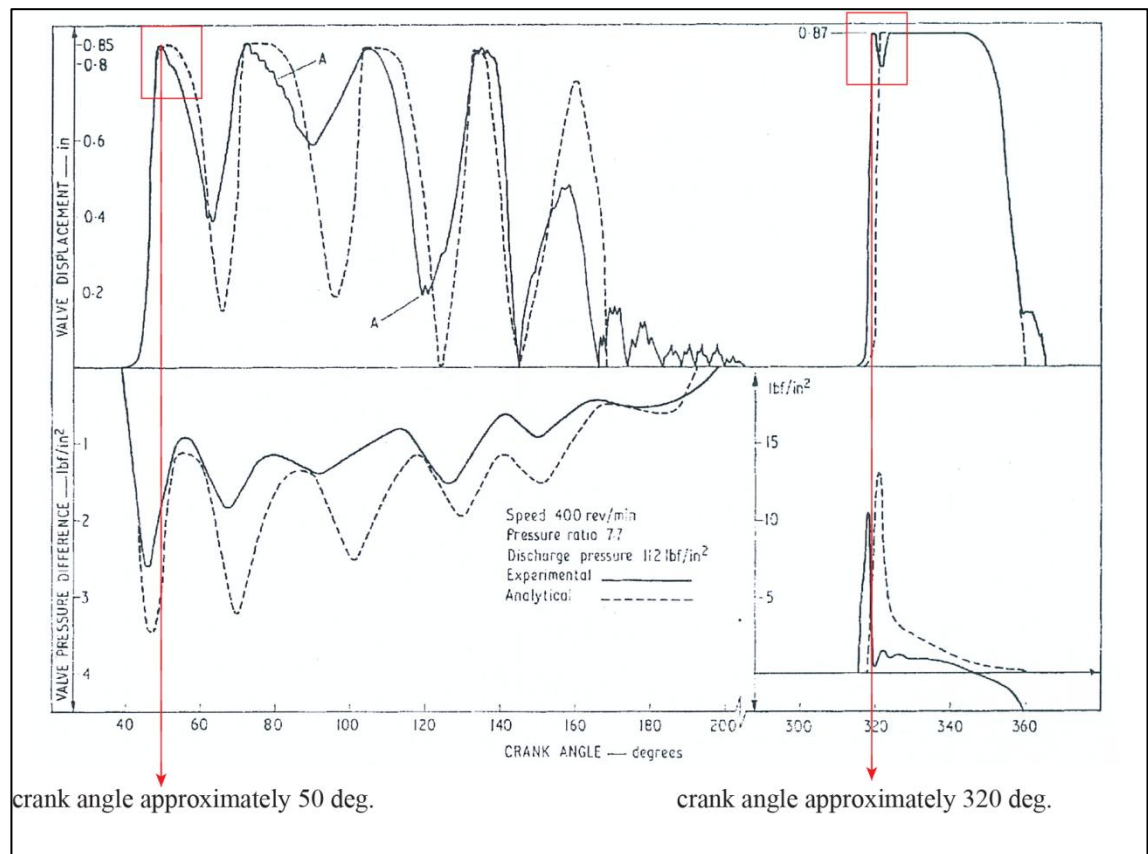


Figure 4.1: Valve displacements and pressure difference at its corresponding crank angle (MacLaren and Kerr, 1969)

As displayed in Figure 4.2, the suction valve in AE and vibration signals started to open at crank angle approximately 60° , which is almost the same as that in Figure 4.1. This finding shows that both signals are good in revealing the valve opening motion. Nevertheless, the discharge valve timing obtained from this study occurred at crack angle approximately 250° - 360° , which is much earlier than the result obtained from MacLaren and Kerr (1969). The earlier discharge valve timing in the current study is attributed to the zero load of test compressor, as opposed the full load of test bed in MacLaren and Kerr (1969), which recorded a pressure ratio of 7.7.

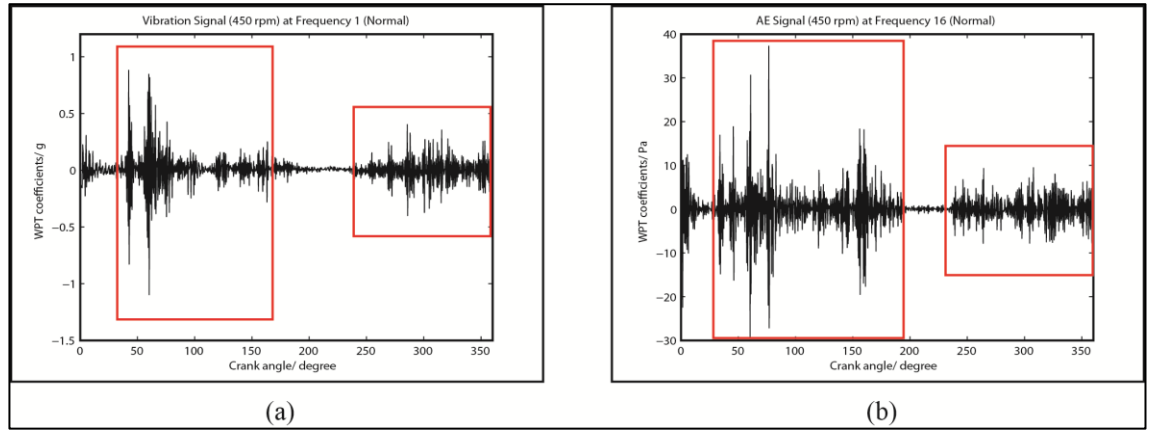


Figure 4.2: Comparison of (a) Vibration (b) AE signal at 450 rpm under normal condition

The validation shows that both AE and vibration signals correlate well with the major valve motion. Further comparisons of both signals at different speeds and valve conditions will be presented in the next section.

4.2.2 Comparison of signals under different valve conditions

The AE and vibration signal acquired at suction valve were compared at low and high speed (450 and 800 rpm) under different valve conditions. Figure 4.3 shows both signals at its corresponding crank angle after WPT decomposition. The valve opening event is displayed by a sudden rise of vibration signal at crank angle approximately 60° under normal valve condition, when the piston was moving from top dead centre (TDC) to bottom dead centre (BDC) as shown in Figure 4.3(d). Nevertheless, the impact of valve opening event cannot be observed from AE signal at low speed (450 rpm) and low frequency range, F1 (0 – 3.2 kHz), as displayed in Figure 4.3(a). Only flow of fluid into cylinder can be observed at the crank angle approximately 100° . However, this valve opening event can be seen clearly at higher speed (800 rpm) as higher speed creates larger pressure differential and thus higher rate of flow of fluid which can be detected easily by AE sensor.

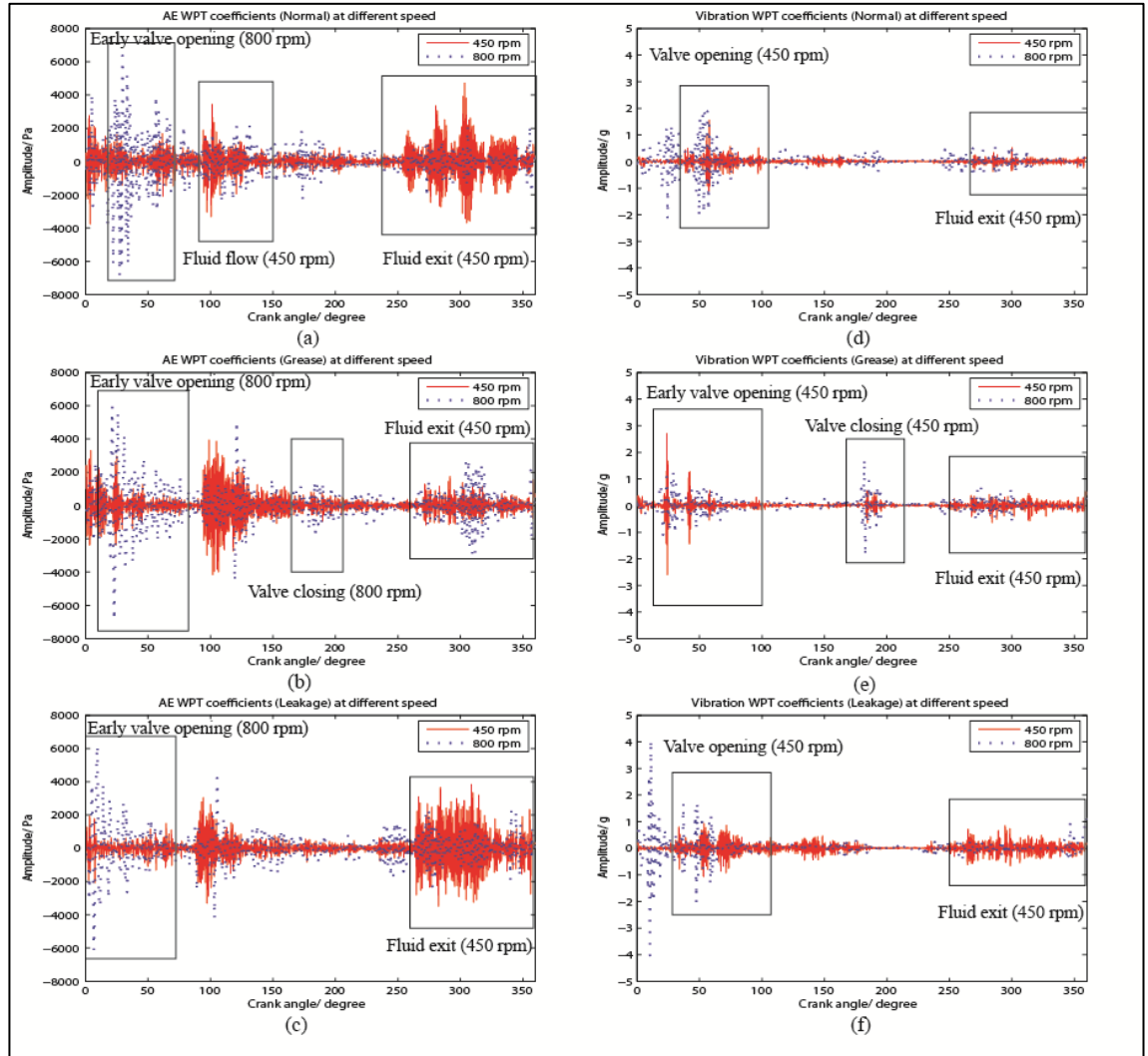
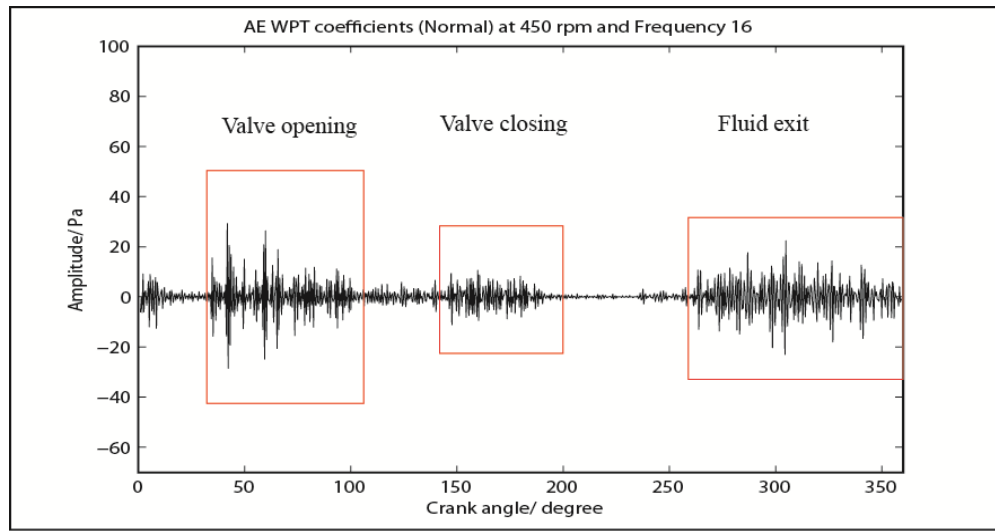


Figure 4.3: AE (a) – (c) and vibration (d) – (f) signal acquired at F1(0 – 3200 Hz) under different conditions and speeds

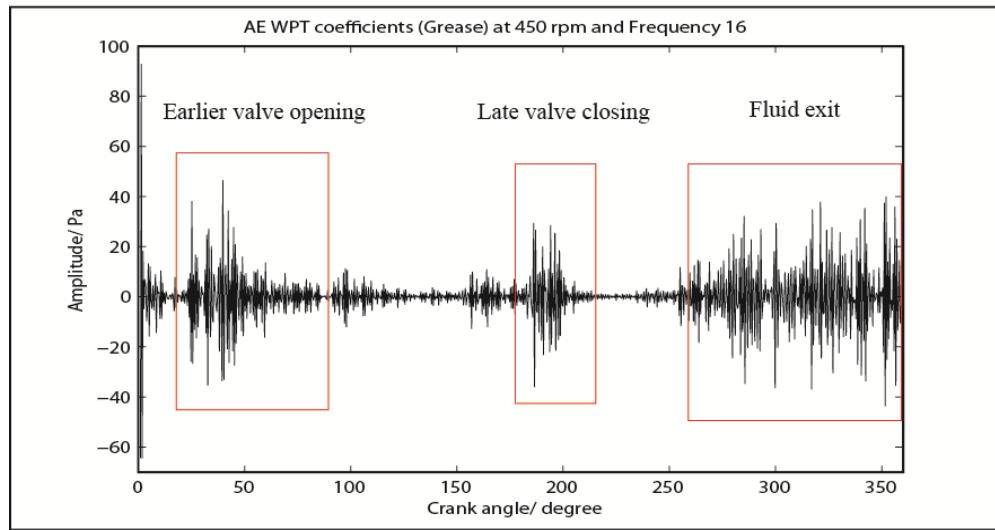
Meanwhile, under normal valve condition, a few transient events can be observed at crank angle 250° - 360° , which is equivalent to the movement of piston from BDC to TDC. Indeed, during the compression cycle, the pressure within cylinder increased when the piston was moving towards the TDC, thereby increasing pressure difference between cylinder and discharge line. When the pressure difference is sufficient to push open discharge valve, fluid from cylinder will exit through discharge valve, as shown in Figure 4.3(a) and (d) from 250° - 360° . However, the flow of fluid

into discharge valve is not obvious in vibration signal if compared to AE signal. It can be deduced that accelerometer is more sensitive in detecting mechanical motion of adjacent structure (localized vibration). As accelerometer was mounted at suction valve cover, it might not be sensitive enough to detect discharge valve opening event. In contrast, AE sensor is good in detecting both mechanical and fluid motion (Gill, et al., 1998). Hence, the flow of fluid into discharge valve can be seen clearly from AE sensor which was mounted at suction valve cover.

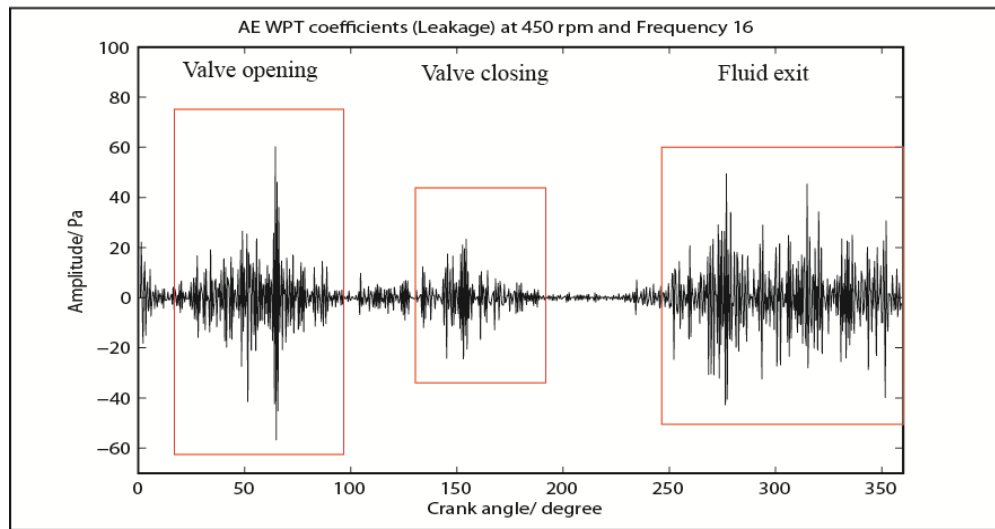
In addition, by comparing Figure 4.3(d) and (e), it can be seen from vibration signal that the valve opening event under grease condition occurred slightly earlier than that under normal condition at 450 rpm, with the valve timing almost the same as the opening event at 800 rpm under normal condition. It can be deduced that the valve stickiness condition causes the suction valve to open partially, thus resulting in earlier valve opening timing as pressure required to open suction valve is significantly smaller compared to the normal condition. However, this observation is not shown clearly from AE signal at 450 rpm and low frequency range, F1 (0-3.2 kHz). Due to the nature of the transducer, the valve opening event is found significant at higher frequency range, F16 (48 – 51.2 kHz). Figure 4.4(b) shows early valve opening impact of AE signal at high frequency range under grease condition.



(a)



(b)



(c)

Figure 4.4: AE signal at 450 rpm and F16 (48 – 51.2 kHz) under (a) Normal (b) Grease (c) Leakage condition

There is a transient event at crank angle approximately 190° from the vibration and AE signal under grease condition, as depicted in Figure 4.3(e) and Figure 4.4(b). This may attribute to valve fluttering motion during valve closing event, which further demonstrates that the suction valve plate was not fully closed under grease condition.

For suction valve under leakage condition, the valve opening event occurred at crank angle much earlier than that under normal condition, but slightly later than that under grease condition, as displayed in Figure 4.3(f) and Figure 4.4(c). Besides, at the compression cycle, the amplitude of AE and vibration signal increases tremendously from crank angle 250° - 360° compared to normal condition, as illustrated in Figure 4.3(c) and (f). It can be deduced that instead of flowing through discharge valve during compression stroke, a portion of fluid had leaked into suction line through suction valve. Therefore, the amplitude of vibration signal rises almost two folds compared to that under normal condition. Similarly, AE signal under leakage condition has higher amplitude compared to that under normal condition, as displayed in Figure 4.4(c) at high frequency range, F16 (48 – 51.2 kHz).

4.2.3 Comparison of signals at different speed

To examine the effect of rotational speed on valve movement, the AE and vibration signals were compared between the low speed and high speed at F1 (0 – 3.2 kHz) under normal, grease and leakage valve conditions. It can be observed from Figure 4.3(a), (c), (d), and (f) that there are shifts in the valve timing under normal and leakage conditions for both AE and vibration signals. The valve opening event at 800 rpm occurred slightly earlier than the opening event at 450 rpm. It can be inferred that higher rotational speed produces larger pressure difference between the suction valve and cylinder, thus enabling the valve plate to open at a smaller crank angle. In contrast,

lower rotational speed results in smaller pressure difference, therefore piston needs to move slightly further such that the pressure difference is sufficient to push open the valve. Hence, the valve opening event at 450 rpm occurred at a crank angle slightly larger than that at 800 rpm.

However, the shift in valve timing at higher speed is not apparent under grease condition especially for the vibration signal, as displayed in Figure 4.3(e). This is because the grease condition had caused the valve timing to shift to a smaller crank angle compared to the normal condition. Thus the increase of rotational speed does not cause significant change to the valve opening timing.

It is obvious that all valve events of AE signal at F1 (0 – 3.2 kHz) is not as distinct as that of vibration signal. In fact, the AE signal shows a lower signal-to-noise ratio at lower frequency range. Gill et al. (1998) suggested that AE signal appeared to have more noise as it depicted a combination of fluid and mechanical events of valve, as opposed to vibration signal which depicted mostly mechanical event. Since the health condition of the valve is hard to be determined through visual inspection of the AE signal, statistical analysis of parameters through one way analysis of variance (ANOVA) is preferred as the later can ease the inspection and improve the valve diagnosis result.

4.3 Methodology for signal analysis

4.3.1 One way analysis of variance (ANOVA)

Different parameters namely RMS, crest factor, skewness, kurtosis, and normalized energy values computed from 2nd resolution level of WPT coefficients of AE and vibration signal were compared between different conditions. Generally, parameter with the most discriminating power between each valve conditions is selected

as the best parameter representing condition of valve. This is normally performed by comparing the mean value of a set of data under one condition to the other. Parameter which shows the greatest difference between each condition will be selected as the best parameter.

By using the best parameter, the state of valve can be identified by comparing the mean value of this parameter with that under different valve failure conditions, after the signal decomposed at 4th level of WPT decomposition. It should be noted that the resolution level of WPT decomposition is doubled when compared to those during parameter comparison to obtain finer time-frequency segment of the signal. Time-frequency segments which show significant difference of mean value between different valve conditions will be selected as the characteristic segments for monitoring.

Nevertheless, the method of obtaining the best parameter and characteristic time-frequency segments by comparing the difference of mean value between each condition often casts doubt as the difference of mean value between each condition might be resulted from variability of data within each condition. In the current study, one way analysis of variance (ANOVA) was chosen as the signal analysis method in selecting the best parameter and characteristic time-frequency segments representing the condition of valve. It was performed by comparing the variation between each condition to the variation within them. A null hypothesis was made where there are no differences between each condition, and all conditions are normally distributed with the same mean and variance (Ross, 2004). In other words, the mean of one condition was assumed to be equal to all other conditions. This hypothesis was tested at 0.05 significance level. If the probability computed is less than 0.05, the null hypothesis can be rejected and thus the values measured are from different condition.

To determine the probability of null hypothesis, the F -ratio, which is the ratio of between to within group (condition) variance, is computed as in Equation 4.1. The variance of between group σ_b^2 and within group σ_w^2 are displayed in Equation 4.2 and 4.3,

$$F = \frac{\sigma_b^2}{\sigma_w^2} \quad (4.1)$$

$$\sigma_b^2 = n \sum_{i=1}^c \frac{(\bar{X}_i - \bar{X})^2}{c-1} \quad (4.2)$$

$$\sigma_w^2 = \sum_{i=1}^c \sum_{j=1}^n \frac{(X_{ij} - \bar{X}_i)^2}{c(n-1)} \quad (4.3)$$

$$\bar{X} = \frac{\sum_{i=1}^c \sum_{j=1}^n X_{ij}}{cn} \quad (4.4)$$

where c denotes the total number of groups (conditions) to be compared, n represents the total number of samples within each group (conditions), \bar{X}_i denotes the mean in i^{th} group (condition), X_{ij} represents the value of parameter in i^{th} group (condition) and j^{th} samples, and \bar{X} denotes the total mean value computed over all i^{th} groups (conditions) and j^{th} samples. The formulation of \bar{X} is shown in Equation 4.4.

Table 4.1 shows a summary of one way ANOVA. In fact, the two mean squares (variance), σ_b^2 and σ_w^2 were computed by dividing the sum of squares by its corresponding number of degrees of freedom (d.o.f.). Besides, the total sum of squares (variation) is equal to the sum of the between-group and within group sum of squares.

Table 4.1: One way ANOVA

Source of variation	Sum of squares	d.o.f.	Mean square
Between groups (between conditions)	$n \sum_{i=1}^c (\bar{X}_i - \bar{X})^2$	$c - 1$	σ_b^2
Within groups (residual variation)	$\sum_{i=1}^c \sum_{j=1}^n (X_{ij} - \bar{X}_i)^2$	$c(n - 1)$	σ_w^2
Total variation	$\sum_{i=1}^c \sum_{j=1}^n (X_{ij} - \bar{X})^2$	$cn - 1$	

The F -ratio, σ_b^2 / σ_w^2 can be computed from Table 4.1. From the F -ratio, the probability of null hypothesis can be determined from the F -distribution. If the probability of null hypothesis computed is smaller than 0.05, it can be concluded that at least one group (condition) is significantly different from the other groups (conditions).

4.3.2 Tukey comparison test

If the one way analysis of variance leads to a conclusion that at least one group (condition) is different from others, the Tukey honest and significance difference (HSD) test can identify which pair of groups (conditions) are significantly different from each other. This post-hoc test is frequently used in examining the performance of different research methods (Hu and Loizou, 2007). The confidence interval, C for each pair of groups (conditions) is computed from the studentized range (q) distribution and is shown in Equation 4.5.

$$C = \bar{X}_i - \bar{X}_j \pm \frac{q_{\alpha; c; N-c}}{\sqrt{2}} \hat{\sigma}_\varepsilon \frac{2}{n} \quad (4.5)$$

$$\hat{\sigma}_\varepsilon = \sqrt{\frac{1}{c} \sum_{i=1}^c \sum_{j=1}^n (X_{ij} - \bar{X}_i)^2} \quad (4.6)$$

$\overline{X_i} - \overline{X_j}$ denotes the mean difference between i^{th} group and j^{th} group, $q_{\alpha;c;N-c}$ denotes the critical value of the studentized range at significant level α , c groups and $N-c$ degree of freedom with N represents the total number of samples in all groups, and n represents the number of samples in each group with the assumption that the sample size for each group is equal. The within group mean-square $\hat{\sigma}_e$ can be computed from Equation 4.6.

If the confidence interval, C does not include a zero, the pair of mean differs significantly and vice versa. This is because zero value indicates overlapping of confidence interval between different groups (conditions). Thus, time-frequency segment with zero crossing is not suitable for monitoring as parameter within this segment does not show significant difference of mean value between each condition (Sim et al., 2012). In fact, parameter with the highest number of non-zero crossing of time-frequency segments will be selected as the best parameter. Similarly, the performance of AE and vibration signals in detecting valve failures was assessed by analyzing number of characteristic time-frequency segments under different speeds. Results of one-way ANOVA in selecting the best parameter and characteristic time-frequency segment will be displayed and discussed in the following section.

4.4 Parameter selection

As visual inspection of signal is subjective, some parameters were introduced to provide better indication on health condition of valves. A few parameters such as RMS, crest factor, skewness, kurtosis, and normalized energy were compared under different conditions by analysing the result of one-way ANOVA.

4.4.1 Results

4.4.1.1 AE Signal at 450 rpm

One way ANOVA was performed on 5 parameters at each time-frequency segments. Each analysis produced an ANOVA table similar to Table 4.1. The result of one way ANOVA for kurtosis at F2 (12.8 – 25.6 kHz) and time segment 1 (F2T1) is displayed in Table 4.2. As there were only 3 groups (conditions) considered in this study, the number of degree of freedom (d.o.f.) between groups is 2. Meanwhile, the d.o.f. value within groups is 117, computed according to the formula displayed in Table 4.1. These two d.o.f. values are consistent throughout the entire study.

Table 4.2: One way ANOVA result for kurtosis at F2 and time segment 1 (F2T1)

Source	Sum of squares	df	Mean squares	<i>F</i> -ratio	Prob> <i>F</i>
Columns	39.346	2.000	19.673	2.359	0.099
Error	975.682	117.000	8.339	-	-
Total	1015.028	119.000	-	-	-

The probability of parameter having the same mean value under different conditions was computed from the *F*-ratio. Table 4.3 shows the *p* value for all parameters of AE signal at 450 rpm. It can be observed from Table 4.3 that the *p* values greater than 0.05 are highlighted in bold. The mean value obtained from these time-frequency segments failed to show difference between groups significantly. In other words, the three mean values obtained from different valve conditions are of the same distribution statistically. Thus, valve conditions cannot be identified by comparing the mean value at these time-frequency segments.

Parameters such as normalized energy and RMS value give better indication on condition of valves as all of the time-frequency segments are of p value smaller than 0.001. Thus, it can be concluded that at least one group is significantly different from other groups in these segments. In contrast, parameters with their differentiating power listed in descending order are kurtosis, crest factor and skewness. The skewness performed worst as there are only two time-frequency segments with non-bolded p value.

Table 4.3: p value for all parameters at 450 rpm (AE signal)

AE 450 Kurtosis (p value)				
Frequency	Time			
	1	2	3	4
1 (0 - 12.8k Hz)	< 0.001	< 0.001	0.034	< 0.001
2 (12.8 – 25.6k Hz)	0.099	< 0.001	< 0.001	< 0.001
3 (25.6 – 38.4k Hz)	0.503	< 0.001	< 0.001	0.032
4 (38.4 – 51.2k Hz)	0.026	< 0.001	< 0.001	0.007
AE 450 Crest factor (p value)				
Frequency	Time			
	1	2	3	4
1 (0 - 12.8k Hz)	< 0.001	0.265	0.132	< 0.001
2 (12.8 – 25.6k Hz)	0.129	< 0.001	< 0.001	0.578
3 (25.6 – 38.4k Hz)	0.611	< 0.001	< 0.001	0.477
4 (38.4 – 51.2k Hz)	0.030	< 0.001	< 0.001	0.021
AE 450 Normalized energy (p value)				
Frequency	Time			
	1	2	3	4
1 (0 - 12.8k Hz)	< 0.001	< 0.001	< 0.001	< 0.001
2 (12.8 – 25.6k Hz)	< 0.001	< 0.001	< 0.001	< 0.001
3 (25.6 – 38.4k Hz)	< 0.001	< 0.001	< 0.001	< 0.001
4 (38.4 – 51.2k Hz)	< 0.001	< 0.001	< 0.001	< 0.001
AE 450 RMS (p value)				
Frequency	Time			
	1	2	3	4
1 (0 - 12.8k Hz)	< 0.001	< 0.001	< 0.001	< 0.001
2 (12.8 – 25.6k Hz)	< 0.001	< 0.001	< 0.001	< 0.001
3 (25.6 – 38.4k Hz)	< 0.001	< 0.001	< 0.001	< 0.001
4 (38.4 – 51.2k Hz)	< 0.001	< 0.001	< 0.001	< 0.001
AE 450 Skewness (p value)				
Frequency	Time			
	1	2	3	4
1 (0 - 12.8k Hz)	< 0.001	< 0.001	0.501	0.059
2 (12.8 – 25.6k Hz)	0.706	0.643	0.201	0.087
3 (25.6 – 38.4k Hz)	0.671	0.500	0.786	0.522
4 (38.4 – 51.2k Hz)	0.865	0.736	0.864	0.395

In evaluating the pair of groups which are significantly different from each other, a post-hoc test namely Tukey comparison test was conducted on the time-frequency segments with p value smaller than 0.05. Figure 4.5 shows the Tukey test result for kurtosis at F2 and time segment 1 (F2T1). The overlapping of confidence interval between all three groups further proved that time-frequency segment with p value greater than 0.05 cannot be characteristic segment to monitor valve conditions. Nevertheless, even the segments have p value smaller than 0.05, there are also possibilities for these segments to have overlapping confidence interval, as one way ANOVA only ensures that at least one group is significantly different from the others, instead of all groups. Figure 4.6 shows the overlapping confidence interval of group 2 (grease condition) and group 3 (leakage condition) of RMS at F3T3 although its p value is smaller than 0.001. Hence, F3T3 cannot be the characteristic segment as not all groups are completely separable.

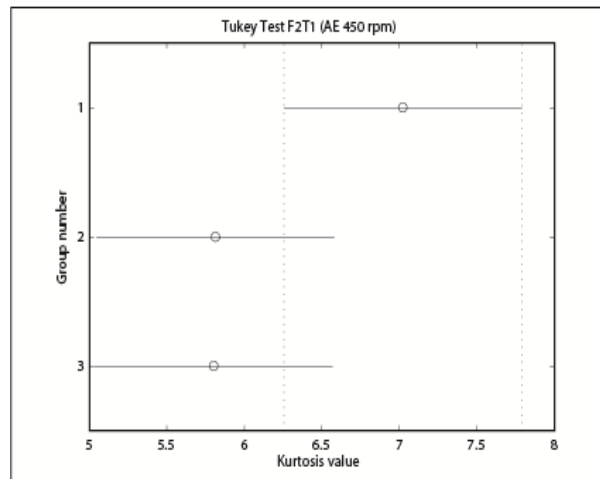


Figure 4.5: Tukey test result for kurtosis at F2 and time segment 1 (F2T1)

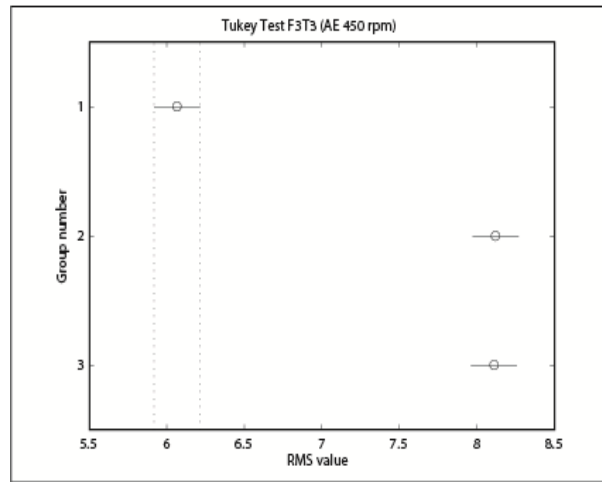


Figure 4.6: Tukey test result for RMS at F3 and time segment 3 (F3T3)

Time-frequency segments with separable confidence interval for all conditions are regarded as characteristic segments. The condition of valves can be identified clearly by observing the mean value in these segments. Figure 4.7 shows that F1T1 of normalized energy can be the characteristic segment as the mean value are completely separable in all groups. The results of Tukey comparison test for all parameters are attached in Appendix A.

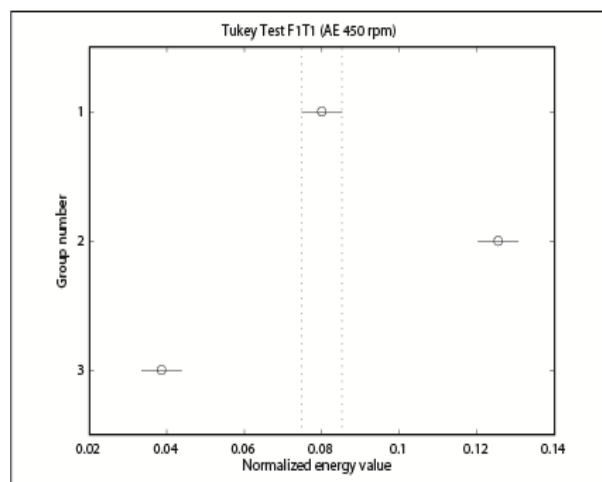


Figure 4.7: Tukey test result for normalized energy at F1 and time segment 1 (F1T1)

Table 4.4 shows a summary of characteristic segments for all parameters obtained from Tukey test. It is obvious that 2 parameters namely crest factor and skewness are not suitable to be the indicator for valve monitoring as none of the time-frequency segments of these parameters have completely separable confidence interval. This might happen because the change of valve impact under different conditions is not large enough to impose significant changes to the mean value. As opposed to RMS and normalized energy which evaluate the average value of signal, crest factor and skewness are more dependent on the peak amplitude within the time segments. Thus, smaller changes in impact resulted in the poor performance of crest factor and skewness.

Table 4.4: Characteristic segments for all parameters at 450 rpm (AE signal)

AE (450 rpm)				
Parameter	Frequency			
	F1	F2	F3	F4
RMS	T1	T1, T3, T4	T1, T2, T4	T3, T4
Crest factor				
Skewness				
Kurtosis	-	-	-	T2
Normalized energy	T1, T2	T1, T4	T1, T2, T4	T1, T2, T4

Meanwhile, normalized energy is the best parameter indicating condition of valves, followed by the RMS value. In fact, normalized energy just performed slightly better than RMS value, where the former has 10 characteristic segments while the later has 9 characteristic segments. However, most of the characteristic segments of normalized energy have larger gap between confidence intervals of different groups if compared to RMS value. Therefore, normalized energy is selected as the monitoring parameter for AE signal under 450 rpm.

4.4.1.2 Vibration Signal at 450 rpm

Table 4.5 shows the p value of vibration signal at 450 rpm for all parameters. Generally, the performance of parameter for vibration signal is almost the same as AE signal. Normalized energy and RMS performed the best as all of the time-frequency segments have p value smaller than 0.001, followed by kurtosis, crest factor and skewness. In fact, for vibration signal, the number of time-frequency segments with p value smaller than 0.001 are same as that in AE signal for crest factor and kurtosis. Nevertheless, in search of characteristic segments, none of the time-frequency segment of kurtosis and skewness has completely separable confidence interval, as displayed in

Table 4.6. This is slightly different from the result of AE signal. In addition, the total number of characteristic segments for normalized energy and RMS are lesser compared to AE signal. For vibration signal, normalized energy occupies a number of 8 characteristic segments while RMS has 7 characteristic segments. Due to larger number of characteristic segments, normalized energy is selected as the best parameter for vibration signal at 450 rpm. Tukey test results for all parameters can be referred from Appendix A.

Table 4.5: p value for all parameters at 450 rpm (Vibration signal)

Vib 450 Kurtosis (p value)				
Frequency	Time			
	1	2	3	4
1 (0 - 12.8k Hz)	< 0.001	< 0.001	< 0.001	0.831
2 (12.8 - 25.6k Hz)	0.141	< 0.001	< 0.001	0.033
3 (25.6 - 38.4k Hz)	0.031	< 0.001	< 0.001	0.016
4 (38.4 - 51.2k Hz)	< 0.001	< 0.001	< 0.001	0.003
Vib 450 Crest factor (p value)				
Frequency	Time			
	1	2	3	4
1 (0 - 12.8k Hz)	< 0.001	< 0.001	< 0.001	0.704
2 (12.8 - 25.6k Hz)	0.150	< 0.001	< 0.001	0.464
3 (25.6 - 38.4k Hz)	0.146	< 0.001	< 0.001	0.134
4 (38.4 - 51.2k Hz)	< 0.001	< 0.001	< 0.001	0.277
Vib 450 Normalized energy (p value)				
Frequency	Time			
	1	2	3	4
1 (0 - 12.8k Hz)	< 0.001	< 0.001	< 0.001	< 0.001
2 (12.8 - 25.6k Hz)	< 0.001	< 0.001	< 0.001	< 0.001
3 (25.6 - 38.4k Hz)	< 0.001	< 0.001	< 0.001	< 0.001
4 (38.4 - 51.2k Hz)	< 0.001	< 0.001	< 0.001	< 0.001
Vib 450 RMS (p value)				
Frequency	Time			
	1	2	3	4
1 (0 - 12.8k Hz)	< 0.001	< 0.001	0.003	< 0.001
2 (12.8 - 25.6k Hz)	< 0.001	< 0.001	< 0.001	< 0.001
3 (25.6 - 38.4k Hz)	< 0.001	< 0.001	< 0.001	< 0.001
4 (38.4 - 51.2k Hz)	< 0.001	< 0.001	< 0.001	< 0.001
Vib 450 Skewness (p value)				
Frequency	Time			
	1	2	3	4
1 (0 - 12.8k Hz)	0.025	< 0.001	0.848	0.458
2 (12.8 - 25.6k Hz)	0.788	0.280	0.954	0.611
3 (25.6 - 38.4k Hz)	0.197	0.041	0.701	0.793
4 (38.4 - 51.2k Hz)	0.170	0.540	0.490	0.983

Table 4.6: Characteristic segments for all parameters at 450 rpm
(Vibration signal)

Vibration (450 rpm)				
Parameter	Frequency			
	F1	F2	F3	F4
RMS	T2, T4	T1, T4	T4	T3, T4
Crest factor	T2	-	-	-
Skewness				
Kurtosis				
Normalized energy	T2, T3, T4	T2, T3, T4	T2	T1

4.4.1.3 AE Signal at 800 rpm

For AE signal at 800 rpm, almost all of the parameters have time-frequency segments with p value smaller than 0.05. Table 4.7 shows that for crest factor, normalized energy and RMS, there exists at least one group in all of the time-frequency segments which differs significantly from the other groups. Therefore, all segments in these parameters have higher possibility of becoming characteristic segments. Meanwhile, for kurtosis, there is only one time-frequency segment with no significant difference across all other groups. Skewness performed the worst as there are only 5 time-frequency segments with p value smaller than 0.05.

In comparing the significant difference between each and every pair of groups, it was found that RMS performed the best with 12 characteristic segments, followed by skewness and kurtosis with 2 characteristic segments each. Crest factor and normalized energy performed the worst with 1 characteristic segment each, as displayed in Table 4.8. It can be deduced that AE signal acquired at higher speed has lower signal-to-noise ratio due to limitation of data acquisition device, which can only achieve a maximum sampling rate of 102.4 kHz. Therefore, the valve opening event acquired at this speed was not distinctive to cause significant change to the value of crest factor and

normalized energy at different valve conditions. Since these parameters are the ratio of peak/ energy within a time segment to mean value/ total energy in a given signal, higher noise can easily cover the valve impact event and thus producing little difference to these parameters. Nevertheless, RMS can produce better result as this value measures and compares a combination of impacts and noise at different conditions. Thus, RMS is selected as the best parameter for AE signal at 800 pm.

Table 4.7: p value for all parameters at 800 rpm (AE signal)

AE 800 Kurtosis (p value)				
Frequency	Time			
	1	2	3	4
1 (0 - 12.8k Hz)	< 0.001	0.069	< 0.001	0.003
2 (12.8 – 25.6k Hz)	< 0.001	< 0.001	< 0.001	0.008
3 (25.6 – 38.4k Hz)	< 0.001	< 0.001	< 0.001	< 0.001
4 (38.4 – 51.2k Hz)	< 0.001	< 0.001	< 0.001	< 0.001
AE 800 Crest factor (p value)				
Frequency	Time			
	1	2	3	4
1 (0 - 12.8k Hz)	< 0.001	0.042	< 0.001	0.015
2 (12.8 – 25.6k Hz)	< 0.001	< 0.001	< 0.001	0.007
3 (25.6 – 38.4k Hz)	< 0.001	< 0.001	0.003	< 0.001
4 (38.4 – 51.2k Hz)	< 0.001	< 0.001	< 0.001	< 0.001
AE 800 Normalized energy (p value)				
Frequency	Time			
	1	2	3	4
1 (0 - 12.8k Hz)	< 0.001	< 0.001	< 0.001	0.010
2 (12.8 – 25.6k Hz)	< 0.001	< 0.001	< 0.001	< 0.001
3 (25.6 – 38.4k Hz)	< 0.001	< 0.001	< 0.001	< 0.001
4 (38.4 – 51.2k Hz)	< 0.001	< 0.001	< 0.001	< 0.001
AE 800 RMS (p value)				
Frequency	Time			
	1	2	3	4
1 (0 - 12.8k Hz)	< 0.001	< 0.001	< 0.001	< 0.001
2 (12.8 – 25.6k Hz)	< 0.001	< 0.001	< 0.001	< 0.001
3 (25.6 – 38.4k Hz)	< 0.001	< 0.001	< 0.001	< 0.001
4 (38.4 – 51.2k Hz)	< 0.001	< 0.001	< 0.001	< 0.001
AE 800 Skewness (p value)				
Frequency	Time			
	1	2	3	4
1 (0 - 12.8k Hz)	0.048	< 0.001	< 0.001	< 0.001
2 (12.8 – 25.6k Hz)	0.887	0.715	0.366	0.022
3 (25.6 – 38.4k Hz)	0.782	0.935	0.334	0.127
4 (38.4 – 51.2k Hz)	0.605	0.904	0.970	0.742

Table 4.8: Characteristic segments for all parameters at 800 rpm
(AE signal)

AE (800 rpm)				
Parameter	Frequency			
	F1	F2	F3	F4
RMS	T1, T2, T3	T1, T2, T3, T4	T1, T3, T4	T1, T4
Crest factor	T3	-	-	-
Skewness	T2, T3	-	-	-
Kurtosis	T3	-	-	T3
Normalized energy	-	-	T4	-

4.4.1.4 Vibration Signal at 800 rpm

Opposing to AE signal at 800 rpm, vibration signal produces better result at higher speed. Table 4.9 shows that all parameters in all time-frequency segments have p value smaller than 0.05, except skewness. It can be deduced that higher speed produces greater mechanical impacts which can be detected by the accelerometer easily. Thus, the impact of valve motion is more significant in vibration signal compared to AE signal as the former is more sensitive to mechanical motion and less sensitive to other noises. Skewness remained as the worst parameter as the impacts still insufficient to alter the skewness of distribution.

The performance of Tukey comparison test listed in descending order is normalized energy, RMS, and crest factor. Normalized energy performed the best with 7 characteristic segments, followed by RMS with 6 characteristic segments, and crest factor with 2 characteristic segments. It can be seen from Table 4.10 that there are no characteristic segments in kurtosis and skewness. This might happen when the noise masked the impact event and caused little changes to the distribution. In contrast, normalized energy and RMS value are sensitive to the combination of impacts and noise in signal as they measure the energy ratio/ average value of signal. Due to the excellent

performance of normalized energy, it is selected as the best parameter for vibration signal at 800 rpm.

Table 4.9: p value for all parameters at 800 rpm (Vibration signal)

Vib 800 Kurtosis (p value)				
Frequency	Time			
	1	2	3	4
1 (0 - 12.8k Hz)	< 0.001	< 0.001	< 0.001	0.034
2 (12.8 - 25.6k Hz)	< 0.001	< 0.001	< 0.001	0.009
3 (25.6 - 38.4k Hz)	< 0.001	< 0.001	< 0.001	< 0.001
4 (38.4 - 51.2k Hz)	< 0.001	< 0.001	< 0.001	< 0.001
Vib 800 Crest factor (p value)				
Frequency	Time			
	1	2	3	4
1 (0 - 12.8k Hz)	< 0.001	0.001	< 0.001	< 0.001
2 (12.8 - 25.6k Hz)	< 0.001	< 0.001	< 0.001	0.014
3 (25.6 - 38.4k Hz)	< 0.001	< 0.001	< 0.001	< 0.001
4 (38.4 - 51.2k Hz)	< 0.001	< 0.001	< 0.001	< 0.001
Vib 800 Normalized energy (p value)				
Frequency	Time			
	1	2	3	4
1 (0 - 12.8k Hz)	< 0.001	< 0.001	< 0.001	< 0.001
2 (12.8 - 25.6k Hz)	< 0.001	< 0.001	< 0.001	< 0.001
3 (25.6 - 38.4k Hz)	< 0.001	< 0.001	< 0.001	0.004
4 (38.4 - 51.2k Hz)	< 0.001	< 0.001	< 0.001	< 0.001
Vib 800 RMS (p value)				
Frequency	Time			
	1	2	3	4
1 (0 - 12.8k Hz)	< 0.001	< 0.001	< 0.001	< 0.001
2 (12.8 - 25.6k Hz)	< 0.001	0.011	0.252	< 0.001
3 (25.6 - 38.4k Hz)	< 0.001	< 0.001	< 0.001	< 0.001
4 (38.4 - 51.2k Hz)	< 0.001	< 0.001	< 0.001	< 0.001
Vib 800 Skewness (p value)				
Frequency	Time			
	1	2	3	4
1 (0 - 12.8k Hz)	0.351	0.002	0.004	0.107
2 (12.8 - 25.6k Hz)	0.209	0.909	0.003	0.642
3 (25.6 - 38.4k Hz)	0.666	0.863	0.993	0.932
4 (38.4 - 51.2k Hz)	0.102	0.824	0.953	0.672

Table 4.10: Characteristic segments for all parameters at 800 rpm
(Vibration signal)

Vibration (800 rpm)				
Parameter	Frequency			
	F1	F2	F3	F4
RMS	T3, T4	T4	T3, T4	T1
Crest factor	T1	-	-	T2
Skewness				
Kurtosis				
Normalized energy	T2, T3, T4	T3	T2	T3, T4

4.4.2 Discussions

It can be observed from previous section that parameters such as crest factor, skewness, and kurtosis are not reliable indicators to valve condition, though they have been applied widely in monitoring of other rotating equipment namely bearings. This is because these parameters require large changes in signal to alter their values significantly, i.e. insensitive to insignificant variation of data. In contrast, parameters such as normalized energy and RMS value are more sensitive to changes in valve conditions. They can identify each valve conditions though the signal was covered with noise. Therefore, these two parameters remained as the best parameter for both AE and vibration signal at 450 rpm and 800 rpm.

Nevertheless, normalized energy performed poorly for AE signal at higher compressor speed, i.e.800 rpm. It can be postulated that the sampling rate used in this study is insufficient to capture the characteristic of AE signal due to excessive fluid noise at higher speed. In order to obtain a clean AE signal, it is advisable to acquire the signal at higher sampling rate, preferably at sampling rate above 1 MHz. However, RMS value has excellent performance at this speed, with 12 characteristic segments from a total of 16 time-frequency segments. Indeed, RMS is less susceptible to noise as this value computes the average value of signal which is inclusive of noise, in contrast

to normalized energy which computes the ratio of energy in a given time segment to the total energy of signal. The later will have little difference between conditions if the noise masked the impact event and caused the impact to be insignificant compared to total energy.

At lower compressor speed (450 rpm), normalized energy performed the best while RMS ranked secondly. Meanwhile, crest factor, skewness, and kurtosis performed poorly at lower speed. AE signal is better in detecting the difference between conditions compared to vibration signal as the former has more characteristic segments for both normalized energy and RMS. This is consistent with the observation from previous research which stated that AE signal is superior in monitoring of bearings at low speed (McFadden and Smith, 1983).

However, at higher compressor speed (850 rpm), AE signal performed poorly compared to vibration signal. Normalized energy computed at higher speed is poor in representing valve conditions due to low signal-to-noise ratio of AE signal. Nevertheless, RMS can replace normalized energy as the best parameter since it is less affected by noise. In fact, all other parameters performed poorly for AE signal at higher speed except RMS value. This further proved that AE signal is inferior to vibration signal at higher speed. In contrast, the normalized energy and RMS value computed from vibration signal are capable to indicate different valve conditions clearly. This might happen as higher speed resulted in greater mechanical impact which produced distinct peak from intensely noised signal.

It was found that both skewness and kurtosis have no characteristic segments at low and high compressor speed. It can be deduced that the valve opening impact is not large enough to change the distribution of signal significantly. Meanwhile, for AE signal, there are no characteristic segment for crest factor and skewness at low speed.

However, at high speed, crest factor, skewness and kurtosis have at least 1-2 characteristic segments due to the higher mechanical impacts. It is believed that these three parameters can perform better if the AE signal is acquired at higher sampling rate.

In short, normalized energy is selected as the best parameter of AE signal and vibration signal for valve monitoring due to their good performance discussed above, except for AE signal acquired at 800 rpm. Although RMS is a better parameter for AE signal at high speed, normalized energy is still chosen for signal analysis in the following section to enable equal comparison with other operating conditions. The following section presents results of one way ANOVA for normalized energy under 4th resolution level of WPT. It is encouraging that the performance of normalized energy for AE signal at high speed improved at higher level of resolution, with more characteristic segments compared to that during parameter comparison. This shows that normalized energy is still a good parameter for AE signal at high speed.

4.5 Signal Analysis

To enable detailed signal analysis, raw AE and vibration signals were decomposed into the 4th level of resolution, which is equivalent to 16 frequency ranges. Signals in each frequency range were further segregated into 4 time segments which correspond to different valve movements, resulting in 64 time-frequency segments for each signal. Characteristic segments of each signal under different speed were identified through one way ANOVA and Tukey test. The results showed characteristics of AE and vibration signal at different speed.

4.5.1 Results

4.5.1.1 Signals acquired at low speed (450 rpm)

Table 4.11 shows characteristic segments of AE and vibration signal from the result of Tukey test. Detailed result can be found in Appendix B. AE signal performed the best at higher frequency range, namely F9 (25.6 – 28.8 kHz), F11 (32.0 – 35.2 kHz), F12 (35.2 – 38.4 kHz), F14 (41.6 – 44.8 kHz) and F15 (44.8 – 48.0 kHz). They were considered as the best frequency ranges as they have the most characteristic segments compared to other frequency range. At these frequency ranges, the mean values of normalized energy at different conditions are significantly different at 3 time segments. The 95% confidence interval (C.I) of these time-frequency segments is displayed in Table 4.12.

Table 4.11: Characteristic segments of AE and vibration signal at 450 rpm

Frequency	450 rpm	
	AE	Vibration
F1 (0 – 3.2 kHz)	T1, T2	T1
F2 (3.2 – 6.4 kHz)	T1, T4	T1 T2 T4
F3 (6.4 – 9.6 kHz)	T2, T3	T1 T4
F4 (9.6 – 12.8 kHz)	T1	T2 T3
F5 (12.8 – 16.0 kHz)	T1	T2
F6 (16.0 – 19.2 kHz)	T2, T4	T2 T3
F7 (19.2 – 22.4 kHz)	T2, T3	T2 T3
F8 (22.4 – 25.6 kHz)	T1, T4	T2 T3
F9 (25.6 – 28.8 kHz)	T1, T2, T4	T2
F10 (28.8 – 32.0 kHz)	T1, T3	T2 T3
F11 (32.0 – 35.2 kHz)	T1, T2, T4	T3
F12 (35.2 – 38.4 kHz)	T1, T3, T4	T2 T3
F13 (38.4 – 41.6 kHz)	T1, T4	T2 T3 T4

Table 4.11, continued

Frequency	450 rpm	
	AE	Vibration
F14 (41.6 – 44.8 kHz)	T1, T2, T4	T2
F15 (44.8 – 48.0 kHz)	T1, T2, T4	T4
F16 (48.0 – 51.2 kHz)	T1, T2	T2 T3 T4

Table 4.12 displays interval of normalized energy of AE signal for identification of valve conditions. As their probability of hypothesis was greater than 0.05, these intervals were proven to be sensitive to valve condition, instead of fluctuations or errors within measurements. Hence, the condition of plate valve can be identified by comparing its normalized energy value with the confidence interval, for compressors operated at 450 rpm. However, this method of inspection is more reliable for valves suffering from grease or leakage problem as other valve conditions have not been tested in this study.

Table 4.12: 95% confidence interval (C.I) of AE signal at 450 rpm in the best frequency range

Frequency range	Valve conditions		
	Normal	Grease	Leakage
F9T1	0.0228 - 0.0294	0.0369 - 0.0436	0.0027 - 0.0093
F9T2	0.437 - 0.485	0.178 - 0.226	0.361 - 0.409
F9T4	0.295 - 0.350	0.545 - 0.600	0.469 - 0.524
F11T1	0.031 - 0.038	0.055 - 0.062	0.001 - 0.009
F11T2	0.362 - 0.395	0.143 - 0.176	0.302 - 0.335
F11T4	0.350 - 0.396	0.583 - 0.628	0.477 - 0.522
F12T1	0.017 - 0.027	0.050 - 0.060	0 - 0.010
F12T3	0.183 - 0.215	0.150 - 0.181	0.100 - 0.131
F12T4	0.290 - 0.339	0.611 - 0.661	0.417 - 0.467
F14T1	0.030 - 0.040	0.055 - 0.064	0.003 - 0.013
F14T2	0.413 - 0.447	0.181 - 0.215	0.305 - 0.338
F14T4	0.355 - 0.402	0.573 - 0.620	0.502 - 0.549
F15T1	0.052 - 0.074	0.094 - 0.116	0.012 - 0.035
F15T2	0.407 - 0.441	0.145 - 0.178	0.320 - 0.354
F15T4	0.347 - 0.395	0.527 - 0.575	0.441 - 0.489

From Table 4.12, it can be observed that the characteristic of AE signal for a particular valve condition is similar in the same time segment, regardless of frequency range. At time segment 1 (T1), which is equivalent to crank angle 0° - 18.8° , the lowest value of C.I is obtained from valve under leakage condition. C.I computed from normal valve condition ranked second while grease condition has the largest value of C.I. This sequence is the same for all confidence intervals computed at T1, as highlighted in yellow colour in Table 4.13.

Table 4.13: Sequence of confidence interval (C.I) of AE signal at 450 rpm in ascending order (1: lowest mean value and 3: highest mean value)

Frequency range	Valve conditions		
	Normal	Grease	Leakage
F9T1	2	3	1
F9T2	3	1	2
F9T4	1	3	2
F11T1	2	3	1
F11T2	3	1	2
F11T4	1	3	2
F12T1	2	3	1
F12T3	3	2	1
F12T4	1	3	2
F14T1	2	3	1
F14T2	3	1	2
F14T4	1	3	2
F15T1	2	3	1
F15T2	3	1	2
F15T4	1	3	2

Similar trend can be seen in time segment 2 (T2). At crank angle 18.8° - 131.4° , which corresponds to event of valve opening, the lowest value of C.I is achieved by that under grease condition. This is followed by C.I under leakage and normal condition, which ranked second and third respectively. The consistency of the trend can be seen clearly in Table 4.13, where those similar segments are coloured in green. It further

shows that AE signal under the same valve condition has same characteristic in the same time segment, which is obvious especially in the best frequency range.

From Table 4.13, it is apparent that only F12 (35.2 – 38.4 kHz) has characteristic segment in the third time segment 3 (T3), which corresponds to suction valve closing event at crank angle 131.4°-244°. In this time segment, C.I under leakage condition has the lowest value, followed by grease and normal condition which ranked second and third respectively. It was found that T3 can be a better segment in detecting grease condition if the length of time segment is shortened. From Figure 4.8, it is noticeable that there is a delay from the impulse in T3 under grease condition. For normal and leakage condition, this impulse occurred at crank angle approximately 131°-175°. On the other hand, under grease condition, a sudden impulse appeared at crank angle approximately 175° - 200°. It can be postulated that the stickiness of valve plate resulted in the delay of impulse, which signifies delay of valve closing event. In fact, it can be observed from Appendix C that the delay is consistent in all frequency ranges except F1 (0 – 3.2 kHz) as the impulse was masked by other machinery noise in low frequency range. Thus, time segment of crank angle 175° - 200° can be the key characteristic for valve suffered in grease condition, which promotes a more effective way to detect greased valve compared to the current T3 time segment.

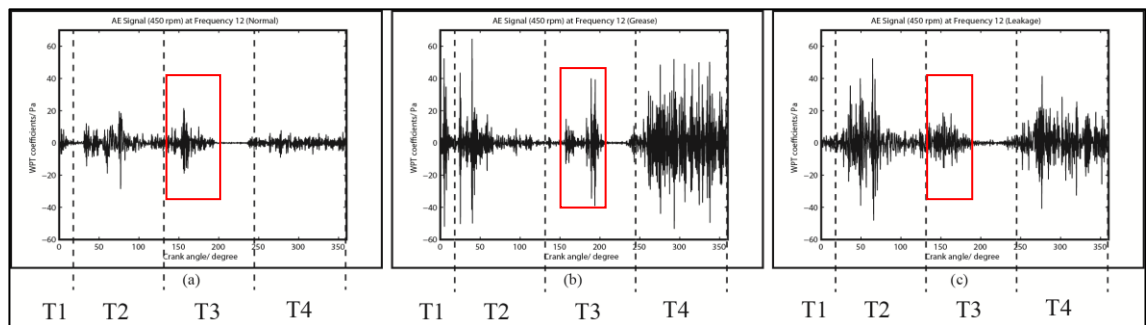


Figure 4.8: Comparison of AE signal at F12 (35.2 – 38.4 kHz) and 450 rpm under (a) normal (b) grease (c) leakage condition

At the fourth time segment (T4) with crank angle 244° - 360° , normalized energy under normal condition shows the lowest C.I. Meanwhile, normalized energy under leakage condition has the second largest C.I. The largest value of C.I is attained by that under grease condition. The blue colour highlighted in Table 4.13 shows the traits of AE signal at time segment 4 (T4) under different frequency ranges.

Meanwhile, for vibration signal, although the Tukey test result displayed in Table 4.11 shows a number of characteristic segments at high frequency ranges, these frequency ranges are beyond operating frequency range of accelerometer. Therefore, characteristic segments in the higher frequency range are not reliable for valve monitoring. It has been shown further in Figure 4.9 and Figure 4.10 that the valve opening impact in the higher frequency range (F7) is less distinctive compared to that in the lower frequency range (F1).

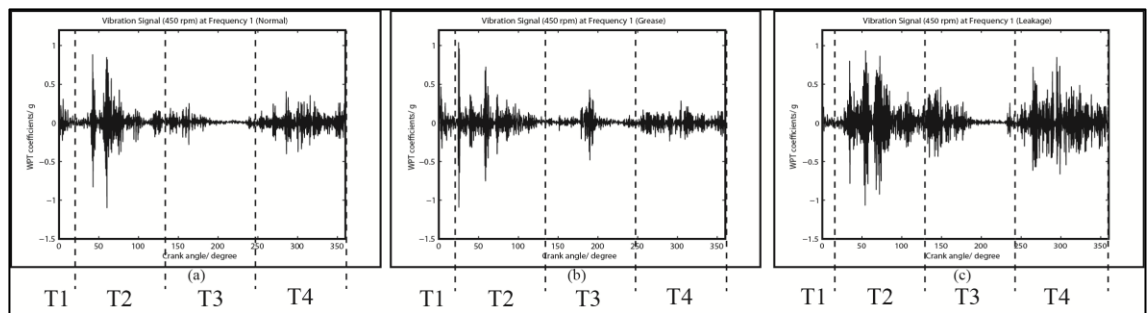


Figure 4.9: Comparison of vibration signal at F1 (0 – 3.2 kHz) and 450 rpm under (a) normal (b) grease (c) leakage condition

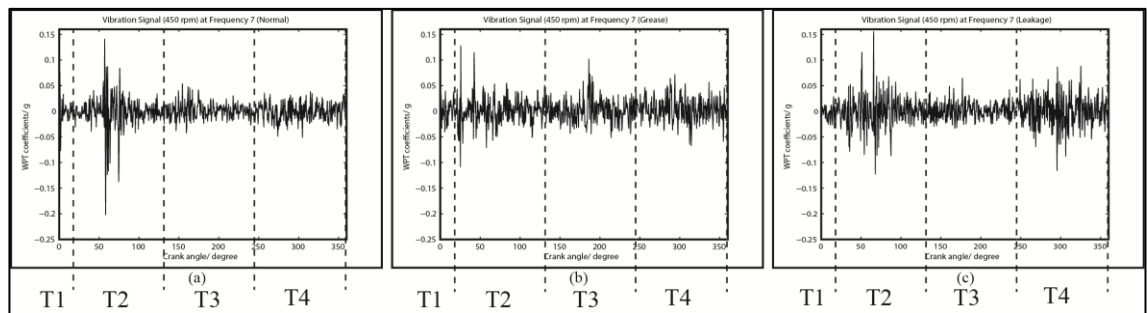


Figure 4.10: Comparison of vibration signal at F7 (19.2 – 22.4 kHz) and 450 rpm under (a) normal (b) grease (c) leakage condition

In fact, it can be observed from Appendix C that vibration signals started to contain more noise and have less distinct peaks in frequency range greater than F6 (16 – 19.2 kHz). This due to the fact that the operating frequency of accelerometer in this research is in the range of 0.35 – 15000 Hz, at 3dB tolerance level, as shown in Appendix D. Thus, despite having many characteristic segments in the higher frequency range, the best frequency range was found in F2 (3.2 – 6.4 kHz), F3 (6.4 – 9.6 kHz), and F4 (9.6 – 12.8 kHz), with 3, 2, 2 characteristic segments respectively, as shown in Table 4.11.

Table 4.14 shows the C.I of characteristic segments for vibration signal at 450 rpm in the best frequency range. Although the value of C.I differs compared to that in AE signal, the sequence of C.I in ascending order is exactly the same as in AE signal, regardless of frequency range, except time segment 3 (T3). From Table 4.14, at time segment 1 (T1), C.I under leakage condition has the lowest value, followed by the normal condition which ranked second. Normalized energy obtained under grease condition has the largest value of C.I. On the other hand, for time segment 2 (T2), grease condition shows the lowest value of C.I, followed by leakage and normal condition which ranked second and third respectively. In the fourth time segment (T4), the lowest value of C.I is achieved by normal condition, while leakage condition has the second largest of C.I. The highest C.I was found under grease condition.

Table 4.14: 95% confidence interval (C.I) of vibration signal at 450 rpm in the best frequency range

Frequency range	Valve conditions		
	Normal	Grease	Leakage
F2T1	0.018 - 0.027	0.047 - 0.056	0.002 - 0.011
F2T2	0.603 - 0.664	0.195 - 0.256	0.530 - 0.590
F2T4	0.229 - 0.295	0.590 - 0.656	0.341 - 0.407
F3T1	0.009 - 0.015	0.029 - 0.036	0.001 - 0.006
F3T4	0.189 - 0.256	0.451 - 0.518	0.269 - 0.336
F4T2	0.791 - 0.839	0.620 - 0.667	0.712 - 0.759
F4T3	0.084 - 0.107	0.121 - 0.144	0.056 - 0.079

By comparing Table 4.13 and Table 4.15, it is obvious that the sequence of C.I in both tables is the same for the same time segment. Therefore, it can be said that AE and vibration signals obtained at the best frequency range are good in representing the valve conditions as both signals correlated well. From the result presented, it is clear that under low rotating speed, AE signal can perform better in the high frequency region while vibration signal is more reliable in the low frequency region.

Table 4.15: Sequence of confidence interval (C.I) of vibration signal at 450 rpm in ascending order (1: lowest mean value and 3: highest mean value)

Frequency range	Valve conditions		
	Normal	Grease	Leakage
F2T1	2	3	1
F2T2	3	1	2
F2T4	1	3	2
F3T1	2	3	1
F3T4	1	3	2
F4T2	3	1	2
F4T3	2	3	1

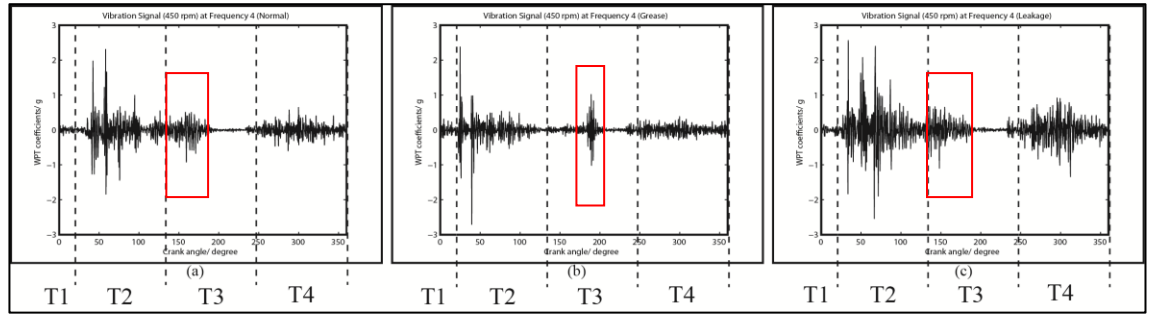


Figure 4.11: Comparison of vibration signal at F4 (9.6 – 12.8 kHz) and 450 rpm under (a) normal (b) grease (c) leakage condition

Nevertheless, the sequence of C.I at time segment 3 (T3) is different between AE and vibration signal. It can be seen from Table 4.15 that leakage condition has the lowest value of C.I, followed by normal and grease condition, which is different from AE signal at the second and third rank. This might due to the long time segment of T3 which causes the segment insensitive to changes of valve condition. However, the delay of impulse at T3 under grease condition is the same for both AE and vibration signal, as displayed in Figure 4.11 for vibration signal at F4 (9.6 – 12.8 kHz). In fact, the ability of vibration signal to detect grease valve problem can be further improved if the length of T3 is shortened to 175° - 200° . It is believed that with the improved T3, the sequence of C.I between AE and vibration signal can be the same.

4.5.1.2 Signals acquired at high speed (800 rpm)

Table 4.16 shows characteristic segments of AE and vibration signal at 800 rpm. Frequency ranges shaded in grey represents no characteristic segments within the frequency range. Detailed result of Tukey test can be found in Appendix E while a sample of AE and vibration signals at all frequency range can be seen in Appendix F.

Table 4.16: Characteristic segments of AE and vibration signal at 800 rpm

Frequency	800 rpm	
	AE	Vibration
F1 (0 – 3.2 kHz)		T3 T4
F2 (3.2 – 6.4 kHz)	T3 T4	T2 T4
F3 (6.4 – 9.6 kHz)	T4	T2
F4 (9.6 – 12.8 kHz)	T4	T2 T4
F5 (12.8 – 16.0 kHz)		T3
F6 (16.0 – 19.2 kHz)	T4	T2 T4
F7 (19.2 – 22.4 kHz)	T1 T2	
F8 (22.4 – 25.6 kHz)	T3	
F9 (25.6 – 28.8 kHz)	T4	
F10 (28.8 – 32.0 kHz)	T2	T3 T4
F11 (32.0 – 35.2 kHz)		T2
F12 (35.2 – 38.4 kHz)		T2 T3
F13 (38.4 – 41.6 kHz)		T3
F14 (41.6 – 44.8 kHz)	T3 T4	T2
F15 (44.8 – 48.0 kHz)	T2	
F16 (48.0 – 51.2 kHz)	T3 T4	T4

It can be scrutinized that AE signal characterizes valve condition better at frequency range namely F2 (3.2 – 6.4 kHz), F7 (19.2 – 22.4 kHz), F14 (41.6 – 44.8 kHz) and F16 (48.0 – 51.2 kHz). On the other hand, vibration signal shows better performance at F1 (0 – 3.2 kHz), F2 (3.2 – 6.4 kHz), F4 (9.6 – 12.8 kHz) and F6 (16.0 – 19.2 kHz). As mentioned in previous section, characteristic segments of vibration signal beyond F6 are neglected as these frequencies lie above the working range of

accelerometer, thus causing them to be less reliable and less effective in representing valve conditions.

Table 4.17 shows the C.I of normalized energy for AE signal in the best frequency range. By comparing normalized energy value in a particular frequency range and time segment, condition of valve can be deduced.

Table 4.17: 95% confidence interval (C.I) of AE signal at 800 rpm in the best frequency range

Frequency range	Valve conditions		
	Normal	Grease	Leakage
F2T3	0.0555 - 0.0851	0.316 - 0.345	0.0898 - 0.119
F2T4	0.265 - 0.315	0.206 - 0.256	0.331 - 0.382
F7T1	0.00324 - 0.0497	0.0781 - 0.125	0.270 - 0.316
F7T2	0.786 - 0.847	0.653 - 0.715	0.522 - 0.583
F14T3	0.101 - 0.141	0.228 - 0.267	0.0577 - 0.0975
F14T4	0.137 - 0.164	0.0413 - 0.0684	0.0785 - 0.106
F16T3	0.111 - 0.156	0.232 - 0.277	0.0558 - 0.101
F16T4	0.111 - 0.137	0.0383 - 0.0648	0.0810 - 0.107

For time segment 1 at F7 (F7T1), it is obvious that C.I increases from normal, grease to leakage condition. On the contrary, under the same frequency range F7, C.I decreases from normal, grease to leakage condition at time segment 2. It can be postulated that valve opening event occurred earlier under leakage condition, resulted in highest C.I among other conditions at T1. Consequently, during the valve opening event of normal and grease condition as represented by T2, leakage condition has the lowest value of C.I. Similarly, since there was no leakage under normal valve condition, it has the lowest value of C.I at T1 and the highest value of C.I at T2. As grease condition has little leakages, its C.I lies between the two conditions at T1 and T2.

For time segment 3 under higher frequency range F14 and F16, it can be seen that leakage condition has the lowest value of C.I, followed by normal and grease

condition. These same sequences of segments are highlighted in orange colour as displayed in Table 4.18. However, the sequence of C.I is different at F2. At this frequency range, the lowest value of C.I is achieved by normal condition, followed by leakage and grease condition. The difference in sequence at F2 might happen as AE signal is prone to be influenced by other noises at lower frequency range. In fact, vibration signal has the same sequence of C.I as in F14 and F16 at F1, as highlighted in orange in Table 4.20. This further supports the postulation that F2 might not good in representing valve conditions. The intense noise of AE signal at F2 compared to F14 and F16 can be seen clearly from Figure 4.12.

Table 4.18: Sequence of confidence interval (C.I) of AE signal at 800 rpm in ascending order (1: lowest mean value and 3: highest mean value)

Frequency range	Valve conditions		
	Normal	Grease	Leakage
F2T3	1	3	2
F2T4	2	1	3
F7T1	1	2	3
F7T2	3	2	1
F14T3	2	3	1
F14T4	3	1	2
F16T3	2	3	1
F16T4	3	1	2

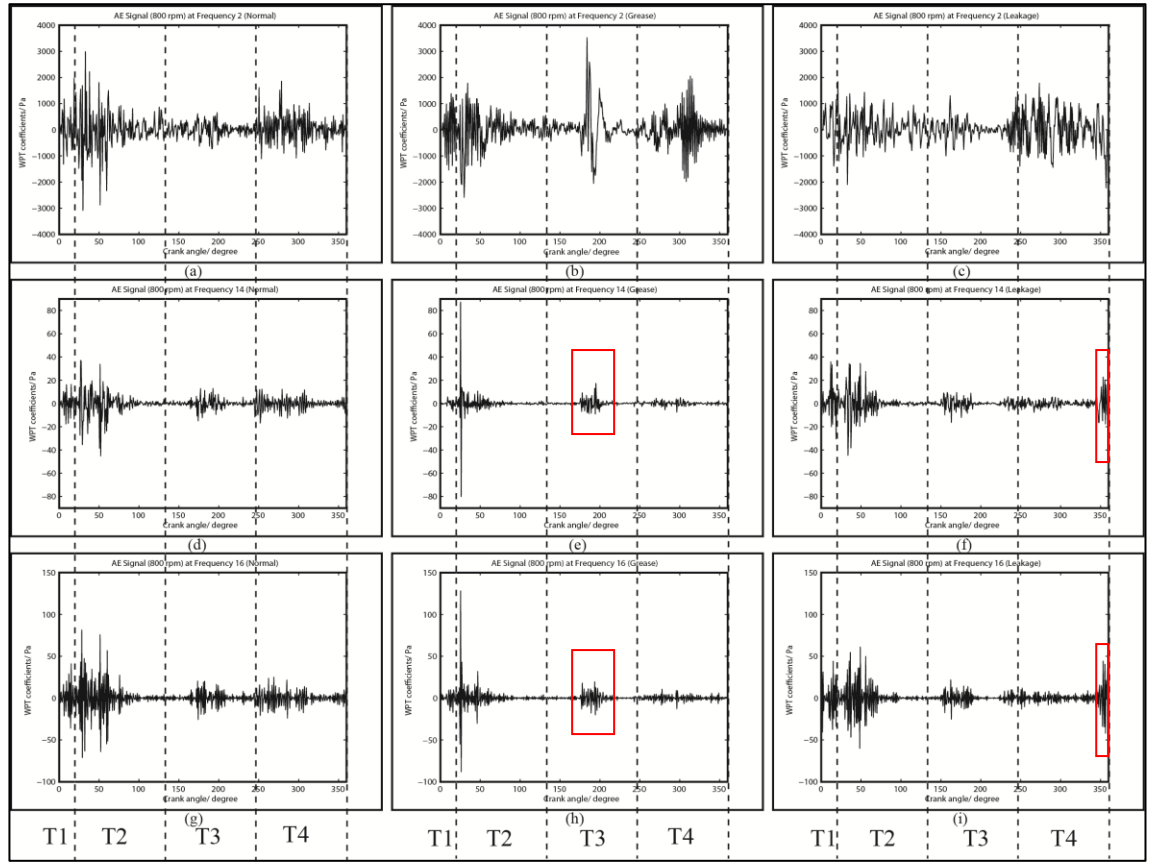


Figure 4.12: Comparison of AE signal at F2 (a) – (c), F14 (d) – (f), and F16 (g) – (i) under different valve conditions at 800 rpm

As stated in the previous section, one of the characteristic of greased valve condition at 450 rpm is the delay of transient event at time segment 3 compared to that under normal valve condition. However, this delay is not obvious for signal captured at higher speed. It can be seen from Figure 4.12 (e) and (h) that there are little delay of transient event in T3 at F14 and F16 compared to normal condition. The difference of transient event at low and high speed will be explained in the discussion section.

It can be observed that F14 and F16 have same sequence of C.I at time segment 4, as highlighted in red in Table 4.18. At this time segment, grease condition ranked first, followed by leakage and normal condition. However, for F2T4, the lowest value of C.I is achieved by grease condition, followed by normal and leakage condition. The

inconsistency of sequence of C.I can be attributed to the low signal-to-noise ratio of AE signal at lower frequency range namely F2.

Table 4.19 shows the C.I of vibration signal in the best frequency range. By comparing the sequence of C.I at time segment 2, it was found that AE and vibration signal have the same sequence, as highlighted in green colour in Table 4.18 and Table 4.20. At this time segment, leakage condition shows the lowest value of C.I, followed by grease and normal condition. This is consistent with the postulation that leakage causes earlier valve opening and therefore resulted in lowest C.I at T2 compared to normal and grease condition.

Table 4.19: 95% confidence interval (C.I) of vibration signal at 800 rpm in the best frequency range

Frequency range	Valve conditions		
	Normal	Grease	Leakage
F1T3	0.169 - 0.199	0.249 - 0.279	0.0115 - 0.0415
F1T4	0.180 - 0.215	0.224 - 0.259	0.0674 - 0.102
F2T2	0.779 - 0.838	0.538 - 0.596	0.351 - 0.409
F2T4	0.0818 - 0.126	0.135 - 0.179	0.217 - 0.262
F4T2	0.887 - 0.944	0.821 - 0.878	0.469 - 0.526
F4T4	0.0330 - 0.0452	0.0462 - 0.0584	0.0181 - 0.0303
F6T2	0.844 - 0.897	0.694 - 0.747	0.443 - 0.496
F6T4	0.0622 - 0.0811	0.105 - 0.124	0.0341 - 0.0529

Similarly, vibration and AE signal at higher frequency range have same sequence of C.I at T3, as highlighted in orange in Table 4.18 and Table 4.20. As grease condition shows the highest value of C.I in T3 consistently for both vibration signal and AE signal at higher frequency range, this time segment T3 can be the feature for greased valve condition. Nevertheless, opposing to AE signal which shows little delay of

transient event at higher speed, vibration signal demonstrates more distinct delay and higher amplitude of transient event at T3 and 800 rpm, as displayed in Figure 4.13. This is because accelerometer is able to detect mechanical impacts better especially at higher rotational speed compared to AE signal. It is suggested that performance of AE signal can be improved by increasing sampling rate of data acquisition system, due to the fact that AE sensor needs higher resolution to represent signal at higher speed.

Table 4.20: Sequence of confidence interval (C.I) of vibration signal at 800 rpm in ascending order (1: lowest mean value and 3: highest mean value)

Frequency range	Valve conditions		
	Normal	Grease	Leakage
F1T3	2	3	1
F1T4	2	3	1
F2T2	3	2	1
F2T4	1	2	3
F4T2	3	2	1
F4T4	2	3	1
F6T2	3	2	1
F6T4	2	3	1

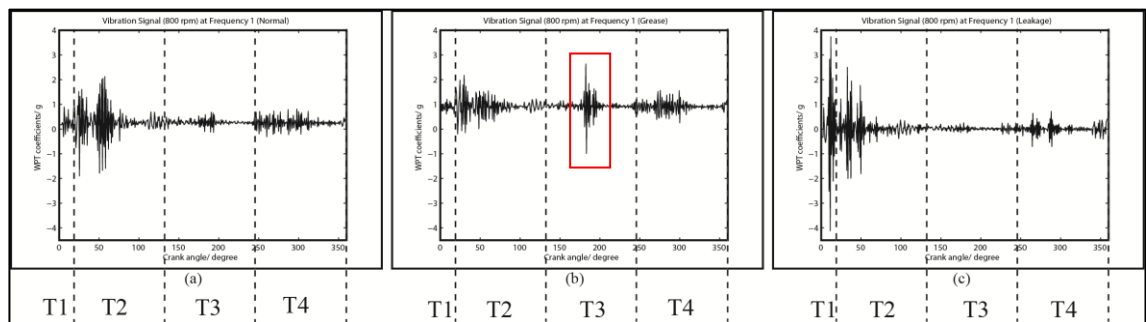


Figure 4.13: Comparison of vibration signal at F1 and 800 rpm under (a) normal (b) grease (c) leakage condition

For time segment 4, sequence of C.I at F1, F4, and F6 are the same, as highlighted in blue in Table 4.20. Leakage condition has the lowest value of C.I, followed by normal and grease condition. Nevertheless, at F2, the lowest value of C.I is achieved under normal condition, followed by grease and leakage condition. It is deduced that some of the signal characteristics are confined in the frequency range of 3.2 - 6.4 kHz (F2), thus causes different sequence of C.I at F2 compared to other frequency range. However, more studies are needed to confirm the deduction.

The following section discusses Tukey test result at low (450 rpm) and high (800 rpm) speed for both AE and vibration signals.

4.5.2 Discussions

By comparing Tukey test result of AE and vibration signal under low speed (450 rpm), it is obvious that both signals have same sequence of C.I at T1, T2, and T4 regardless of best frequency ranges, as displayed in Table 4.13 and Table 4.15. This consistency shows that C.I in these characteristic segments are reliable for effective valve monitoring as sampling rate selected in this study is sufficient to capture characteristics of signal under different valve conditions at low speed.

Nevertheless, sequences of C.I for both signals are different at T3 under 450 rpm. As mentioned in previous section, the sequences might be the same if the length of T3 is shortened. It was found that sequence of C.I of vibration signal under lower speed is the same as that under higher speed, for vibration signal and AE signal at higher frequency range, as displayed in Table 4.15, Table 4.18, and Table 4.20. Indeed, grease condition shows significant peak at higher speed, thus resulted in highest C.I value among other conditions. It is postulated that higher speed causes larger suction volume

flow rate and thus greater impact forces during valve fluttering event. This is further supported by the fact that C.I at higher speed lies in the range of 0.23 – 0.28 (for vibration and AE signal at higher frequency range), which is much higher than that at lower speed, which lies between 0.12 – 0.18 (for AE and vibration signal).

In fact, valve dynamics under different conditions can be deduced clearly from the sequence of C.I of both signals. For normal and leakage condition, valve opening event occurred at T2 (18.8°-131.4°). The opening impact causes normal condition to show highest C.I value at T2. As leakage condition has less opening impact, it recorded lower C.I value compared to normal condition. Meanwhile, for grease condition, valve opening event occurred earlier at T1 (0°-18.8°), resulted in highest C.I value at T1 and lowest C.I value at T2. In addition, leakage condition has lowest C.I value at T1 as the simulated leak is too small to cause significant changes at lower speed. However, leakage condition is accounted for significant changes of C.I value in T1 at higher speed. This will be discussed in the later part of this section.

The valve closing event is postulated at T3 (131.4°-244°), when piston was in transition between expansion and compression stroke. This event is most significant under grease condition due to valve fluttering motion. For vibration signal, the C.I value shows approximately 0.13 under grease condition, while normal and leakage condition has C.I value around 0.096 and 0.068 respectively. It is deduced that during this transition period, as pressure is built up consistently, suction plate closes from valve guard to valve seat, resulted in transient event at approximately 131° – 200° for normal and leakage condition, and a sharper peak at 175° - 200° for grease condition. In fact, the grease condition causes delay in timing as larger crank angle is needed to increase pressure which is sufficient to close the suction valve. This delay is consistent for both

AE and vibration signal, and therefore it can be a key feature in identifying greased valve.

The opening event of discharge valve occurred at T4 (244°-360°). Grease condition shows highest value of C.I as part of the fluids leaked through suction valve instead of discharge valve during compression cycle. This is because valve plate was not fully closed under grease condition. Hence, this condition has C.I value greater than 0.5 for all frequency ranges. Compared to normal condition which recorded C.I value around 0.3, at least 20% of energy is lost through suction valve under grease condition. Similarly, leakage condition has second highest C.I value due to the leakage of fluid across simulated passage at valve plate. In fact, the C.I value of leakage condition around 0.4 signifies approximately 10% of energy lost into suction valve. Lowest C.I value is achieved by normal condition as most fluids flow through discharge valve.

On the other hand, at higher speed, the sequence of C.I is different. This indicates different valve event compared to that under lower speed. Indeed, as opposed to 450 rpm which shows lowest C.I value in T1 under leakage condition, the C.I value is highest at 800 rpm. AE signal attained C.I value of approximately 0.29, which is very much higher, compared to grease and normal condition, where they recorded C.I value of 0.10 and 0.026 respectively. This is due to the fact that more fluid leaked into cylinder through simulated groove at higher speed, resulting in earlier valve opening event. Besides, loose closing of valve plate under grease condition also causes its C.I value at T1 to be the second highest after leakage condition. Consequently, leakage and grease condition shows lowest and second lowest C.I value at T2 respectively. As valve plate under normal condition closed tightly, greater valve opening impact can be observed and thus accounted for highest C.I value at T2. It was found that sequence of C.I has no difference between AE and vibration signal at T2. This feature can be the key

characteristic in detecting valve failures at higher speed. Nevertheless, more studies are needed in future to obtain the relationship between C.I value and severity level of different valve conditions.

With regard to valve closing timing at T3, it is obvious that vibration signal performed better in detecting valve closing impact and valve fluttering motion both at lower and higher speed. On the other hand, AE signal shows little delay in the valve fluttering event, as opposed to sharp delay of vibration signal, for grease condition at higher speed. In fact, higher rotation speed results in chaotic turbulent flow, increases the difficulty of signal processing of AE signal compared to vibration signal, due to broad frequency range of the former compared to the later. It is postulated that the current sampling frequency of 102.4 kHz is insufficient to extract actual mechanical and fluid motion at higher speed. Higher sampling rate of 1 MHz is suggested for improved performance of AE signal in future.

Inadequacy in sampling frequency is further shown in T4 at higher speed. Table 4.21 and Table 4.22 displayed combined C.I of AE and vibration signals at T3 and T4 under low and high speed. It can be seen that C.I value in T4 is much higher at lower speed under all valve conditions. Besides, by comparing both tables, it can be observed that the difference of C.I value between T3 and T4 at higher speed is almost the same while the difference is much larger at lower speed. These findings further support the postulation that discharge valve opening event at higher speed is not depicted well in AE and vibration signal. It also explained the inconsistency of C.I value between AE and vibration signal. Nevertheless, delay of discharge valve opening event can be seen clearly in Figure 4.12 (f) and (i) at F14 and F16. Due to fluid leakages, piston needs to move further upwards, producing larger crank angle and pressure difference in order to

open the discharge valve. As mentioned previously, larger sampling frequency may improve result of AE signal at higher speed.

Table 4.21: Joint confidence interval (C.I) of AE and vibration signal at T3 under different speed and valve conditions

Speed	AE and vibration C.I at T3		
	Normal	Grease	Leakage
450 rpm	0.084 - 0.22	0.12 - 0.18	0.056 - 0.13
800 rpm	0.056 - 0.20	0.23 - 0.28	0.012 - 0.10

Table 4.22: Joint confidence interval (C.I) of AE and vibration signal at T4 under different speed and valve conditions

Speed	Joint C.I at T4		
	Normal	Grease	Leakage
450 rpm	0.19 - 0.4	0.45 - 0.66	0.27 - 0.55
800 rpm	0.033 - 0.32	0.038 - 0.26	0.018 - 0.38

4.5.3 Conclusions

This sub-section compares the effect of speed and valve conditions on AE and vibration signal. It was found that effect of grease is greater at lower speed while leakage shows larger impact at higher speed. This causes difference in sequence of C.I in T1, T2 and T4 at different speed. Nevertheless, sequence of C.I at T3 is the same at both speeds, where grease condition records highest C.I value consistently regardless of speed. This feature can be the key characteristic of grease condition.

In comparing performance of AE and vibration signal at different speed and valve conditions, it is clear that AE is more sensitive in higher frequency range (19.2 kHz and above) while vibration signal shows better result at lower frequency range

(19.2 kHz and below). These two signals are consistent at lower speed (450 rpm) with same sequence of C.I regardless of frequency range. However, both signals show different sequence of C.I at higher speed (800 rpm), especially during compression stroke at T4. Due to complexity of fluid flow at higher speed, AE signal requires higher resolution and advanced signal processing technique to depict the fluid flow and mechanical motion. It is believed that the performance of AE signal can be further improved if the sampling frequency is increased to 1 MHz.

Statistical theory suggested that better estimation of C.I can be achieved with larger sample size. Therefore more data can be collected from specific time interval in future for better representation of valve conditions from C.I. It must be noted that the C.I computed in this study is limited to compressors in the same operating condition, namely rotational speed and work load.

In the coming section, the data collected from compressor operating in gas cooling plant will be compared with the test result in the current section.

4.6 Test data study

A compressor operated in Makhostia KLCC Gas District Cooling plant is selected as the test compressor for this study. Three measurements were taken over 4 months (August 2012 – December 2012), with 40 samples in each measurement, from a suction valve cover. Figure 4.14 and Figure 4.15 show the plan view and actual view while Table 4.23 displays specifications of this double acting, horizontal compressor. The objective of this test data study is to monitor condition of suction valve in the compressor, besides examining characteristics of AE and vibration signal compared to that in the test rig.

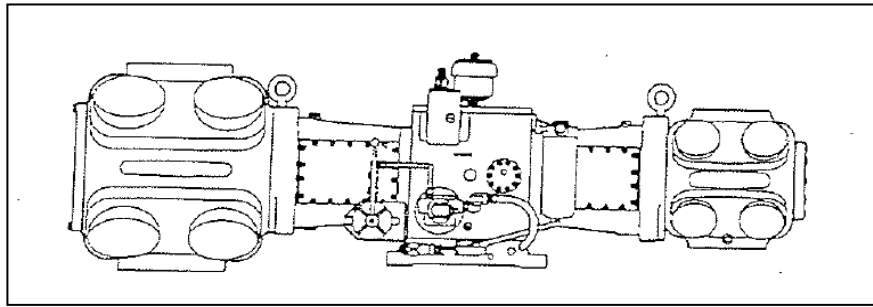


Figure 4.14: Plan view of test compressor JGJ/2



Figure 4.15: Test compressor JGJ/2

Table 4.23: Specification of test compressor JGJ/2

Model No	JGJ/ 2
Type	Double acting, horizontal compressor
Number of throw	2
Speed	1485 rpm
Fluid	Methane
Pressure suction line (kPaG)	722.98
Temperature suction line (Deg C)	46.23
Pressure discharge line (kPaG)	2862.97
Temperature discharge line (Deg C)	142.15

As the speed of compressor in plant is almost twice the speed of test rig, more noise can be seen from raw signal acquired. Hence, it is necessary to perform WPT decomposition in order to obtain signal with high signal-to-noise ratio. Figure 4.16 and Figure 4.17 show comparison between raw and WPT decomposed signal. It is obvious that raw AE signal contains more noise compared to raw vibration signal as it detects both mechanical and fluid motion. After decomposing these raw signals into 16 frequency ranges, it was found that these test signals correlates well with that in the test rig. Suction valve opening event can be seen clearly at crank angle approximately 35° - 45° while valve closing event is shown at crank angle approximately 165° - 175° for both signal at F16 (48.0 – 51.2 kHz), as displayed in Figure 4.16 (b) and Figure 4.17(b). Due to high rotational speed which produces larger mechanical impact, vibration signal remain clear in F16.

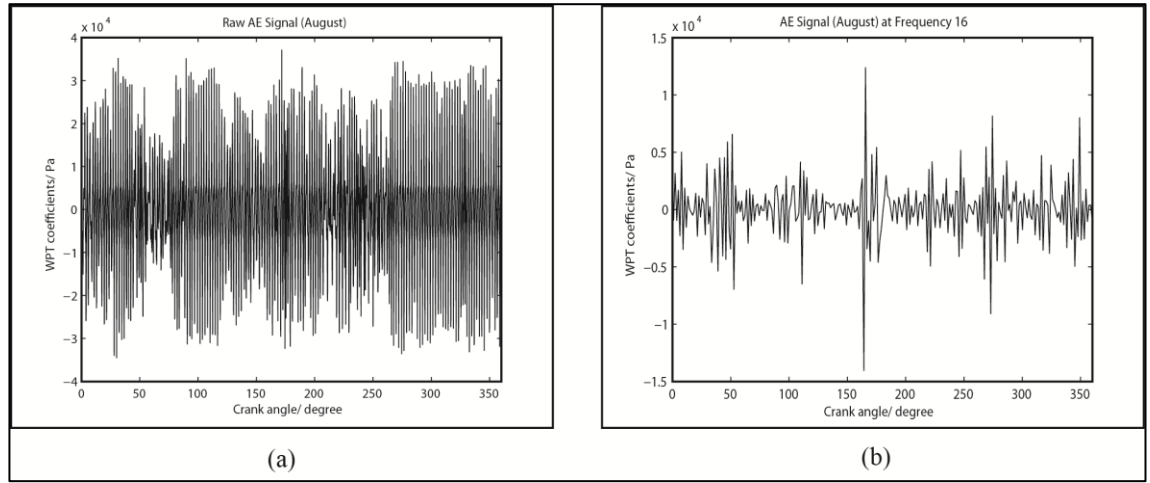


Figure 4.16: Comparison of AE signal (a) Raw signal (b) WPT decomposed signal

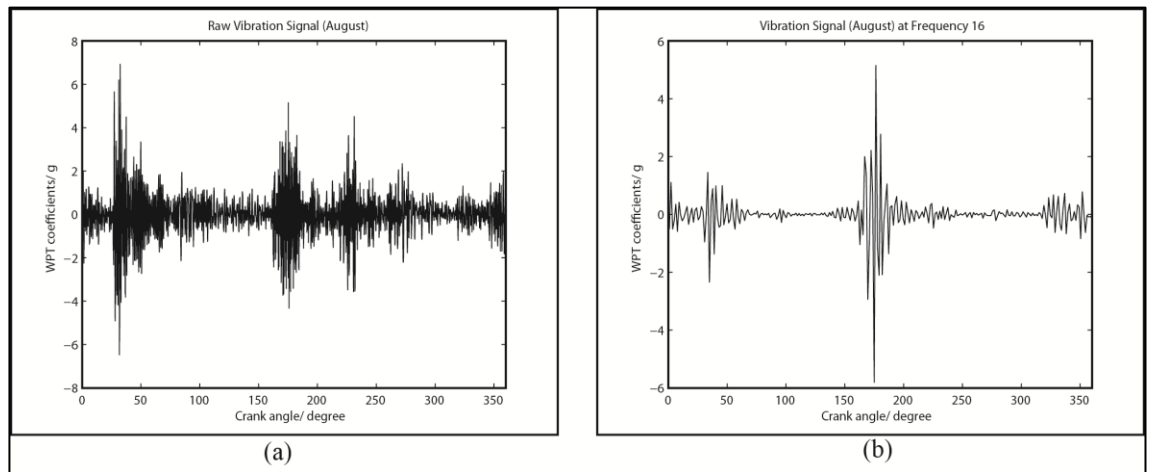


Figure 4.17: Comparison of vibration signal (a) Raw signal (b) WPT decomposed signal

Result from test rig suggested that under grease valve condition, valve opening event occurred at crank angle smaller than 50^0 . For valve closing event, grease condition shows delay in valve timing at crank angle approximately 175^0 , with amplitude almost the same as the valve opening impact. Figure 4.18 (c) shows increased amplitude of valve closing event while Figure 4.18 (d) shows delay in valve closing event, for vibration and AE signal acquired from test rig under grease condition at 800

rpm. Earlier valve opening event at crank angle approximately 25^0 under grease condition can be observed in Figure 4.18 (d) for AE signal.

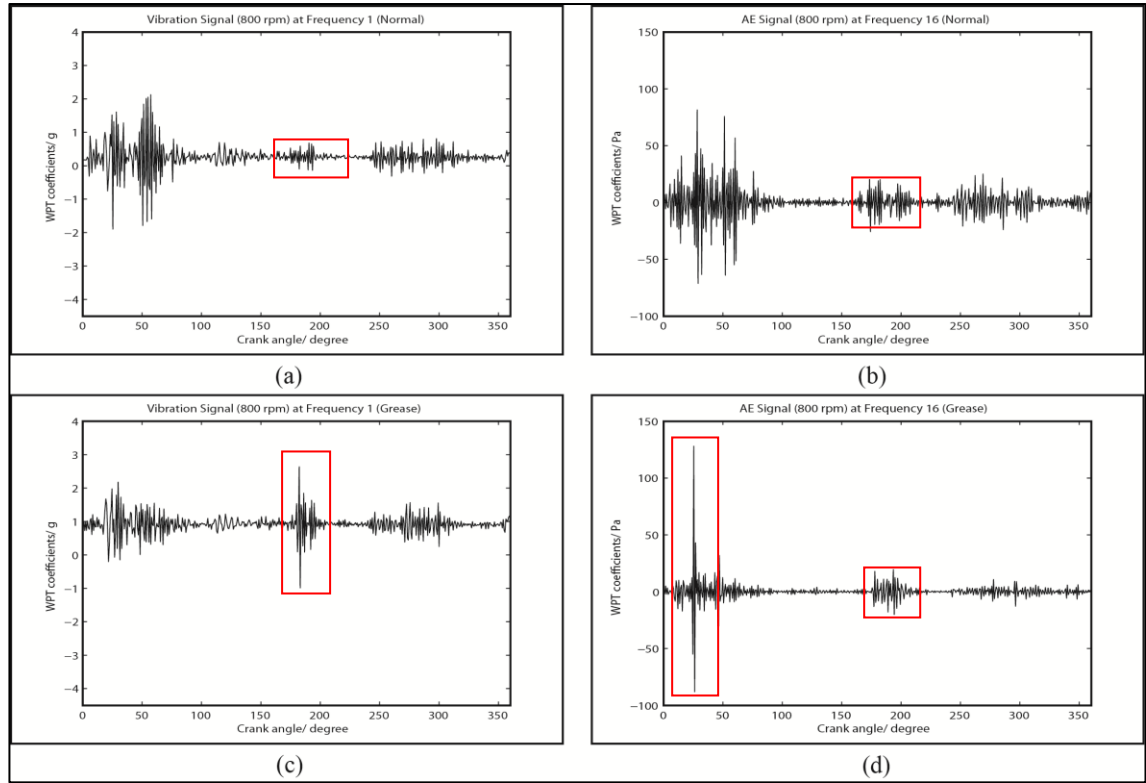


Figure 4.18: Comparison of vibration and AE signal at 800 rpm under normal (a)-(b) and grease (c)-(d) condition

In fact, early opening of valve at crank angle approximately 30^0 can be seen consistently over three measurements from vibration signals acquired from plant, as displayed in Figure 4.20. For AE signal, the opening impact is most distinct during September, as shown in Figure 4.19 (b). Both signals show characteristic of greased valve condition.

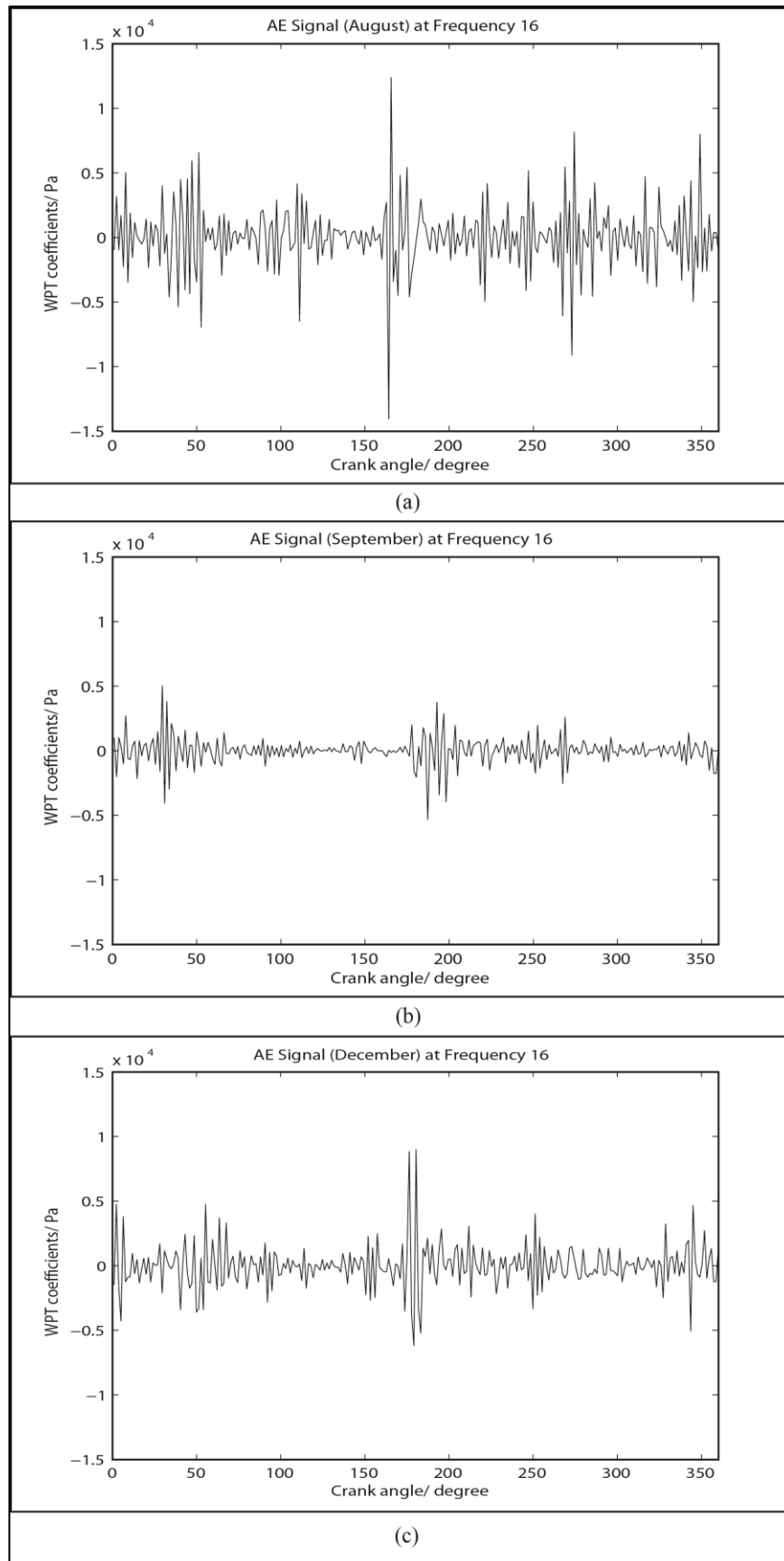


Figure 4.19: Comparison of AE signal during different months (a) August (b) September (c) December

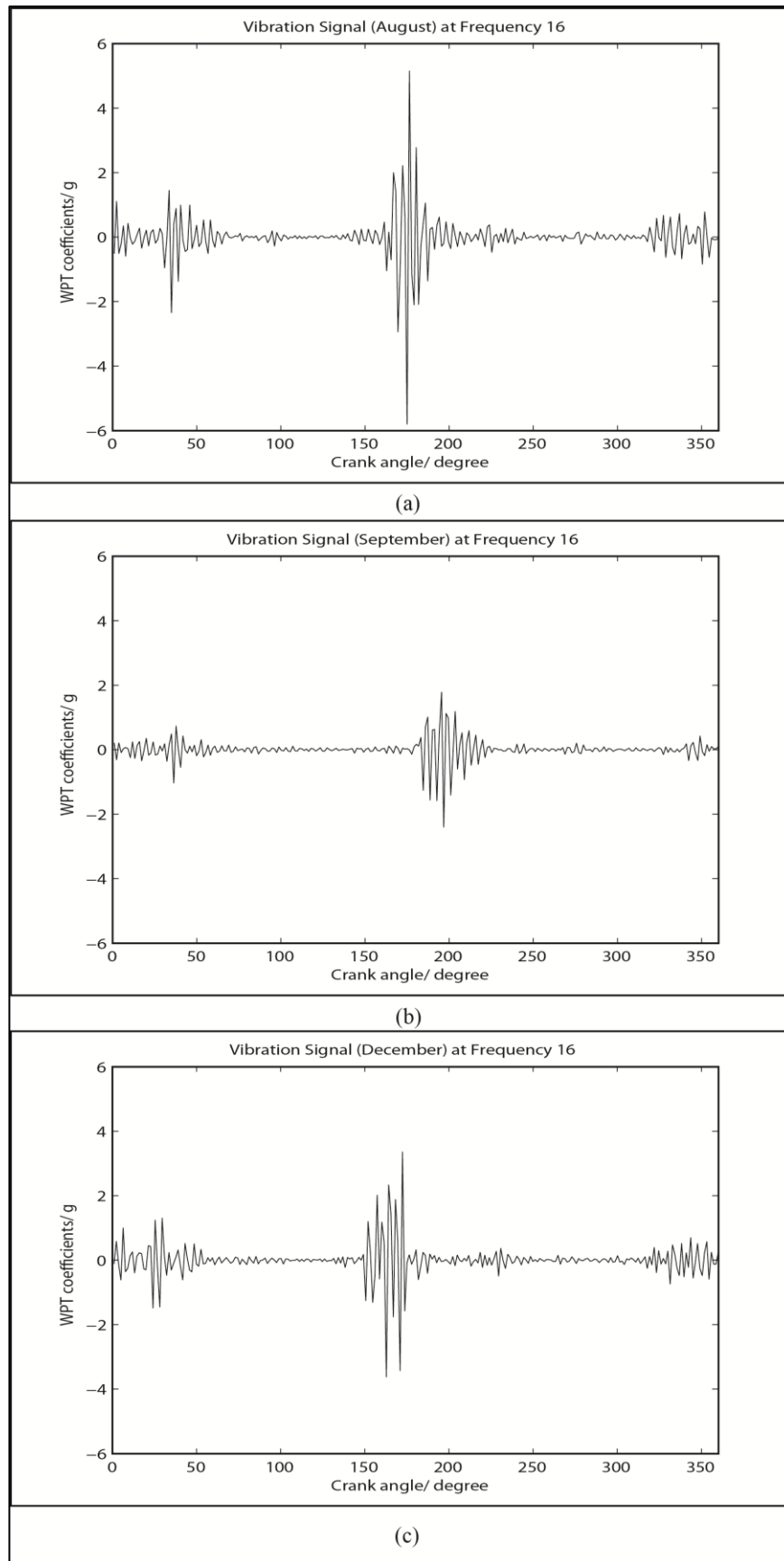


Figure 4.20: Comparison of vibration signal during different months (a) August (b) September (c) December

For valve closing event, AE and vibration signal shows delayed valve timing at crank angle approximately 175° during August and December. Nevertheless, the valve closing timing is approximately 200° during September, as shown in Figure 4.19 (b) and Figure 4.20 (b). More measurements are needed in future to confirm the postulation of increasing grease condition in the suction valve.

In comparing amplitude trend of normalized energy for AE and vibration signals over three measurements, mean of 40 samples was computed for each measurement.

Figure 4.21 shows normalized energy value of both signals in different time segments over three measurements from August to December 2012. It was found that normalized energy value during valve closing event increases consistently from August to December for AE signal, which further supports the postulation of grease condition in the suction valve. Similarly, vibration signal shows highest peak at T3 for each measurement, with a slight decrease during September. As the normalized energy value during valve closing event (T3) is significantly larger than that during valve opening event (T2) for all measurements, it is deduced that valve fluttering event occurred at T3 due to grease valve condition. However, more measurements should be taken to confirm the diagnosis.

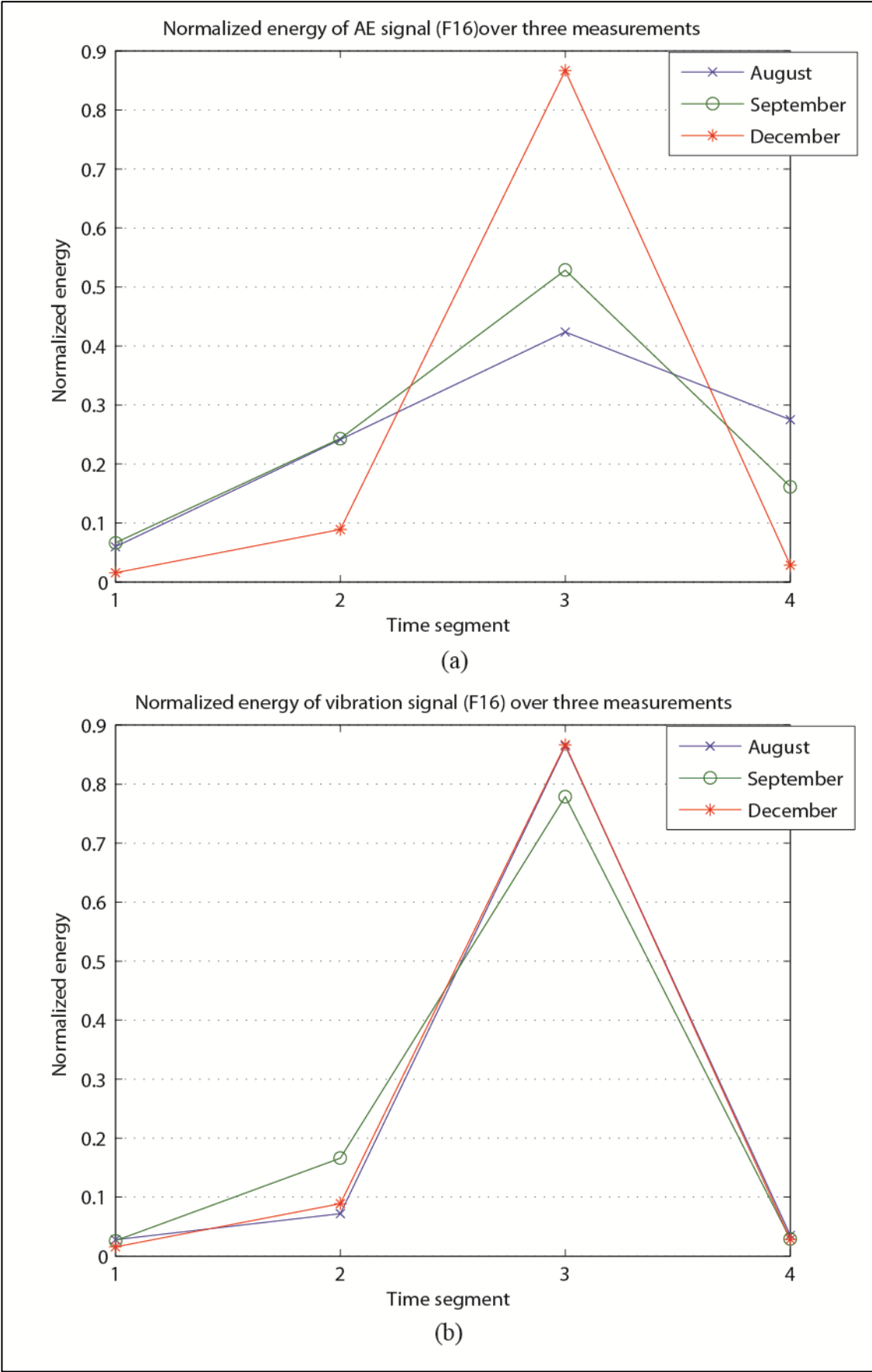


Figure 4.21: Comparison of normalized energy over three measurements for (a) AE signal (b) Vibration signal

It must be noted that characteristics of signals obtained from test rig under different simulated condition were based on the assumption that compressor was working in the same operating condition. Nevertheless, in actual plant measurement, there are always possibilities that compressor operating condition altered due to increasing workload or changing of suction line pressure. These external factors may affect the signal trend monitored. Thus, it is advisable to gather all plant information before valve diagnosis. Machine learning techniques such as support vector machines can ease valve diagnosis in future by training each and every characteristics of signal under different operating condition. Valve diagnosis result will then be obtained in consideration of compressor operating condition, thus providing fast and accurate estimation of valve condition.

4.7 Summary

This chapter began with signal comparison of AE and vibration signal under different conditions and speeds. To enable fast and effective inspection of valve, a few parameters were suggested as indicators for valve monitoring. By employing one way analysis of variance (ANOVA) and Tukey comparison test, normalized energy was selected as the best parameter representing valve conditions. Characteristics of AE and vibration signals were obtained later by comparing sequence of C.I of normalized energy under different speeds and valve conditions. It was found that effect of valve leakage is more significant at higher speed, as it showed much earlier valve opening impact than grease condition at higher speed.

In addition, grease condition showed early valve opening event and late valve closing event at both low and high speed. Besides, amplitude of valve closing event was extremely high under grease condition due to valve fluttering motion. The characteristics of greased valve signal were found in a test data study in the last section of the chapter. However, more measurements are needed to confirm the diagnosis result.

Next chapter presents an advanced valve diagnosis technique by using machine learning method. As C.I computed in this chapter requires large sampling size for better estimation of valve condition, it often causes inconvenience among plant personnel as it is impractical to collect and analyze huge amount of information from the plant. Machine learning in the next chapter can overcome this deficiency by classifying signals into its corresponding condition automatically without interpretation from plant personnel. In fact, this method can be further improved in future by including compressor operating condition into the system, thus enabling fast and efficient valve diagnosis.

CHAPTER 5 SIGNAL CLASSIFICATION

5.1 Overview

One way analysis of variance (ANOVA) and Tukey test in the previous chapter identified characteristic time-frequency segments which described condition of valves. For automated classification of signals, these time-frequency segments will serve as the input vectors as they carry much information about the valve conditions. This chapter explains classification of normal, grease, and leakage condition of valves through support vector machine (SVM). SVM is a supervised learning technique developed based on statistical learning theory, with the objective of obtaining optimal separating hyper-plane which separates two classes being tested with maximum distance.

To apply the SVM technique in signal classification, some of the theoretical backgrounds of this technique must first to be understood. Hence, this chapter begins with some mathematical backgrounds of SVM concept before proceeds to the methodology of signal classification. This is followed by parameter tuning to obtain the best parameters for SVM classifiers. The chapter ends with comparison of classification results between AE and vibration signals at low speed (450 rpm) and at high speed (800 rpm).

5.2 Theoretical background

5.2.1 Risk minimization

There are various ways to classify two sets of data. The classical pattern recognition method such as the artificial neural networks (ANN) involves obtaining a set of coefficient values (weights), $w = (w^1, \dots, w^n)$ representing a set of linear indicator functions through empirical risk minimization (ERM), which minimizes the error of

training data. This set of linear indicator function will be substituted into the learning/decision function to classify test data. Nevertheless, upper bound of the actual risk, $R(w)$ is actually dependent on the empirical risk and the Vapnik Chervonenkis (VC) confidence (Vapnik, 1995), as shown in Equation 5.1. The first term on the right hand side is empirical risk, $R_{emp}(w)$ which measures error on training data while the second term is VC confidence, which incorporates the VC dimension, h , total number of training data, l , and confidence level, η in its formulation. Equation 5.2 displays the empirical risk, $R_{emp}(w)$ formulation, where l denotes total number of training data, y_j denotes actual output of training data, $f(x_j, w)$ denotes decision function in which the predicted output is determined, and w is the coefficient values (weights) for the indicator function.

$$R(w) \leq R_{emp}(w) + \sqrt{\frac{h(\log(2l/h) + 1) - \log(\eta/4)}{l}} \quad (5.1)$$

$$R_{emp}(w) = \frac{1}{l} \sum_{j=1}^l (y_j - f(x_j, w))^2 \quad (5.2)$$

In fact, the VC confidence is affected by VC dimension, h where it measures capacity of learning machine (decision functions). A right balance should be made between training accuracy and capacity of the learning machine for best generalization performance, which is the ability to learn any training set without errors (Burges, 1998). As most of the classical pattern recognition methods such as the ANN develop their algorithms mainly based on ERM, which minimizes the first term of Equation 5.1, they tend to over-fit data especially when the network is too complex for the given number of training data. This is because the VC confidence will still be large due to large VC dimension even the algorithm can minimize empirical risk to zero. Moreover, coefficient values (weights) found by using ERM through back propagation method are

not guaranteed to be the global minimum as the empirical risk functional has many local minima (Vapnik, 1999). The optimization procedures might converge to some local minimum and thus lead to large testing error.

To minimize actual risk, it is necessary to minimize empirical risk while controlling VC dimension of the learning machine. It can be achieved through structural risk minimization (SRM). SRM introduces the concept of structure, where possible sets of learning (decision) function S are composed of nested subsets of functions, as displayed in Equation 5.3, where each subset has its own capacity. Figure 5.1 shows the nested subsets of functions with increasing capacity h . SRM involves finding subsets which minimizes bounds on the actual risk (Burges, 1998). In other words, SRM minimizes both the empirical risk and the VC confidence at the same time.

$$S_1 \subset S_2 \subset S_3 \subset S_4 \dots S_n \quad (5.3)$$

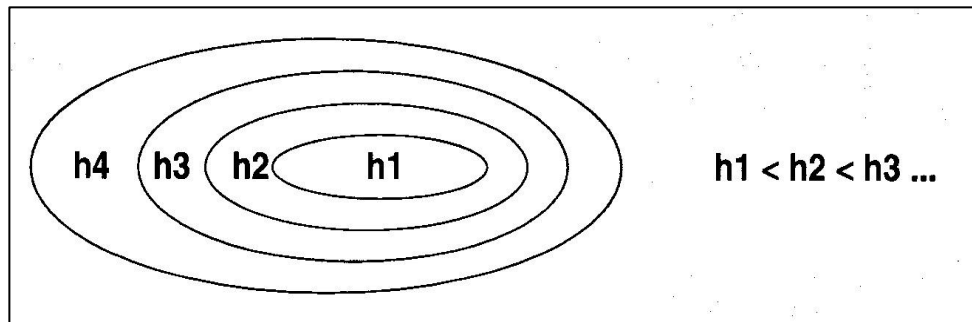


Figure 5.1: Nested subset of functions (Burges, 1998)

5.2.2 Support vector machine (SVM)

As shown in Figure 5.2, there are several possible ways to separate two classes. Support vector machine (SVM) involves getting the optimal separating hyper-plane which separates two different classes with maximal margin without error.

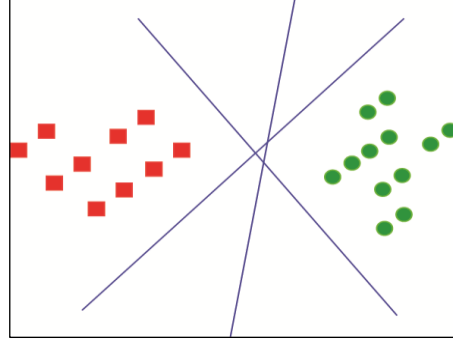


Figure 5.2: Possible hyper-planes to separate two classes

In fact, maximizing the margin is equivalent to minimizing VC dimension h , as illustrated in Equation 5.4, where Δ denotes the margin, R denotes radius of the hyper-sphere enclosing all data points and n denotes dimension of the space.

$$h \leq \min \left(\left\lceil \frac{R^2}{\Delta^2} \right\rceil, n \right) + 1 \quad (5.4)$$

According to Vapnik (1999), VC dimension of the set of linear indicator functions in n dimensional coordinate space is equal to $h = n + 1$. By maximizing the margin between the two classes Δ , upper bound of the VC dimension h can be minimized and thus reducing the VC confidence. This can ultimately reduce the actual risk.

Suppose there are l sets of training data, as shown in (5.5), which can be separated by the optimal separating hyper-plane into two classes, $y_i = +1$ and $y_i = -1$.

$$(x_1, y_1), \dots, (x_l, y_l), \quad x_i \in \mathfrak{R}^n, \quad y \in \{+1, -1\} \quad (5.5)$$

$$H : \{\vec{x}_i | (\vec{x}_i \cdot \vec{w}) + b = 0\} \quad (5.6)$$

The optimal separating hyper-plane H in Equation 5.6 separates the two classes in such a way that the distance between the hyper-plane and the nearest data points in each class is maximal. Thus, sign of hyper-plane H can be decision function for classifier, as expressed in Equation 5.7, where data which fall in the range of $\vec{x}_i \cdot \vec{w} + b \geq 0$ belong to class $y = +1$ while data in the range of $\vec{x}_i \cdot \vec{w} + b \leq 0$ belong to class $y = -1$.

$$f(x) = \text{sign}(\vec{w} \cdot \vec{x}_i + b) \quad (5.7)$$

Nevertheless, redundancy occurs when there are many planes with $(\vec{x}_i \cdot k\vec{w}) + kb = 0$ for any $k \neq 0$. Thus, Vapnik (1995) introduced a canonical hyper-plane by enforcing constraint which states that the closest points to the hyper-plane should be at a unit distance from the plane. Equation 5.8 and 5.9 describe this concept:

$$H_1 : \{\vec{x}_i | \vec{x}_i \cdot \vec{w} + b \geq +1 - \xi\} \quad \text{for } y_i = +1 \quad (5.8)$$

$$H_2 : \{\vec{x}_i | \vec{x}_i \cdot \vec{w} + b \leq -1 + \xi\} \quad \text{for } y_i = -1 \quad (5.9)$$

$$\xi_i \geq 0 \quad \forall i \quad (5.10)$$

where, \vec{x}_i is the training data, \vec{w} is the vector normal to the hyper-plane and b defines location of the plane. To enable SVM classifier to classify data with some tolerance for misclassification, especially when training data are non-separable, the positive slack variable ξ_i is introduced, as expressed in Equation 5.10. Equation 5.8 and 5.9 can be combined to form Equation 5.11.

$$y_i(\vec{x}_i \cdot \vec{w} + b) \geq 1 - \xi \quad \forall i \quad (5.11)$$

Figure 5.3 shows classification of two classes through SVM concept. It should be noted that the nearest data points to optimal hyper-plane H lie in plane H_1 and H_2 . They are termed as the support vectors (SVs) and displayed as black and white circles in Figure 5.3. The optimal hyper-plane H will lie in the middle of H_1 and H_2 . Perpendicular distance from the optimal hyper-plane H to origin, O is computed as $|b|/\|\vec{w}\|$ while distance from the plane of one class (H_1 or H_2) to the misclassified data is computed as $\xi_i/\|\vec{w}\|$, where $\|\vec{w}\|$ is the Euclidean norm of \vec{w} .

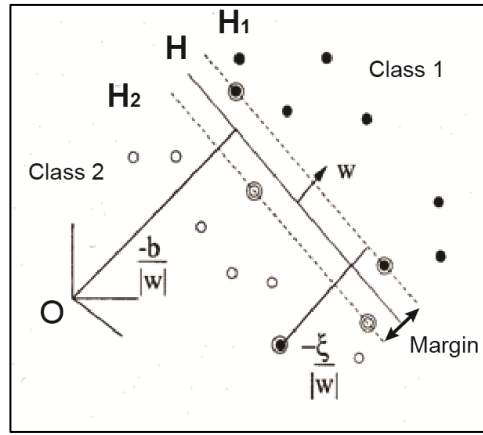


Figure 5.3: Classification of two classes using SVM

In Figure 5.3, margin of SVM classifier Δ is the distance from plane H_1 to H_2 . It can be computed as in Equation 5.12 (Gunn, 1998). Hence, to maximize the margin, $\|\vec{w}\|$ needs to be minimized.

$$\Delta = \frac{2}{\|\vec{w}\|} \quad (5.12)$$

An objective function can be constructed to achieve this goal, as stated in Equation 5.13, under the constraints shown in Equation 5.10 and 5.11. Thus, by minimizing the objective function, margin Δ can be maximized while training errors can

be minimized, as $\sum_i \xi_i$ represents upper bound of number of training errors. C is the penalty parameter determined by user, where larger C corresponds to assigning higher penalty to the training errors.

$$\min_{\vec{w}, b, \xi} \frac{1}{2} \vec{w}^T \vec{w} + C \sum_{i=1}^l \xi_i \quad (5.13)$$

The optimal hyper-plane can be obtained by solving this quadratic programming problem. A primal Lagrangian is formed where the constraint equations are multiplied by positive Lagrange multipliers and subtracted from the objective function, as displayed in Equation 5.14:

$$L_p = \frac{1}{2} \|\vec{w}\|^2 + C \sum_i \xi_i - \sum_i \alpha_i \{y_i (\vec{x}_i \cdot \vec{w} + b) - 1 + \xi_i\} - \sum_i \mu_i \xi_i \quad (5.14)$$

where, α_i and μ_i are positive Lagrange multipliers for the constraint, and i is the index of training data, with $i=1, \dots, l$. In fact, μ_i is the Lagrange multiplier introduced to ensure the positivity of ξ_i . For a convex quadratic programming problem, the primal Lagrangian L_p can be solved by obtaining derivatives of L_p with respect to \vec{w} , b , and ξ_i at its optimal point, as shown in Equation 5.15 to 5.17.

$$\frac{\partial L_p}{\partial \vec{w}} = \vec{w} - \sum_i \alpha_i y_i \vec{x}_i = 0 \quad (5.15)$$

$$\frac{\partial L_p}{\partial b} = -\sum_i \alpha_i y_i = 0 \quad (5.16)$$

$$\frac{\partial L_p}{\partial \xi_i} = C - \alpha_i - \mu_i = 0 \quad (5.17)$$

It must be noted that the Lagrangian has to be minimized with respect to \vec{w} and b and maximized with respect to $\alpha_i \geq 0$ (Gunn, 1998). This Lagrangian duality enables the problem to be solved either in the primal or dual way. In other words, the solution can

be obtained by minimizing the primal Lagrangian L_P with respect to \vec{w} and b or maximizing the dual Lagrangian L_D subjects to the constraint that the derivative of L_P with respect to \vec{w} and b vanish and $\alpha_i \geq 0$, as displayed in Equation 5.18.

$$\max_{\alpha} L_D = \max_{\alpha} \left(\min_{w, b} L_P \right) \quad (5.18)$$

As dual Lagrangian offers a much easier way to solve the problem, solution of the derivatives, Equation 5.19 and 5.20, will be substituted back into Equation 5.14 to form dual Lagrangian. Hence, the solution can be obtained by maximizing L_D with respect to α , as displayed in Equation 5.21, subject to constraints as shown in Equation 5.20 and 5.22. The penalty error C will serve as the upper bound of α_i to ensure $\xi_i=0$ (Burges, 1998).

$$\vec{w} = \sum_i \alpha_i y_i \vec{x}_i \quad (5.19)$$

$$\sum_i \alpha_i y_i = 0 \quad (5.20)$$

$$L_D = \sum_i \alpha_i - \frac{1}{2} \sum_{i,j} \alpha_i \alpha_j y_i y_j \vec{x}_i \cdot \vec{x}_j \quad (5.21)$$

$$0 \leq \alpha_i \leq C \quad (5.22)$$

Thus, by maximizing Equation 5.21, the Lagrange multiplier α_i of every training point can be obtained. Those points with $\alpha_i > 0$ are termed “support vectors” as they are closest to the optimal hyper-plane, and lie on one of the hyper-plane H_1 or H_2 . The solution \vec{w} can be found by substituting α_i of every training point into Equation 5.19 while the value of b can be obtained by substituting the value of \vec{w} , α_i , ξ_i and training samples (x_i, y_i) into Equation 5.23.

$$\alpha_i \{y_i (\vec{x}_i \cdot \vec{w} + b) - 1 + \xi_i\} = 0 \quad (5.23)$$

Support vectors on hyper-plane H_1 or H_2 will decide location of the optimal separating hyper-plane, which serves as a decision boundary for data classification. Once the optimal separating hyper-plane was found, all other training samples can be removed from the SVM classifier. Other samples can be tested on this classifier for its classification performance.

5.3 Methodology for SVM signal classification

5.3.1 Non-linear classification kernel

The optimal separating hyper-plane above is obtained based on the assumption that the decision function is a linear function of data. However, in real world applications, data acquired might not be linearly separable. To enable classification of non-linearly separable data, data are mapped from its original input space X to a higher dimensional feature space F , as shown in Equation 5.24.

$$\Phi : \vec{x}_i \mapsto \Phi(\vec{x}_i) \in F \quad (5.24)$$

Therefore, data which are not linearly separable in the original space X might be linearly separable after transforming them into higher dimensional feature space F , as illustrated in Figure 5.4. The optimal separating hyper-plane will be constructed in this feature space to classify transformed feature vectors $\Phi(\vec{x}_i)$. The feature vectors $\Phi(\vec{x}_i)$ will then be transformed back to its original space X . Thus, the linear decision boundary in F will appear as a non-linear decision boundary in X .

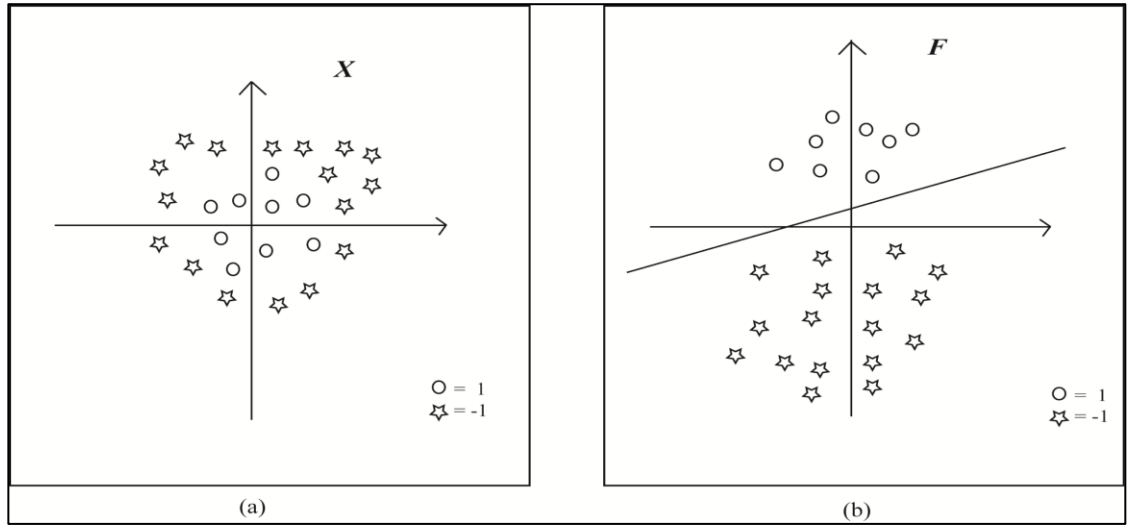


Figure 5.4: (a) Data in original input space X (b) Data in transformed feature space F

Nevertheless, it is computationally intensive to transform all input data \vec{x}_i into its corresponding feature vectors $\Phi(\vec{x}_i)$. Since the objective and decision function in the classifier involve only the inner product of input vectors $\vec{x}_i \cdot \vec{x}_j$, kernel function $K(\vec{x}_i, \vec{x}_j)$ is introduced to compute the inner products of feature vectors $\Phi(\vec{x}_i) \cdot \Phi(\vec{x}_j)$ from the input vector \vec{x}_i , without computing each feature vector explicitly, as shown in Equation 5.25. Therefore, the decision function is computed in the form of kernel function, as expressed in Equation 5.26.

$$K(\vec{x}_i, \vec{x}_j) = \Phi(\vec{x}_i) \cdot \Phi(\vec{x}_j) \quad (5.25)$$

$$f(\vec{x}_j) = \text{sign} \left(\sum_i y_i \alpha_i K(\vec{x}_i, \vec{x}_j) + b \right) \quad (5.26)$$

The kernel function enables efficient non-linear mapping from input space X to feature space F . Nevertheless, only functions that satisfy Mercer's condition can be considered as kernel function (Vapnik, 1995). Generally there are four common kernel functions in SVM classification, namely linear, polynomial, Gaussian radial basis, and

sigmoid function. These kernel functions are computed according to the list of formulae in Table 5.1.

Table 5. 1: Type of kernel functions

Type of kernel	Kernel function, $K(\vec{x}_i \cdot \vec{x}_j)$
Linear	$\vec{x}_i \cdot \vec{x}_j$
Polynomial	$(\vec{x}_i \cdot \vec{x}_j + 1)^p$
Gaussian radial basis	$\exp\left(-\gamma\ \vec{x}_i - \vec{x}_j\ ^2\right)$
Sigmoid	$\tanh(\kappa\vec{x}_i \cdot \vec{x}_j - \delta)$

In fact, the selection of kernel function is depending on the classification problem. Gaussian radial basis function is chosen as the kernel function in the present study due to its popularity and high success rate in various classification problems (Wang et al., 2009). Besides, the number of hyper-parameters is lesser in Gaussian radial basis function compared to polynomial function. These hyper-parameters are not desirable as they may affect complexity of model selection (Hsu, et al., 2010). Moreover, the Gaussian radial basis function has fewer numerical difficulties, as its value lies in the range of 0 to 1, as opposed to the polynomial function where its value may reach infinity. On the other hand, the sigmoid function is not preferable as not all sigmoid functions fulfil the Mercer's condition (Vapnik, 1995). It is often used as a proxy for neural networks.

However, linear function is preferable over Gaussian radial basis function if the number of features is large (Hsu, et al., 2010). In this study, as there are only four features being tested, the Gaussian radial basis function still remains as the most

suitable kernel function. The best value of γ in the kernel function is obtained through cross-validation technique and included in section 5.4.

5.3.2 Multiclass classification

Since SVM classifier is a binary classifier in nature, it can only perform classification for a two-class problem. Nevertheless, most of the real world problems are multiclass problem. In the current study, three classes were investigated, namely the normal, grease, and leakage conditions. Hence, a multiclass classification strategy should be developed to extend the binary classifier to a multiclass classifier. This can be achieved by either solving a few larger optimization problems which includes data from all classes or by combining several binary classifiers through a voting system. Detailed explanations regarding the two strategies are described in the following section.

5.3.2.1 One-against-all (OAA)

One-against-all (OAA) strategy is the earliest implementation of SVM multiclass classification. It constructs k SVM classifiers where k is the number of classes. In s^{th} SVM classifier, one class is trained with data from the s^{th} class and labelled as positive while the other class is trained with all the other data and labelled as negative. Hence for l training data $(x_1, y_1), \dots, (x_l, y_l)$, where $x_i \in \mathcal{R}^n$, $i = 1, \dots, l$ and $y_i \in \{1, \dots, k\}$ is the class for x_i , the s^{th} SVM classifier solves the optimization problem as in Equation 5.27 subject to the constraints imposed by Equation 5.28 to 5.30, where C is the penalty parameter.

$$\min_{\vec{w}^s, b^s, \xi^s} \frac{1}{2} (\vec{w}^s)^T \vec{w}^s + C \sum_{i=1}^l \xi_i^s \quad (5.27)$$

$$(\vec{w}^s)^T \phi(\vec{x}_i) + b^s \geq 1 - \xi_i^s \quad \text{if} \quad y_i = s \quad (5.28)$$

$$(\vec{w}^s)^T \phi(\vec{x}_i) + b^s \leq -1 + \xi_i^s \text{ if } y_i \neq s \quad (5.29)$$

$$\xi_i^s \geq 0, i=1, \dots, l \quad (5.30)$$

The function ϕ mapped the training data \vec{x}_i to a higher dimensional space for non-linear classification. Solving Equation 5.27 will result in k decision functions. The class of data, c will be the class having the largest value of the decision function, as illustrated in Equation 5.31. The concept of OAA method is shown in Figure 5.5.

$$c \equiv \arg \max_{s=1, \dots, k} \left((\vec{w}^s)^T \phi(x) + b^s \right) \quad (5.31)$$

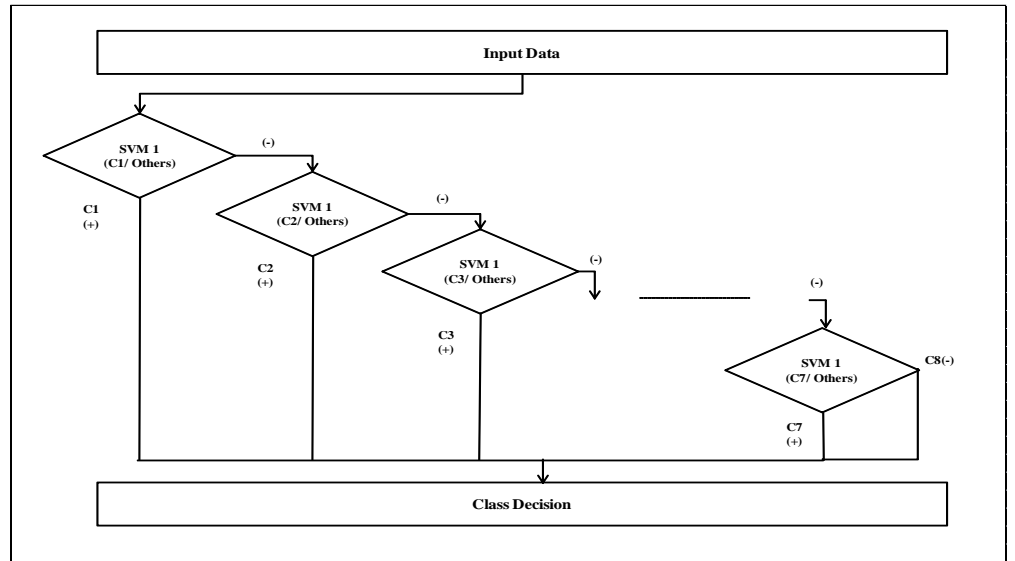


Figure 5.5: One-against-all (OAA) strategy

5.3.2.2 One-against-one (OAO)

The one-against-one (OAO) method trains all possible pair of classes and the final class is determined through a voting system. Generally, it constructs $k(k-1)/2$ classifiers where each one is trained on data from two classes. The classification problem is solved as in Equation 5.32 for training data obtained from s^{th} and m^{th} classes, subject to constraints 5.33 to 5.35.

$$\min_{\vec{w}^{sm}, b^{sm}, \xi^{sm}} \frac{1}{2} (\vec{w}^{sm})^T \vec{w}^{sm} + C \sum_{i=1}^l \xi_i^{sm} \quad (5.32)$$

$$(\vec{w}^{sm})^T \phi(\vec{x}_i) + b^{sm} \geq 1 - \xi_i^{sm} \quad \text{if } y_i = s \quad (5.33)$$

$$(\vec{w}^{sm})^T \phi(\vec{x}_i) + b^{sm} \leq -1 + \xi_i^{sm} \quad \text{if } y_i = m \quad (5.34)$$

$$\xi_i^{sm} \geq 0, i = 1, \dots, l \quad (5.35)$$

To determine the class of data, a voting strategy is applied on the result of decision function (Friedman, 1996). If the decision function $\text{sign}((\vec{w}^{sm})^T \phi(x) + b^{sm})$ shows that the training data \vec{x}_i is from s^{th} class, one vote will be given to the s^{th} class. Else, the vote for m^{th} class will be added by one. The class of data c will be the class having the largest vote. For the case where two classifiers have the same vote, the classifier with smaller index will be selected, though it may not be a good strategy. This voting approach is described as the Max Win strategy. The concept of OAO method is illustrated in Figure 5.6.

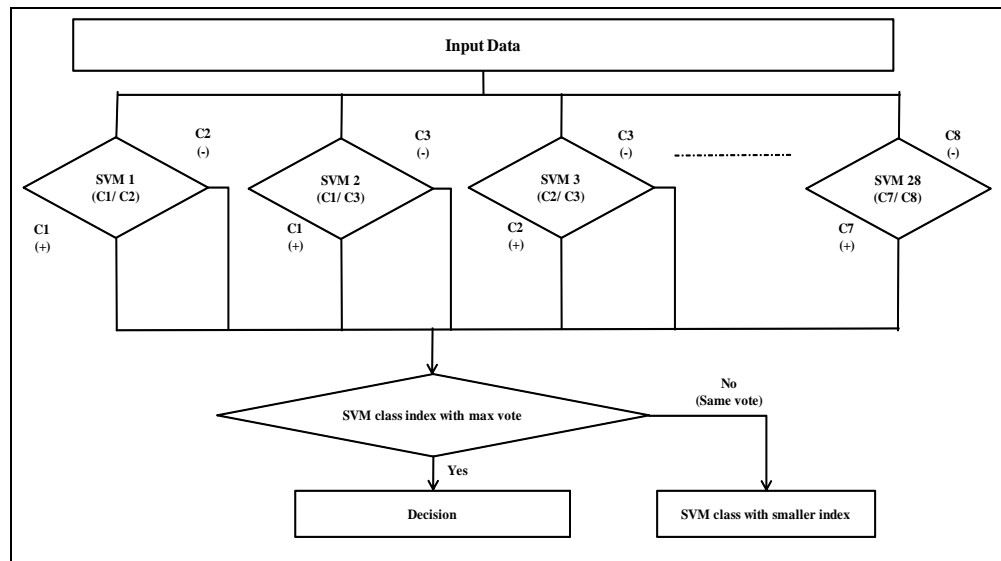


Figure 5.6: One-against-one (OAO) strategy

This study employed one-against-one (OAO) approach for multi-class classification. Though number of classifiers constructed are usually larger compared to one-against-all (OAA) approach, the OAO strategy requires lesser training time, thus it is more suitable for practical usage (Hsu and Lin, 2002). This is because training data for each classifier are usually smaller under OAO strategy. In fact, for the OAO strategy, each classifier requires $\left(\frac{2l}{k}\right)^d$ training data, where d is the dimension size of the optimization problem. Meanwhile, for the OAA method, each classifier requires l^d training data. Hence, as the number of class k increases, training data required for each classifier are generally smaller for OAO method compared to OAA, although the total training data for OAO is $\frac{k(k-1)}{2}O\left(\left(\frac{2l}{k}\right)^d\right)$, which is in fact larger than the OAA method, as the later requires a total training data of $kO(l^d)$ (Lin, 2006).

5.3.3 Process flow for SVM classification

Signal classification of AE and vibration signal began with feeding input vectors of 4 features into the classifier. These input vectors are normalized energy value at 4 time segments obtained from the previous chapter, which represent 4 main features of signals. To enable non-linear classification, the data were transformed into a higher dimensional space through Gaussian radial basis kernel function.

There are two parameters to be determined for the Gaussian radial basis function kernel classifier, namely penalty error C from the objective function (Equation 5.32) and γ from the Gaussian radial basis function. To obtain better classification result, the best (C, γ) should be chosen. A cross-validation procedure was proposed to identify suitable (C, γ) such that the classifier can predict unknown data (testing data) accurately.

As there were three valve conditions simulated in this study, three binary classifiers were constructed, namely Class 1-2, Class 1-3, and Class 2-3 where Class 1, Class 2, and Class 3 represent normal, grease, and leakage condition respectively.

Each classifier obtained its best (C, γ) from cross validation. These (C, γ) values were then fed into its corresponding classifier for training purposes. During the training process, SVM algorithm computes support vectors α_i and b for optimal hyper-plane construction. This optimal hyper-plane can classify unknown data into its corresponding class if they have similar features as trained data. Finally, a set of test data were fed into the classifier to examine its performance by computing the classification success rate of these data. Figure 5.7 shows SVM classifiers with 2 time segments as features. Data displayed in circles are support vectors for optimal hyper-plane construction. In this study, all time segments are included as features. Due to its large dimensionality (4D), this optimal separating hyper-plane cannot be displayed in a 2-D graph.

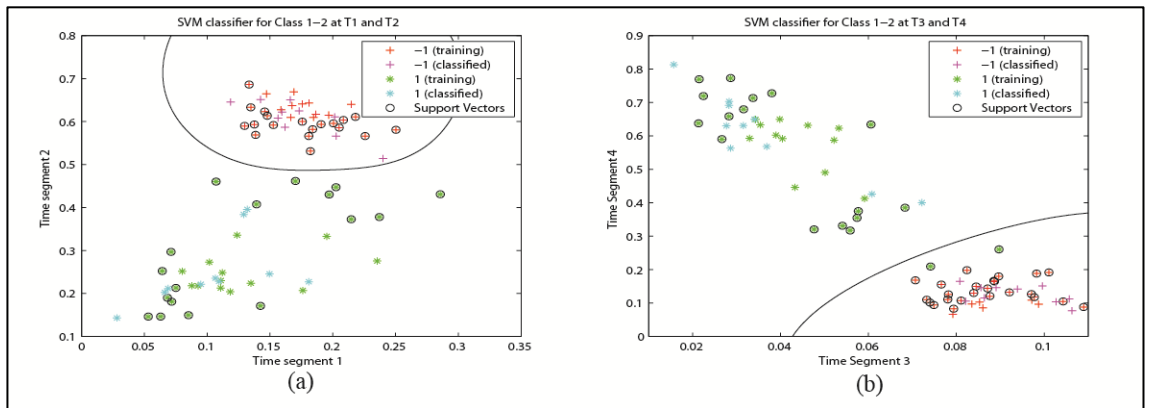


Figure 5.7: Optimal separating hyper-plane with features from (a) Time segment 1 and 2 (b) Time segment 3 and 4

Lastly, all binary classifiers were integrated into a multiclass classifier through one-against-one (OAO) strategy. The test data will serve as input vectors for Class 1-2,

Class 1-3, and Class 2-3 classifier. If the test data have similar patterns as that in Class 1, one vote will be given each from Class 1-2 and Class 1-3 classifier to Class 1. Thus, Class 1 has the highest number of votes and displays as the final class decision. Figure 5.8 displays a summary of process flow for SVM classification.

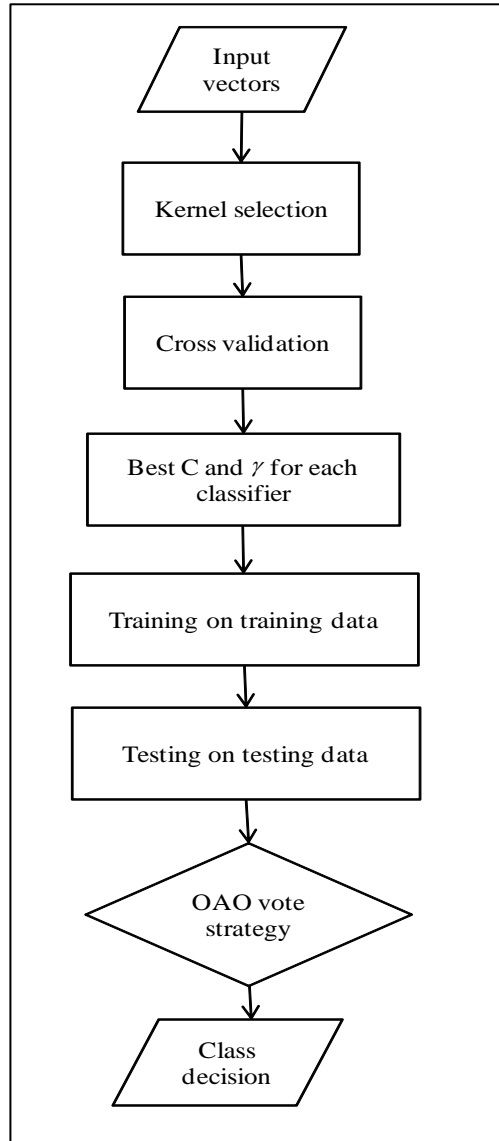


Figure 5.8: Flow chart for signal classification

5.4 Cross validation

Cross validation procedure involves tuning parameter C and γ for best testing accuracy. Three binary classifiers, namely Class 1-2, Class 1-3, and Class 2-3 were

constructed to train data from the normal (Class 1), grease (Class 2) and leakage (Class 3) condition before they were integrated into a multiclass classification system through one-against-one (OAO) strategy. In the present study, data in each condition (40 samples) were segregated into 4 sets with 10 samples each. The cross-validation procedure was started by training each classifier on the first 3 sets of data with various pairs of (C, γ) . It was followed by testing the remaining 1 set of data on the trained classifier. Parameter C and γ which produces highest testing accuracy will be considered as best parameter for classification. Indeed, testing accuracy was chosen as classifier's performance indicator over training accuracy to avoid over-fitting problem. If the classifier's performance was assessed based on its training accuracy, the classifier might be over trained and thus produces poor testing result.

The cross validation procedure was conducted through the grid search method (Hsu, et al., 2010). A number of exponentially growing sequences of C and γ were tried on the classifier and the best pair of (C, γ) was chosen based on the best testing accuracy. In this study, the classifier was tested with value of $C = 2^{-5}, 2^{-3}, \dots, 2^{15}$ and $\gamma = 2^{-15}, 2^{-13}, \dots, 2^3$. A loose grid search was conducted first to identify potential region for better testing accuracy. It was followed by a fine grid search on this potential region to identify the pair of (C, γ) for best classification result. The best pair of (C, γ) in each classifier will be substituted into the multiclass classification system to generate final classifier.

5.4.1 Cross validation results

This section compares the cross validation results between AE and vibration signals at F1 (0 - 3.2 kHz) under low speed (450 rpm) and high speed (800 rpm).

Classification success rate of Class 1-2, Class 1-3, and Class 2-3 classifiers within a specified range of C and γ value will be discussed in detail.

5.4.1.1 Low speed (450 rpm)

Figure 5.9 shows the classification success rate of Class 1-2 classifier for loose and fine grid search. This classifier attempted to classify the normal (Class 1) and grease (Class 2) condition of valve plate from the AE signal at F1 (0-3.2 kHz) and 450 rpm. It can be seen that 100% of testing accuracy can be achieved by setting the value of $\log_2 C$ in the range from -5 to 9 and $\log_2 G$ in the range from -15 to 1.

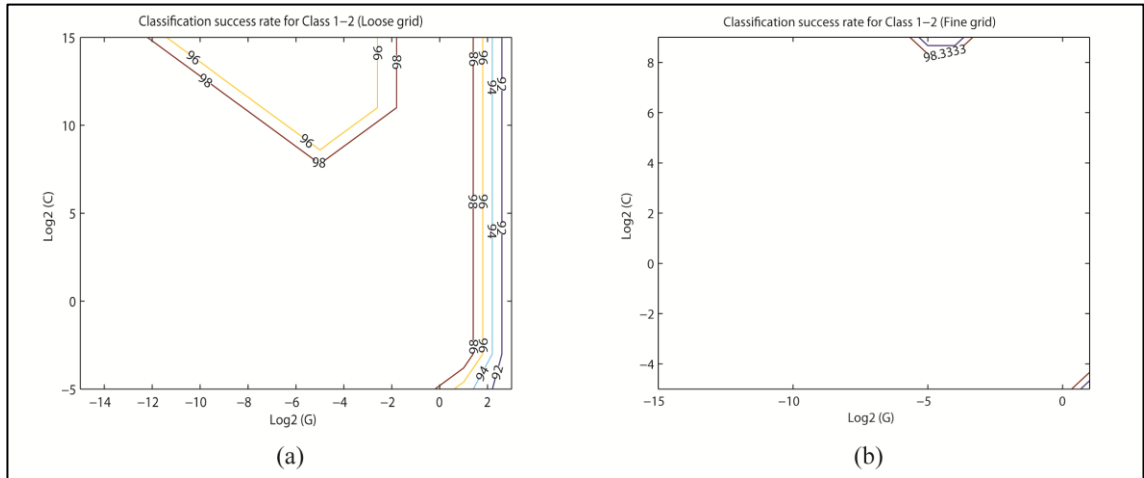


Figure 5.9: Classification success rate for AE signal, Class 1-2 classifier on (a) Loose grid (b) Fine grid at F1 and 450 rpm

The classification success rate of Class 1-3 classifier which classified normal (Class 1) and leakage (Class 3) valve plate condition from AE signal at F1 and 450 rpm is shown in Figure 5.10. The potential region was identified in the loose grid with $\log_2 C$ value range from -3 to 7 and $\log_2 G$ value range from -15 to -5. After performing fine grid search as shown in Figure 5.10 (b), it can be observed that the best parameter of (C, γ) lies in the diagonal of this potential region.

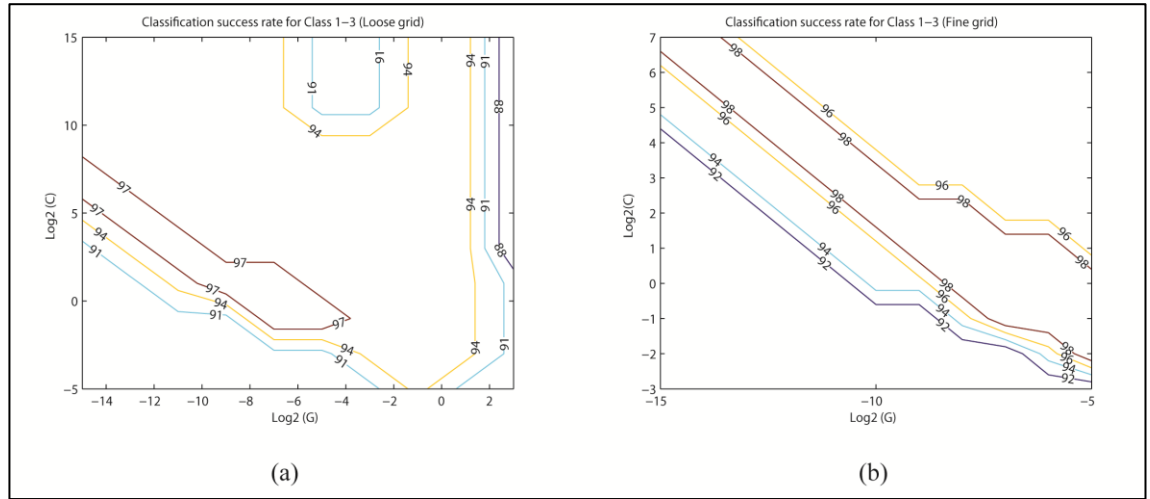


Figure 5.10: Classification success rate for AE signal, Class 1-3 classifier on (a) Loose grid (b) Fine grid at F1 and 450 rpm

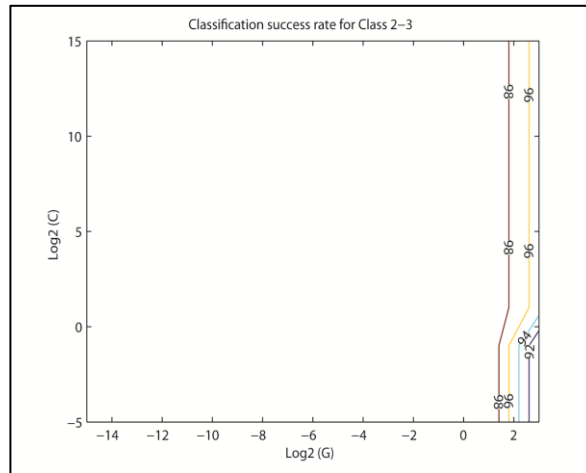


Figure 5.11: Classification success rate for AE signal, Class 2-3 classifier at F1 and 450 rpm

Meanwhile, for the Class 2-3 classifier which classified the AE signal at F1 and 450 rpm from grease (Class 2) and leakage (Class 3) condition, the classification success rate is better than the other two classifiers as a high success rate of more than 95% was achieved even at the loose grid region, as shown in Figure 5.11. Therefore, no fine grid search is needed for the Class 2-3 classifier.

It should be noted that at the loose grid region, both Class 1-2 and Class 2-3 classifier can achieve high success rate of almost 100%. This may attribute to

discriminant features of AE signal under grease condition (Class 2) compared to other conditions at F1 and 450 rpm. Therefore, the trained classifier can obtain high classification success rate on the testing data irrespective of parameter C and γ . Nevertheless, the other 2 conditions namely the normal (Class 1) and leakage (Class 3) condition are still remain discriminant as all of the classifiers achieved more than 88% of success rate even at the coarse grid region.

For the vibration signal, the classification success rate of Class 1-2 classifier at F1 and 450 rpm is displayed in Figure 5.12. By comparing the classification result between AE and vibration signal, it is obvious that AE signal can distinguish between normal and grease valve condition better than vibration signal at this frequency range and speed. This can be observed from the high classification success rate of AE signal at coarse grid, which range from 90% to 100%, compared to the vibration signal, as the later can only have a classification success rate range from 65% to 82%. After performing fine grid search, the Class 1-2 classifier for vibration signal can achieve highest classification success rate of 85%.

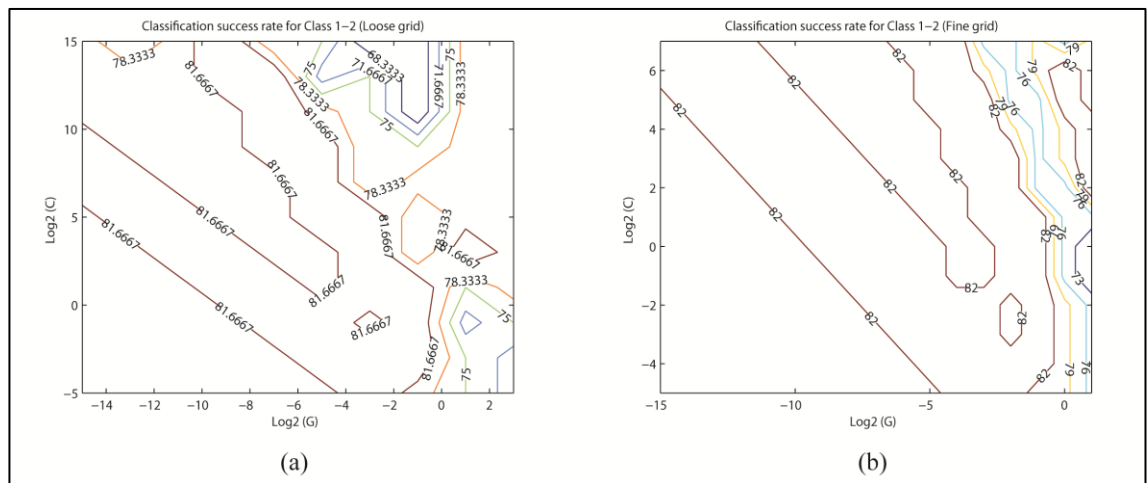


Figure 5.12: Classification success rate for vibration signal, Class 1-2 classifier on (a) Loose grid (b) Fine grid at F1 and 450 rpm

Figure 5.13 displays classification success rate of Class 1-3 classifier at F1 and 450 rpm. Loose grid of Class 1-3 classifier shows slightly better result than Class 1-2 classifier constructed from vibration signal, with its classification success rate range from 77% to 88%. It can be observed that higher success rate can be achieved at $\log_2 C$ value range from 4 to 12 and $\log_2 G$ value range from -8 to -6. By conducting fine grid search, a 90% success rate can be obtained with C and γ value at this potential region. However, its performance is still lower than the AE signal which has almost 100% of classification success rate at the same frequency range and speed.

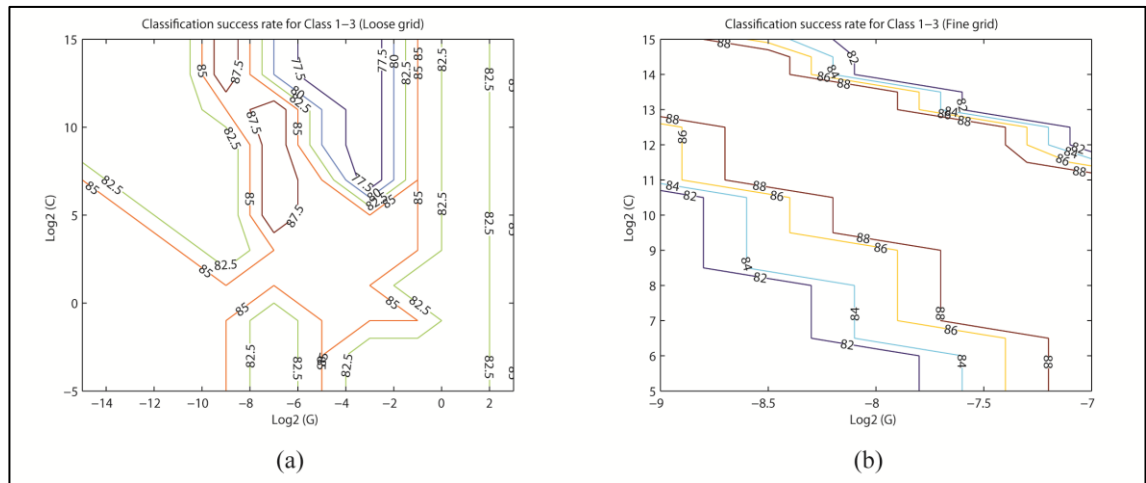


Figure 5.13: Classification success rate for vibration signal, Class 1-3 classifier on (a) Loose grid (b) Fine grid at F1 and 450 rpm

Class 2-3 classifier shows the best result compared to its counterparts, as it displays a minimum classification success rate of 80% even at the loose grid region. Figure 5.14 (b) shows that 90% success rate can be achieved by the classifier after fine grid search. Nevertheless, Class 2-3 classifier of AE signal still remain as a better classifier compared to that of vibration signal as the former shows its highest performance of almost 100% success rate.

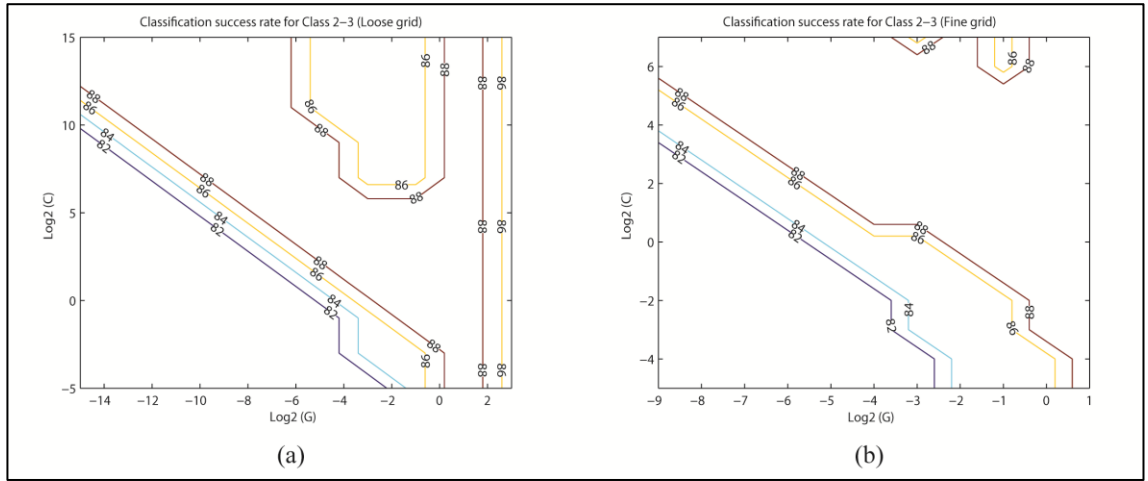


Figure 5.14: Classification success rate for vibration signal, Class 2-3 classifier on (a) Loose grid (b) Fine grid at F1 and 450 rpm

By comparing the region of high classification success rate of the three classifiers for AE and vibration signal, it is obvious that AE signal shows higher classification success rate for all classifiers, irrespective of C and γ value at the specified range. Thus, it can be deduced that AE signal has better discriminating power at F1 and 450 rpm. Comparison of classification success rate between AE and vibration signal at all frequency ranges will be discussed in Section 5.5.

5.4.1.2 High speed (800 rpm)

Figure 5.15 displays classification success rate of Class 1-2 classifier under coarse and fine grid search for AE signal at F1 and 800 rpm. The result at loose grid indicates poorer performance of classifier compared to that at lower speed which achieved almost 100% classification success rate, as Class 1-2 classifier at higher speed has success rate range between 50% and 75%. Finer grid search shows maximum classification success rate of 75% within specified range of $\log_2 C$ and $\log_2 G$, as depicted in Figure 5.15 (b).

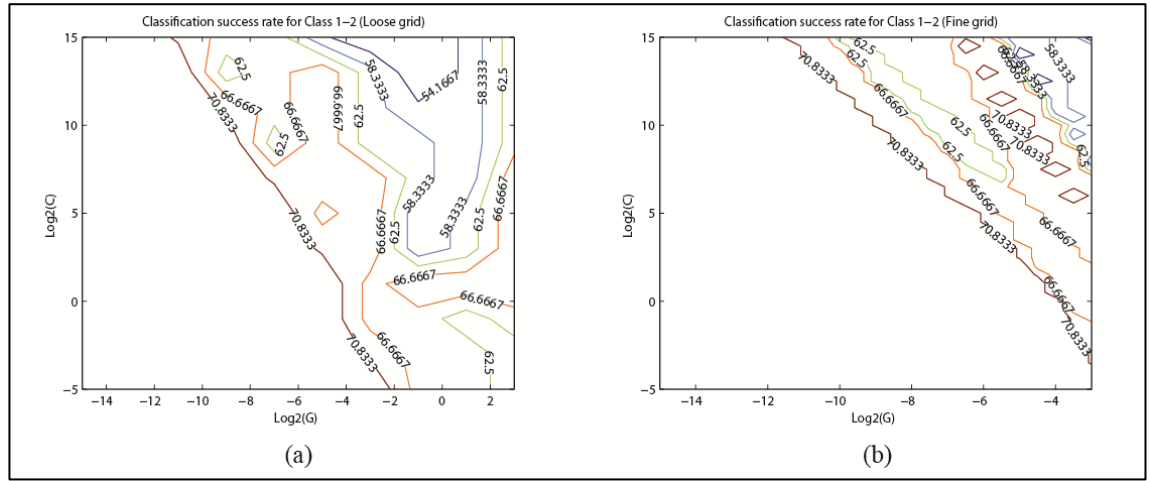


Figure 5.15: Classification success rate for AE signal, Class 1-2 classifier on (a) Loose grid (b) Fine grid at F1 and 800 rpm

Meanwhile, Class 1-3 and Class 2-3 classifier show 100% classification success rate for AE signal at F1 and 800 rpm, at all values of $\log_2 C$ and $\log_2 G$. It can be inferred from the high success rate of both classifiers that leakage condition (Class 3) shows dominant features at higher speed. Thus, it can be distinguished from normal (Class 1) and grease (Class 2) condition easily and achieved 100% of success rate regardless of parameter C and γ . This finding is in line with the deduction from the previous chapter which stated that features of leakage condition are more apparent at higher speed.

On the other hand, vibration signal shows better result in success rate at higher speed, ranging from 75% to 95%, as demonstrated in Figure 5.16 (a). Further fine grid search showed that 100% success rate can be attained at specific $\log_2 C$ and $\log_2 G$ range indicated in Figure 5.16 (b).

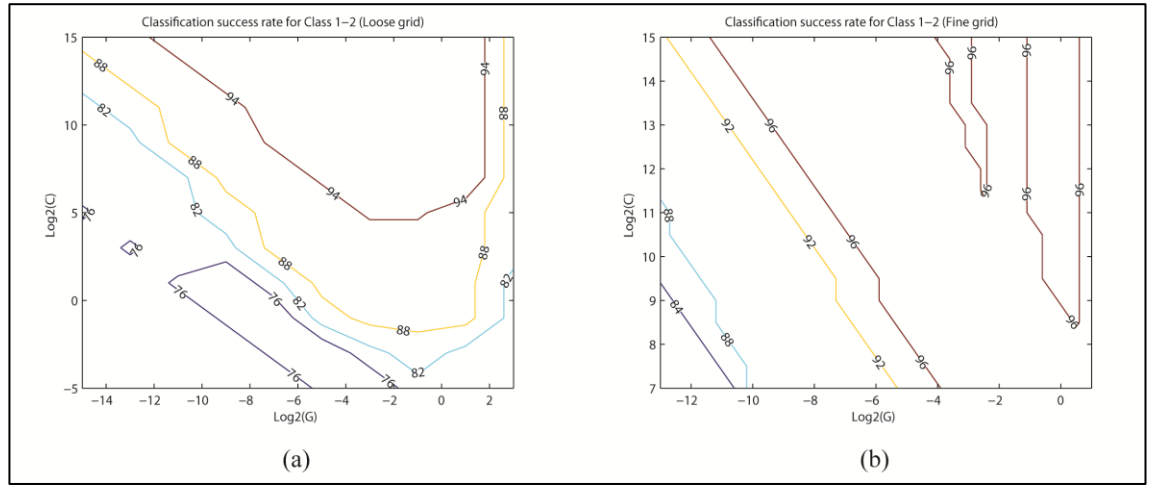


Figure 5.16: Classification success rate for vibration signal, Class 1-2 classifier on (a) Loose grid (b) Fine grid at F1 and 800 rpm

It was found that vibration signal at F1 and 800 rpm performed better than those at lower speed. As opposed to Class 1-3 classifier which shows classification success rate of 77- 90% at lower speed, the Class 1-3 classifier at higher speed achieved 100% classification success rate at all range of $\log_2 C$ and $\log_2 G$. Similarly, Class 2-3 classifier of vibration signal shows higher success rate of almost 100% at higher speed, as displayed in Figure 5.17.

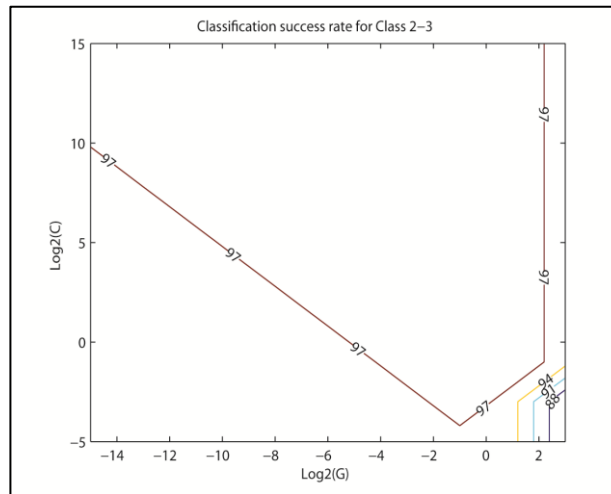


Figure 5.17: Classification success rate for vibration signal, Class 2-3 classifier at F1 and 800 rpm

In comparing performance of classifiers at 800 rpm, it is noticeable that Class 1-3 and Class 2-3 classifier have better success rate results compared to Class 1-2 classifier. In fact, both classifiers from vibration and AE signals have almost 100% classification success rate at higher speed. The consistent trend of both classifiers' performance for vibration and AE signal further supports the postulation that leakage (Class 3) condition is more pronounced at higher speed.

5.4.2 Discussions on cross validation results

5.4.2.1 Classification success rate at low and high speed

The main objective of cross validation procedure is to obtain the best C and γ within a specified range for best testing result. It was found that some classifiers have high classification success rate irrespective of its C and γ value. This finding has lead to the deduction that training data of these classifiers have distinctive features which result in high classification success rate regardless of its C and γ value.

It is observable that AE signal at lower speed shows almost 100% classification result within a specified range ($C = 2^{-5}, 2^{-3}, \dots, 2^{15}$ and $\gamma = 2^{-15}, 2^{-13}, \dots, 2^3$). On the other hand, the highest classification success rate of Class 1-2 classifier is 75% for AE signal at higher speed. These findings show that AE signal at F1 and 800 rpm has poor features in differentiating normal (Class1) and grease (Class 2) condition. Meanwhile, distinct features of AE signal at 450 rpm enable test data to be distinguishable between normal, grease and leakage condition. Nevertheless, higher speed produces more apparent features for signal under leakage condition, resulted in 100% success rate of Class 1-3 and Class 2-3 classifier at higher speed irrespective of C and γ value.

Vibration signal shows poorer classification result compared to AE signal at lower speed. Fine grid search is required to obtain C and γ value with highest success rate. However, at higher speed, vibration signal performed the best in classifying normal (Class 1) and grease (Class 2) condition compared to AE signal. Indeed, the Class 1-2 classifier recorded 100% success rate for vibration signal, compared to 75% success rate for AE signal at higher speed, after fine grid search. For Class 1-3 and Class 2-3 classifier, both shows success rate of 100% due to distinct features of leakage condition at higher speed.

In comparing classification result of vibration signal at low and high speed, it was found that vibration signal showed better result at higher speed. The high performance of all classifiers at higher speed further confirmed the postulate that significant features of vibration signal can be acquired at higher speed as a result of large mechanical impacts during the valve opening and closing event.

Again, one should be reminded that the comparison of AE and vibration signal is confined to signal with frequency content of F1 (0 - 3.2 kHz). More comparisons of both signals at different frequency range will be presented in Section 5.5.

5.4.2.2 Best parameters for Gaussian radial basis kernel

The results from cross validation show that there are a number of pairs of (C, γ) with the same classification success rate. Yang et al. (2005) suggested selecting γ value with the highest classification success rate and considerably low number of support vectors (SVs) as the best parameter. Indeed, the generalization ability of classifiers is affected by number of SVs, as it represent the upper bound of

generalization error. In other words, larger number of SVs will produce higher upper bound of generalization error (Vapnik, 1995; Burges, 1998) .

Figure 5.18 shows classification success rate and number of SVs at different gamma values ($\gamma = 2^{-9}, 2^{-8.5}, \dots, 2^1$) at $C=2$ for Class 2-3 classifier to categorize AE signal at F4 (9.6 – 12.8 kHz) and 450 rpm. It can be seen from Figure 5.18 (a) that maximum classification success rate of 90% was recorded at 14 different γ values. In order to decide the best γ value, number of SVs at different γ value should be taken into consideration. As each classifier was trained with a total of 60 training data, the best γ value should have number of SVs lies between 10 and 60, as too few the number of SVs in a classifier will cause under-fitting problems while too many the number of SVs will result in over-fitting problem. Figure 5.18 (b) shows that the highest classification success rate can be achieved at $\gamma = 0.177$ or $\log_2 G = -2.5$, with the lowest number of SVs at 33. Therefore, this value was chosen as the best parameter for the Class 2-3 classifier.

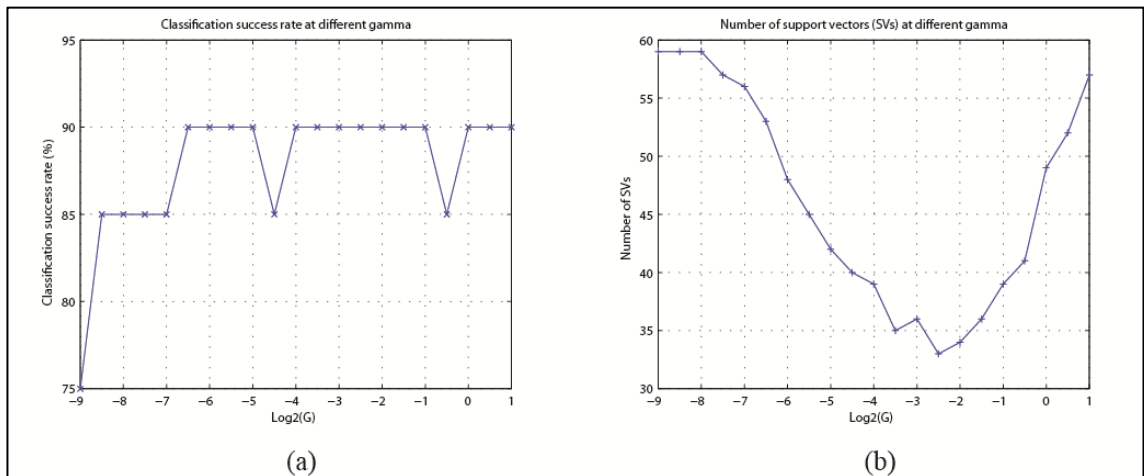


Figure 5.18: Effect of gamma values at $C=2$ on (a) Classification success rate (b) Number of support vectors in Class 2-3 classifier of AE signal at F4 and 450 rpm

It must be noted that penalty parameter C can affect classification result and number of SVs in a classifier, as it represents tolerance level to misclassification error. Higher C value will tolerate more misclassification error. Therefore, if a classifier has the same success rate and considerably low number of SVs at the same γ value, lower C value is always preferred.

Table 5.1 displays the best pair of (C, γ) selected based upon the aforementioned guidelines for Class 1-2, Class 1-3 and Class 2-3 classifier trained with AE and vibration signal at all frequency range and 450 rpm. It is noticeable that some classifiers have (C, γ) value with more than 50 SVs, as shown in bold in Table 5.1. This is inevitable especially if the trained data do not show distinct features between different conditions (class). At this instant, more support vectors are needed to construct the hyper-plane, to the extent that all trained data were utilized as support vectors. To avoid over-fitting problem, more trained data should be added into classifier for better learning of pattern in these data. If the number of SVs remained the same after training, it can be inferred that training data in that particular frequency range failed to capture features of valve condition.

Table 5.1: Best parameters of Gaussian radial basis kernel classifier for AE and vibration signal at 450 rpm

Frequency	Classifier	AE			Vibration		
		C	G	SVs	C	G	SVs
F1	Class 1-2	1.000	0.500	43	2.000	0.125	49
	Class 1-3	2.000	0.008	59	32.000	0.008	37
	Class 2-3	1.000	0.500	41	2.000	0.125	37
F2	Class 1-2	2.000	0.125	45	2.000	0.125	33
	Class 1-3	32.000	0.500	48	128.000	0.125	12
	Class 2-3	32.000	2.000	46	2.000	0.125	24
F3	Class 1-2	4.000	0.177	55	0.125	0.500	60
	Class 1-3	8.000	0.125	46	32.000	0.008	36
	Class 2-3	8.000	0.125	42	2.000	0.125	39

Table 5.1, continued

Frequency	Classifier	AE			Vib		
		C	G	SVs	C	G	SVs
F4	Class 1-2	512.000	0.500	18	8.000	0.008	45
	Class 1-3	11.314	0.008	45	32.000	0.008	48
	Class 2-3	2.000	0.177	33	2.000	0.500	47
F5	Class 1-2	32.000	0.500	24	2.000	0.500	44
	Class 1-3	4096.000	0.008	17	2.000	0.008	58
	Class 2-3	32.000	0.500	18	90.510	0.002	43
F6	Class 1-2	8.000	0.125	38	32.000	0.500	27
	Class 1-3	2.000	0.125	26	1024.000	0.002	42
	Class 2-3	8.000	0.500	26	256.000	0.001	30
F7	Class 1-2	2.000	0.125	40	2.000	0.031	39
	Class 1-3	8.000	0.125	17	8.000	0.008	51
	Class 2-3	1.000	0.022	52	8.000	0.500	25
F8	Class 1-2	2.000	0.031	40	2.000	0.031	38
	Class 1-3	2.000	0.125	33	128.000	0.008	23
	Class 2-3	8.000	2.000	48	2.000	0.125	31
F9	Class 1-2	2.000	0.500	40	2.000	0.125	26
	Class 1-3	4.000	1.414	51	8.000	0.031	34
	Class 2-3	2.000	0.500	38	2.000	0.125	28
F10	Class 1-2	32.000	0.002	35	181.019	1.000	29
	Class 1-3	8.000	0.031	34	0.031	2.000	60
	Class 2-3	2.000	0.125	27	8.000	0.125	36
F11	Class 1-2	128.000	2.000	47	2.000	0.500	46
	Class 1-3	8.000	0.031	33	2.000	0.002	59
	Class 2-3	32.000	0.008	20	4.000	0.354	56
F12	Class 1-2	2.000	0.500	39	2.000	0.125	40
	Class 1-3	1.414	0.044	49	32.000	0.500	43
	Class 2-3	0.500	0.125	44	8.000	0.125	44
F13	Class 1-2	8.000	0.031	18	2.000	0.125	30
	Class 1-3	2.000	0.031	54	8.000	0.008	39
	Class 2-3	2.000	0.125	24	8.000	0.125	37
F14	Class 1-2	2.000	0.125	29	2.000	0.125	29
	Class 1-3	8.000	0.125	35	1.000	0.011	59
	Class 2-3	2.000	0.125	30	2.000	0.125	29
F15	Class 1-2	2.000	0.125	29	2.000	0.125	37
	Class 1-3	2.000	0.031	47	1448.155	0.088	51
	Class 2-3	362.039	0.022	12	2.000	0.125	32
F16	Class 1-2	0.125	2.000	27	2.000	0.125	28
	Class 1-3	8.000	0.031	37	2.000	0.031	41
	Class 2-3	32.000	0.002	43	2.000	0.125	24

Meanwhile, the best parameter of Gaussian radial basis kernel for all classifiers with trained data at 800 rpm is displayed in Table 5.2. It is notable that the *C* value is enormously high for Class 1-2 classifier trained with AE signal at F9 (25.6 – 28.8 kHz).

The high C value of 16384 may due to the postulation that trained data at this frequency range failed to differentiate normal (Class 1) and grease (Class 2) condition, thus requiring higher tolerance level to achieve higher classification success rate. Nevertheless, higher tolerance level may result in under-fitting problem as the classifier tolerates most of the misclassification. More testing data are required to test the classifier in future to verify its performance against different data sets.

Table 5.2: Best parameters of Gaussian radial basis kernel classifier for AE and vibration signal at 800 rpm

Frequency	Classifier	AE			Vibration		
		C	G	SVs	C	G	SVs
F1	Class 1-2	2.000	0.031	58	128.000	0.250	24
	Class 1-3	2.000	0.125	27	32.000	0.002	34
	Class 2-3	2.000	0.125	25	2.000	0.125	39
F2	Class 1-2	16.000	0.006	38	8.000	0.125	29
	Class 1-3	8.000	0.006	38	2.000	0.125	27
	Class 2-3	2.000	0.063	31	2.000	0.125	32
F3	Class 1-2	2.000	0.031	44	8.000	0.125	29
	Class 1-3	2.000	0.008	53	2.000	0.031	46
	Class 2-3	2.000	0.125	30	2.000	0.125	32
F4	Class 1-2	8.000	0.354	54	128.000	2.000	49
	Class 1-3	8.000	0.031	30	2.000	0.125	39
	Class 2-3	32.000	0.031	24	2.000	0.125	41
F5	Class 1-2	181.019	0.354	42	128.000	0.125	50
	Class 1-3	2.000	0.125	41	2.000	0.125	34
	Class 2-3	2.000	0.125	41	2.000	0.125	36
F6	Class 1-2	32.000	0.008	46	8.000	0.500	30
	Class 1-3	2.000	0.125	38	2.000	0.125	33
	Class 2-3	2.000	0.125	40	2.000	0.125	29
F7	Class 1-2	2.000	0.500	44	1.000	0.008	60
	Class 1-3	128.000	0.031	14	128.000	0.031	9
	Class 2-3	512.000	0.008	29	2.000	0.500	45
F8	Class 1-2	32.000	0.500	46	2.000	0.125	40
	Class 1-3	2.000	0.125	28	8.000	0.125	19
	Class 2-3	0.125	2.000	60	2.000	0.500	38
F9	Class 1-2	16384.00	0.031	28	2.000	0.031	49
	Class 1-3	1.000	0.125	34	512.000	5.657	55
	Class 2-3	128.000	0.031	13	0.500	0.125	56
F10	Class 1-2	2.000	0.002	60	2.000	0.500	44
	Class 1-3	2.000	0.125	33	128.000	8.000	50
	Class 2-3	2.000	0.125	36	32.000	0.031	15

Table 5.2, continued

Frequency	Classifier	AE			Vibration		
		C	G	SVs	C	G	SVs
F11	Class 1-2	32.000	0.500	36	2.000	0.031	45
	Class 1-3	32.000	0.500	25	0.031	2.000	60
	Class 2-3	2.000	0.125	34	8.000	0.500	28
F12	Class 1-2	2.000	0.002	60	2.000	0.031	48
	Class 1-3	2.000	0.125	39	2.000	0.125	24
	Class 2-3	2.000	0.125	28	2.000	0.031	36
F13	Class 1-2	2.000	0.002	60	2.000	0.125	33
	Class 1-3	2.000	0.125	42	2.000	0.125	22
	Class 2-3	2.000	0.031	43	2.000	0.125	24
F14	Class 1-2	2.000	0.125	39	2.000	0.125	32
	Class 1-3	2.000	0.125	38	8.000	2.000	42
	Class 2-3	2.000	0.125	33	2.000	0.125	28
F15	Class 1-2	2.000	0.125	40	2.000	0.125	28
	Class 1-3	2.000	0.031	39	2.000	0.125	36
	Class 2-3	8.000	0.031	20	2.000	0.125	31
F16	Class 1-2	2.000	0.125	40	2.000	0.125	24
	Class 1-3	32.000	0.125	21	2.000	0.125	30
	Class 2-3	2.000	0.125	30	32.000	0.500	19

After obtaining the best parameters for all classifiers trained with data from different conditions and speed, the Class 1-2, Class 1-3 and Class 2-3 classifier at each frequency range were integrated into a multiclass system through one-against-one (OAO) strategy. Next section presents classification results of the multiclass system for AE and vibration signal at different frequency ranges.

5.5 Multiclass classification

In this study, the multiclass system at each frequency range was tested with 3 different sets of data with 10 samples each, which correspond to data under normal (Class 1), grease (Class 2) and leakage (Class 3) condition. Final class decision was given to class with maximum vote. It is assumed that input vectors computed from

normalized energy have distinct features which can discriminate themselves from other conditions, thus preventing chances of getting equal votes in the classifier.

5.5.1 Classification results of each testing class

5.5.1.1 Low speed

Table 5.3 shows classification success rate of multiclass system trained with AE and vibration signals acquired at 450 rpm. The first three columns of each signal (AE/ vibration) from the left represent classification result tested with data from normal (Class1), grease (Class 2) and leakage (Class 3) condition respectively. Final classification result which includes data in all conditions is displayed in shaded column on the right of each signal.

Table 5.3: Classification success rate of multiclass system trained with data at 450 rpm

Frequency	AE				Vibration			
	Class 1	Class 2	Class 3	Total	Class 1	Class 2	Class 3	Total
1	100.0	100.0	100.0	100.0	70.0	90.0	70.0	76.7
2	50.0	80.0	90.0	73.3	100.0	100.0	100.0	100.0
3	80.0	60.0	100.0	80.0	100.0	100.0	90.0	96.7
4	100.0	50.0	90.0	80.0	100.0	90.0	70.0	86.7
5	100.0	80.0	80.0	86.7	100.0	80.0	60.0	80.0
6	70.0	80.0	100.0	83.3	100.0	80.0	80.0	86.7
7	80.0	100.0	90.0	90.0	100.0	100.0	70.0	90.0
8	90.0	100.0	100.0	96.7	100.0	100.0	90.0	96.7
9	80.0	90.0	100.0	90.0	100.0	100.0	90.0	96.7
10	90.0	100.0	90.0	93.3	90.0	90.0	80.0	86.7
11	90.0	90.0	100.0	93.3	90.0	60.0	100.0	83.3
12	100.0	100.0	100.0	100.0	90.0	100.0	70.0	86.7
13	90.0	100.0	100.0	96.7	90.0	80.0	60.0	76.7
14	100.0	100.0	90.0	96.7	100.0	100.0	90.0	96.7
15	90.0	100.0	90.0	93.3	90.0	100.0	80.0	90.0
16	80.0	80.0	80.0	80.0	90.0	100.0	90.0	93.3

It can be seen that the classifiers achieved more than 90% classification success rate at all frequency range except F1 (0 – 3.2 kHz) when tested with vibration signal from normal (Class 1) condition. This is because vibration signal at F1 has only 1 characteristic segment namely time segment 1 (T1), as presented in Table 4.11 (Chapter 4). Due to poorer feature at this time segment compared to T2, and T3 where the later depicted the valve opening and closing event, classification result at its corresponding frequency range recorded a poor result of 70% success rate.

By observing classifiers' performance tested with vibration signal acquired from grease (Class 2) condition, it is obvious that classifier at F11 (32.0 – 35.2 kHz) performed poorly compared to other frequency ranges. It hits the lowest success rate of 60% compared to others which have more than 80% of success rate. This might attribute to insufficient features representing grease condition in F11, as it has only 1 characteristic segment at time segment 3 (T3), as displayed in Table 4.11. As mentioned in Chapter 4, T3 can reflect grease condition better if the length of the time segment is shortened. Due to insufficient characteristic segments and lower signal-to-noise ratio at F11, the classifier has disappointing classification results compared to that in other frequency ranges.

Classification results were less satisfactory when being tested with vibration signals obtained from leakage (Class 3) condition. This supports the postulate in Chapter 4 that the features obtained under leakage condition are less significant at lower speed. Nevertheless, the classifiers achieved 100% classification results at F2 (3.2 – 6.4 kHz) and F11. Signal analysis in the previous chapter suggested that classifier at F2 is more reliable in reflecting leakage condition compared to F11 as the former has more characteristic segments, namely T1, T2, T4 and higher signal-to -noise ratio compared

to the later. Indeed, any unreliable classifier is always not preferred as it may give false alarm to the system.

On the other hand, for classifiers tested with AE signal acquired from normal (Class 1) condition, it was found that the classifiers performed better at higher frequency range, as it attained more than 90% classification success rate from F10 (28.8 – 32.0 kHz) to F15 (44.8 – 48.0), which is in good agreement with findings obtained from previous chapter. Classifiers hits its lowest and second lowest success rate at F2 and F6 (16.0 – 19.2 kHz), with classification result of 50% and 70% respectively. Thus, it is reasonable to infer that AE signal has a lower signal-to-noise ratio at lower frequency range, which resulted in poor performance of classifiers with data tested from these frequency ranges.

Compared to that under normal (Class 1) condition, the classification success rate is slightly better for classifiers tested with AE signal under grease (Class 2) condition. In fact, classifiers achieved 100% success rate at 8 frequency ranges, out of which 6 frequency ranges are from the higher frequency range. Classifiers with the poorest performance come from F3 (6.4 – 9.6 kHz) and F4 (9.6 – 12.8), with 60% and 50% success rate respectively. It further confirms the deduction that AE technique can extract signal features better in higher frequency range.

Surprisingly, classifiers tested with AE signals obtained under leakage (Class 3) condition show better classification result compared to that tested under normal (Class 1) and grease (Class 2) condition. All classifiers have success rate greater than 80% in all frequency range. This is in contrast with the result obtained from vibration signal discussed above, which inferred that leakage condition has less significant features at lower speed. The difference of results between AE and vibration signal implied that AE

technique is more sensitive in detecting fluid motion such as fluid leakages through suction valve compared to vibration technique.

By comparing classifier's performance tested with each testing class, it is obvious that classifier of AE signal achieved 100% classification result for all testing class at F1 and F12 (35.2 – 38.4 kHz), bolded in Table 5.3. However, classifier tested with AE signal at F12 is preferable as it is better in revealing valve events with lesser noise. Meanwhile, classifier of vibration signal attained 100% success rate for all testing class at F2. This finding further supports the postulation that AE technique is more sensitive in higher frequency range (F8 and above) while vibration technique is better in lower frequency range.

5.5.1.2 High speed

Table 5.4 shows classification results of classifiers trained with AE and vibration signals acquired at 800 rpm.

Table 5.4: Classification success rate of multiclass system trained with data at 800 rpm

Frequency	AE				Vibration			
	Class 1	Class 2	Class 3	Total	Class 1	Class 2	Class 3	Total
1	70.0	80.0	100.0	83.3	100.0	100.0	100.0	100.0
2	80.0	90.0	100.0	90.0	100.0	100.0	100.0	100.0
3	90.0	100.0	90.0	93.3	100.0	100.0	100.0	100.0
4	80.0	90.0	100.0	90.0	90.0	90.0	100.0	93.3
5	70.0	70.0	100.0	80.0	80.0	90.0	100.0	90.0
6	80.0	100.0	100.0	93.3	100.0	100.0	100.0	100.0
7	90.0	100.0	80.0	90.0	100.0	100.0	100.0	100.0
8	80.0	60.0	80.0	73.3	100.0	90.0	90.0	93.3
9	90.0	100.0	100.0	96.7	100.0	100.0	100.0	100.0
10	80.0	100.0	100.0	93.3	100.0	100.0	90.0	96.7
11	100.0	100.0	100.0	100.0	100.0	100.0	100.0	100.0
12	80.0	100.0	100.0	93.3	100.0	100.0	100.0	100.0
13	80.0	100.0	100.0	93.3	90.0	100.0	100.0	96.7
14	80.0	100.0	100.0	93.3	100.0	100.0	100.0	100.0
15	90.0	100.0	100.0	96.7	100.0	90.0	100.0	96.7
16	70.0	100.0	100.0	90.0	100.0	90.0	100.0	96.7

Classifiers tested with vibration signals from normal (Class 1) condition demonstrate good results with a minimum of 80% success rate at all frequency ranges. Similarly, the classification results of classifiers tested with vibration signal from grease (Class 2) and leakage (Class 3) condition show at least 90% of success rate at all conditions. It is noteworthy that classifiers tested with data from leakage (Class 3) condition at higher speed show tremendous increase in success rate compared to that at lower speed. In fact, the classifiers have 100% success rate at 14 frequency ranges, which is very much higher, compared to the result of 100% success rate at 2 frequency ranges acquired at lower speed. This is in agreement with previous postulations that features of leakage condition are more apparent at higher speed.

Results from one way analysis of variance (ANOVA) suggested that vibration signals have no significant segments at F7 (19.2 – 22.4 kHz), F8 (22.4 – 25.6 kHz), F9 (25.6 – 28.8 kHz), and F15 (44.8 – 48.0 kHz). Nevertheless, SVM multiclass classifiers show more than 90% success rate for all test data at these frequency ranges. This further proved the superior performance of SVM classifiers in classifying vibration signals to its corresponding conditions (Class) although the input feature vectors are less significant.

Meanwhile, by comparing performance of classifiers tested with AE signal from normal (Class 1) condition, it is apparent that AE signal is less capable in extracting features of normal (Class 1) condition at higher speed. Although all classifiers obtained a minimum of 70% success rate, there is only 1 classifier managed to categorize all normal data correctly, compared to 5 classifiers at lower speed. The 100% success rate of this classifier in F11 (32.0 – 35.2 kHz) is shown in bold in Table 5.4. This finding concurs with previous postulation that AE signal appears to have more noise at higher

speed. Indeed, the noise may mask features of normal (Class 1) condition, resulting in less satisfactory classification result.

Nevertheless, classification results of classifiers tested with grease AE signal improved at higher speed. There are 11 classifiers attained classification result of 100%, out of which 8 classifiers are from higher frequency range (F9 and above). Unlike weak features of normal (Class 1) condition which can be masked by noise easily, it is believed that features of grease (Class 2) condition become more significant at higher speed. By filtering away intense noise, these features can be detected clearly at higher frequency range.

Similarly, when tested with AE signal obtained from leakage (Class 3) condition, the classifiers show improved classification results at higher speed. It can be observed from Table 5.4 that all leakage (Class 3) data were categorized successfully in 13 classifiers, compared to 8 classifiers with 100% success rate at lower speed. It must be noted that the improved results of classifiers tested with grease (Class 2) and leakage (Class 3) condition are in contrast with previous findings obtained from one way ANOVA, where the later suggested poor performance of AE signal at higher speed. Indeed, more noise can be seen from AE signal acquired at higher speed, which eventually mask the signals carry information of valve condition. However, these masked features were intensified after being transformed into a higher dimensional space through Gaussian radial basis kernel. Therefore, the features of grease (Class 2) and leakage (Class 3) condition can be detected at higher speed. Nevertheless, due to less significant features under normal condition (Class 1), the classification success rate does not have great improvement at higher speed. The strength of kernel function also explained good classification results of classifiers in F1 (0 – 3.2 kHz), F5 (12.8 – 16.0 kHz), F11 (32.0 – 35.2 kHz), F12 (35.2 – 38.4 kHz), and F13 (38.4 – 41.6 kHz) though

one way ANOVA results demonstrated no significant segments in these frequency ranges.

5.5.2 Overall classification results

5.5.2.1 Comparison between different signals

Figure 5.19 displays total classification success rate for classifiers tested with AE and vibration signal from a combination of normal (Class 1), grease (Class 2) and leakage (Class 3) condition. Once again, vibration signal shows its superiority over AE signal in identifying valve problems in lower frequency range at lower speed, especially at F2, F3, and F4, each with success rate greater than 85%. Indeed, these frequency ranges were regarded as the best frequency range in Table 4.14 of Chapter 4. Meanwhile, AE signal demonstrates higher success rate than vibration signal at higher frequency range, namely F10, F11, F12, F13, and F15. All these frequency ranges have more than 90% classification result at lower speed. This finding also agrees well with the result of one way ANOVA, which suggested that the best frequency range lays in the higher frequency range namely F9, F11, F12, F14, and F15, as shown in Table 4.13 of Chapter 4.

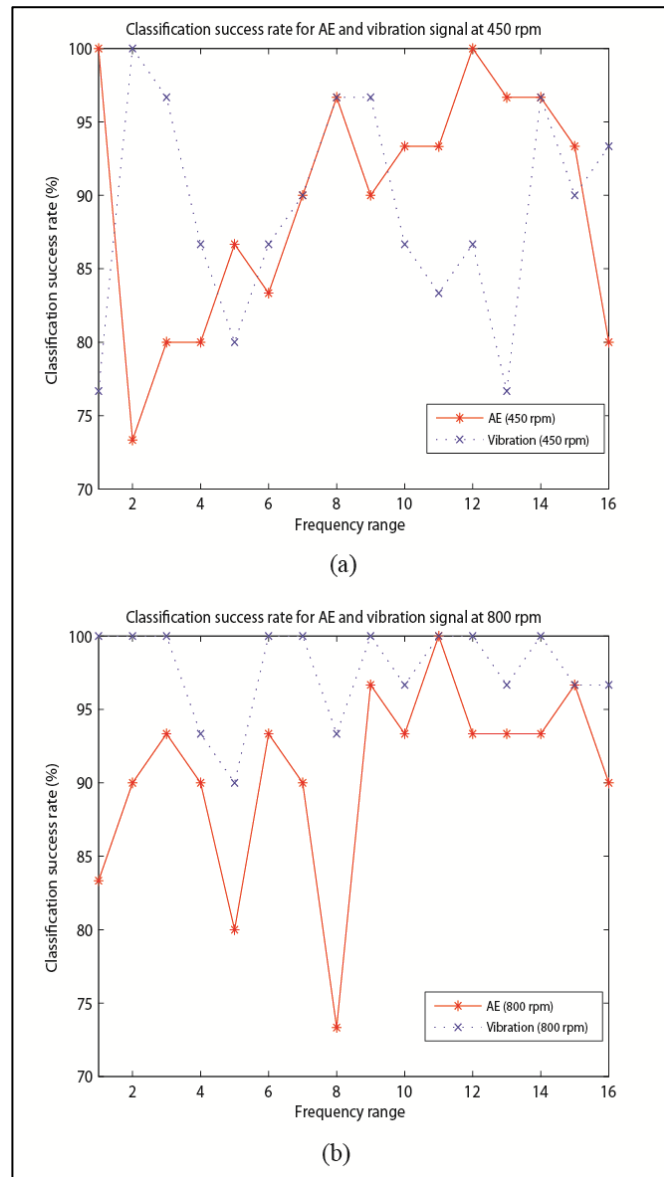


Figure 5.19: Total classification results of AE and vibration signals at (a) 450 rpm (b) 800 rpm

The classification result shows in Figure 5.19 (b) suggested that vibration technique is far better than AE technique at higher speed. Due to larger mechanical impact, vibration signal has 100% success rate at 9 frequency ranges, compared to AE signal at 1 frequency range. Nevertheless, AE signal still perform greatly especially at F9, F11 and F15, each with classification result of 96.7%, 100%, and 96.7% respectively. It is believed that performance of AE technique can be improved by increasing sampling frequency to 1 MHz and above.

5.5.2.2 Comparison between different speed

Figure 5.20 displays total classification success rate of AE and vibration signal at different speed. Compared to the classification results of AE signal at 800 rpm, AE signal at 450 rpm shows better performance in higher frequency range especially F8, F12, F13, and F14. On the contrary, AE signal at 800 rpm demonstrates fluctuating classification success rate across different frequency ranges. It has higher success rate than signal at 450 rpm in lower frequency range, namely F2, F3, F4, and F6 while displays a sudden drop at F8. It is postulated that the poor performance of AE signal (800 rpm) in higher frequency range is attributed to its low resolution. Due to increased speed, the sampling frequency at higher speed needs to be increased for higher resolution. Nevertheless, the signals at both speeds achieved highest success rate at higher frequency range. It can be seen from Figure 5.20 (a) that AE signal at 450 and 800 rpm shows 100% success rate at F12 and F11 respectively. Although 100% classification result of AE signal (450 rpm) can be seen in F1, this frequency range is not as reliable as that in F12 due to its low signal-to-noise ratio discussed previously.

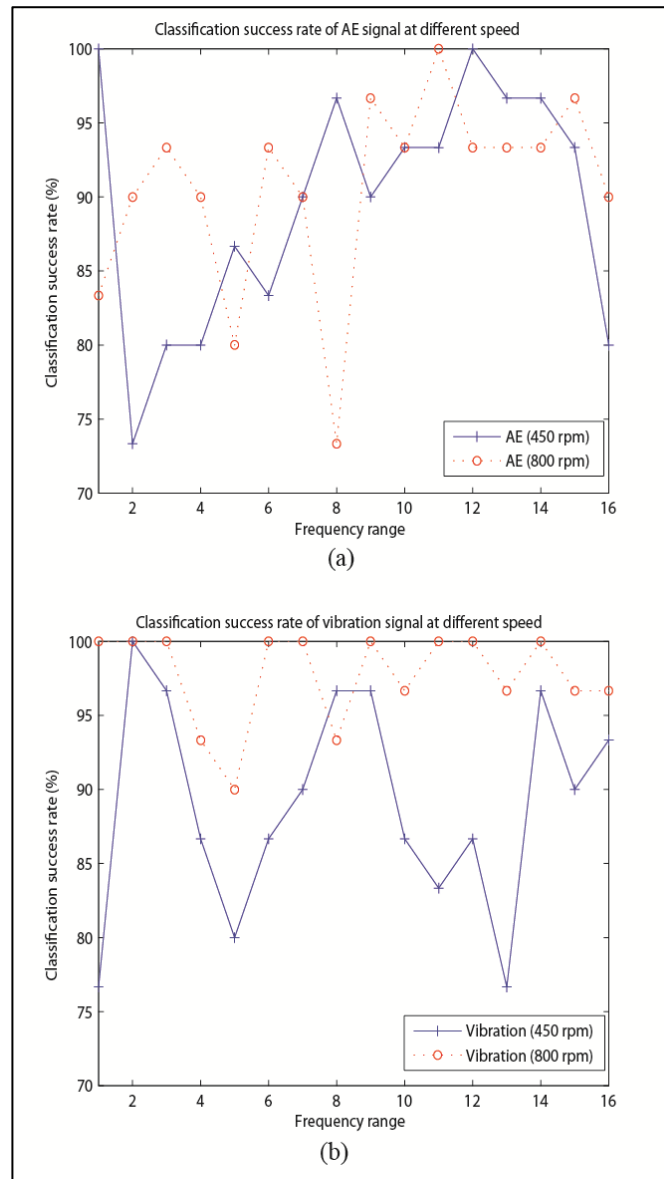


Figure 5.20: Total classification results of (a) AE (b) Vibration signal at different speed

As shown in Figure 5.20 (b), the classification result of vibration signal has improved at higher speed. It displays consistent high classification success rate of 100% at both low and high frequency range. As mentioned in Section 4.4.2 in Chapter 4, higher speed produces greater mechanical impact especially during valve opening and closing motion, resulted in better performance at most of the frequency ranges compared to that at lower speed. In contrast, vibration signal at lower speed shows fluctuations in classification result across different frequency ranges. The signal (450

rpm) hits its maximum classification result of 100% at F2 and experiences a sudden drop at F1, F5, F11, and F13, with success rate of 76.7%, 80%, 83.3%, and 76.7% respectively. The best performance of vibration signal is achieved at F2 as this frequency range lies in the best operating frequency range of accelerometer (0 – 6 kHz), as displayed in Appendix D. However, due to lower mechanical impact and limitation of operating frequency range of accelerometer, the signal (450 rpm) shows poorer performance especially at higher frequency range.

5.6 Summary

In this study, normalized energy values computed in time-frequency segments under 3 different conditions were trained and tested through SVM classifier. These classifiers were optimized by fine tuning the best parameters through cross validation technique before they were tested with a combination of signals acquired under different conditions. It was found that AE technique performed better in the higher frequency range at lower speed while vibration technique precedes AE technique by showing high classification success rate at higher speed. It is postulated that insufficient sampling frequency is accounted for poor classification performance of AE technique at higher speed. Meanwhile, the fluctuating performance of vibration technique in higher frequency at lower speed is elucidated by limitation of accelerometer's operating frequency range. These findings agree well with postulations made in Chapter 4.

CHAPTER 6 CONCLUSIONS AND RECOMMENDATIONS

6.1 Conclusions

Health condition of valves plays a vital role in maintaining high efficiency of reciprocating compressors. This study shows the necessity of valve monitoring to avoid sudden shutdown and reduce maintenance cost of compressors. Poor monitoring of valve will lead to reduction in compressors' efficiency and cause secondary damage to other machine components.

To monitor valve conditions, valve dynamics must first to be understood. Previous studies showed that under normal condition, valve opens at crank angle approximately 50° and closes at approximately 170° . In this study, the impact of valve opening and closing were observed by using AE and vibration technique. By observing AE and vibration signals obtained through fourth level of wavelet packet transform (WPT), three simulated valve conditions namely normal, grease, and leakage condition were monitored.

To identify different valve conditions, a few parameters were suggested as indicators namely crest factor, kurtosis, skewness, RMS (root-mean-square) and normalized energy value. The reliability of these parameters were compared by using one way analysis of variance (ANOVA) and Tukey Test. Results obtained showed best performance of RMS and normalized energy value in distinguishing different valve conditions. Due to better sensitivity in reflecting sudden impacts of valve motion, normalized energy was selected as the monitoring parameter over RMS value.

Features of WPT decomposed AE and vibration signal at different valve conditions were obtained by computing confidence interval (C.I) of normalized energy through Tukey test. Four major time segments of signal were monitored, where each of

them corresponds to features of valve events at different crank angle, namely T1 (0° - 18.8°), T2 (18.8° - 131.4°), T3 (131.4° - 244°), and T4 (244° - 360°). Under normal condition, both AE and vibration signals show highest C.I value in T2 compared to other time segments, as this segment represents the valve opening motion. Meanwhile, under the same condition, valve closing event can be observed in T3 with considerably low C.I value. Results from Chapter 4 demonstrated slight delay of valve closing event and highest amplitude of C.I at T3 under grease valve condition. This key feature of grease condition is consistent for both signals at low (450 rpm) and high (800 rpm) speed. Indeed, the characteristics of greased valve signal were observed in a plant compressor study with speed of 1485 rpm.

By comparing sequence of C.I of both signals at low and high speed, it is obvious that features of signals under different valve conditions change with regards to compressor speed. This study shows that grease signal is more significant at lower (450 rpm) speed while leakage signal shows apparent changes at higher (800 rpm) speed. In fact, at lower speed, grease signal shows highest C.I value at T1 and lowest C.I value at T2 due to early valve opening event. Nevertheless, at higher speed, these features were apparent in leakage signal as the signal shows much earlier valve opening event than grease condition at higher speed. Thus, it is important to consider speed and other operating conditions of compressor being monitored before establishing confidence interval for each valve condition.

To have a better estimation of valve condition, statistical analysis mentioned above requires larger number of data. This often causes inconvenience among plant personnel as it is difficult to collect and analyze huge amount of information from plant. Moreover, complications arise when there are a number of compressors operated at different speeds and working conditions. Therefore, later part of this study presented an

automated classification system to classify normal and abnormal signal through support vector machine (SVM).

Four input vectors obtained from features in 4 time segments were fed into SVM classifiers for automated signal classification. There were 3 binary classifiers constructed at each frequency range, namely Class 1-2, Class 1-3 and Class 2-3 classifier to classify normal (Class 1), grease (Class 2) and leakage (Class 3) condition. By fine tuning (C, γ) value through cross validation technique, the best parameter of each classifier is obtained before integrating them into a multiclass system through one-against-one (OAO) vote strategy.

Results from Chapter 5 suggested good performance of AE signal at the higher frequency range as it displayed high classification success rate at frequency range above F8 (22.4 – 25.6 kHz) at lower speed. On the other hand, vibration signal shows better classification results in lower frequency range namely F2 (3.2 – 6.4 kHz), F3 (6.4 – 9.6 kHz), and F4 (9.6 – 12.8 kHz) at lower speed. These findings agree well with deductions obtained from Chapter 4. However, AE signal shows fluctuating result of classification success rate compared to vibration signal at higher speed. It is deduced that higher sampling rate and advanced signal processing technique are needed to acquire and analyze AE signal which reflects complicated fluid flow at higher speed. In contrast, vibration signal shows 100% classification result at most of the frequency ranges due to pronounced mechanical impacts at higher speed. It is believed that performance of AE signal can be improved by increasing sampling rate to 1MHz and above.

6.2 Recommendations for future works

Some of the recommendations for improvement on the current study are listed as follows:

- a) Sampling rate of AE signal should be increased to 1MHz and above to capture complicated fluid flow in valves. Due to unavailability of equipment, this issue was not addressed during the period of study. The poor performance of AE technique at higher speed can be complemented by vibration technique in this study.
- b) Time segment T3 can be shortened to $175^0 - 200^0$ for better detection of grease condition. This issue was not addressed during the study as the SVM technique is capable of classifying signals into its corresponding valve conditions regardless of delay in valve timing. Nevertheless, the reduction of length in T3 can provide better diagnosis result in signal analysis, especially for analyzing the propagation of defects in future.
- c) Other plant operating conditions such as speed and work load can be included in SVM classifier for better prediction of valve condition. As different operating conditions may result in different features of input vectors, inclusion of these parameters into the classifier can increase the accuracy and robustness of the system.
- d) Other valve problems such as spring deterioration, and fracture plate valve can be considered for future study. These are other common valve problems found in the reciprocating compressor.
- e) More training data should be added in SVM classifiers to avoid over-fitting as some of the classifiers have large number of support vectors.

- f) Continuous monitoring of valve problems which comprised of initiation and propagation of defects should be included in future.

REFERENCES

- API Standard 618. (1995). *Reciprocating compressors for petroleum, chemical and gas industry services* (4th Edition). Washington, D. C.: American Petroleum Institute.
- Afimiwala, K. A. & Woollatt, D. (1984). A diagnostic system for reciprocating compressors. *International Compressor Engineering Conference*, 1063-1072.
- Ahmed, M., Abdusslam, S., Baqqar, M., Gu, F. & Ball, A. D. (2011). Fault classification of reciprocating compressor based on neural networks and support vector machines. *Proceedings of the 17th International Conference on Automation & Computing*, University of Huddersfield, UK, 213-218.
- Ahuja, N., Lertrattanapanich, & Bose, N. K. (2005). *IEEE Proceedings on Vision, Image, and Signal Processing*, **152**(5), 659-664.
- Al-Ghamd, A. M. & Mba D. (2006). A comparative experimental study on the use of acoustic emission and vibration analysis for bearing defect identification and estimation of defect size. *Mechanical Systems and Signal Processing*, **20**, 1537-1571.
- Anderson, J. A. (1972). A simple neural network generating an interactive memory. *Mathematical Bioscience*, **14**, 197-220.
- Balerston, H. L. (1969). The Detection of Incipient Failure in Bearings. *Materials Evaluation*, **27**, 121-128.
- Baydar, N., & Ball, A. (2001). A comparative study of acoustic and vibration signals in detection of gear failures using Wigner-Ville Distribution. *Mechanical Systems and Signal Processing*, **15**(6), 1091-1107.
- Baydar, N., & Ball, A. (2003). Detection of gear failures via vibration and acoustic signals using wavelet transform. *Mechanical Systems and Signal Processing*, **17**(4), 787-804.
- Burges, C. J. C. (1998). A tutorial on support vector machines for pattern recognition. *Data Mining and Knowledge Discovery*, **2**, 121-167.
- Byvatov, E., Fechner, U., Sadowski, J., & Schneider, G. (2003). Comparison of support vector machine and artificial neural network systems for drug/nondrug classification. *Journal of Chemical Information and Computer Sciences*, **43**(6), 1882-1889.
- Chen, H. X., Chua, P. S. K. & Lim, G. H. (2006). Adaptive wavelet transform for vibration signal modelling and application in fault diagnosis of water hydraulic motor. *Mechanical Systems and Signal Processing*, **20**, 2022-2045.
- Chen, Z. & Lian, X. (2010). Fault diagnosis for valves of compressors based on support vector machine. *IEEE Chinese Control and Decision Conference*, 1235 – 1238.
- Courrech, J. (1996). Condition monitoring of machinery. In *Shock and Vibration Handbook* (4th Ed.), pp. 16.1-16.26. McGraw-Hill.

- Cui, H., Zhang, L., Kang, R., & Lan, X. (2009). Research on fault diagnosis for reciprocating compressor valve using information entropy and SVM method. *Journal of Loss Prevention in the Process Industries*, **22**(6), 864-867.
- Daubechies, I. (1992). *Ten lectures on wavelets*. Society for Industrial and Applied Mathematics (SIAM), Philadelphia, PA, USA.
- Davis, G. (2004). Using PV curves to diagnose a reciprocating valve problem. *Orbit Magazine*, 48-54.
- Diab, S. & Howard, B. (2004). Reciprocating compressor management systems provide solid return on investment. *Proceedings of Rotate Conference*.
- Eftekharnajad, B. & Mba, D. (2009). Seeded fault detection on helical gears with acoustic emission, *Applied Acoustics*, **70**, 547-555.
- El-Ghamry, M. H., Reuben, R. L. & Steel, J. A. (2003). The development of automated pattern recognition and statistical feature isolation techniques for the diagnosis of reciprocating machinery faults using acoustic emission. *Mechanical Systems and Signal Processing*, **17**(4), 805-823.
- Elhaj, M., Gu, F., Wright, J. & Ball, A. D. (2001). Early detection of leakage in reciprocating compressor valves using vibration and acoustic CWT features. *Proceedings of the 14th International Congress on Condition Monitoring and Diagnostic Engineering Management (COMADEM)*, Manchester, UK, 749-756.
- Elhaj, M., Gu, F., Ball, A. D., Albarbar, A., Al-Qattan, M. & Naid, A. (2008). Numerical simulation and experimental study of a two-stage reciprocating compressor for condition monitoring. *Mechanical Systems and Signal Processing*, **22**, 374-389.
- Elhaj, M., Almrabet, M., Rgeai, M. & Ehtiawesh, I. (2010). A combined practical approach to condition monitoring of reciprocating compressors using IAS and dynamic pressure. *World Academy of Science, Engineering and Technology*, **63**(39), 186-192.
- Foreman S. (2002). *Compressor valves and unloaders for reciprocating compressors – An OEM's perspective*. Dresser-Rand Technology Report, Dresser-Rand Technology Paper.
- Friedman, J. (1996). *Another approach to polychotomous classification*. Technical report, Department of Statistics, Stanford University.
- Gabbanini, F., Vannucci, M., Bartoli, G. & Moro, A. (2004). Wavelet packet methods for the analysis of variance of time series with application to crack widths on the Brunelleschi Dome. *Journal of Computational and Graphical Statistics*, **13**(3), 639-658.
- Gabor, D. (1946). Theory of communication. *J. Inst. Elec. Eng.*, **93** (III), 429-457.
- Gill, J. D., Brown, E. R., Reuben, R. L., Sandford, P. M., & Steel, J. A. (1998). Monitoring of a Large Reciprocating Compressor. *Proceedings of COMADEM 1998*, Monash University, Australia, 317-326.

- Girdhar, P. (2004). *Practical machinery vibration analysis and predictive maintenance*. Newnes: Elsevier Ltd.
- Goumas, S. K., Zervakis, M. E., & Stavrakakis, G. S. (2002). Classification of washing machines vibration signals using discrete wavelet analysis for feature extraction. *IEEE Transactions on Instrumentation and Measurement*, **51** (3), 497-508.
- Graps, A. (1995). An introduction to wavelets. *IEEE Computer Science and Engineering*, **2**(2), 1-18.
- Griffith, W. A. & Flanaganm, E. B. (2001). Online continuous monitoring of mechanical condition and performance for critical reciprocating compressors. *Proceedings of the 30th Turbomachinery Symposium*, Texas A&M University, Houston.
- Güenal, S., Gökhan Ece, D., & Nezih Gerek, Ö. (2009). Induction machine condition monitoring using notch-filtered motor current. *Mechanical Systems and Signal Processing*, **23**(8), 2658-2670.
- Gunn, S. R. (1998). *Support vector machines for classification and regression*. ISIS technical report, Image Speech & Intelligent Systems Group, University of Southampton.
- Hill, R., Okoroafor, E. U., & Priston, A.-M. (1996). Acoustic emission wave propagation model and issues of damage induction in composites. *Ultrasonics*, **34**, 321-325.
- Hoerbiger Technical Note. (2007). *Valve theory and design*, The Hoerbiger Group.
- Hsu, C. W., Chang, C. C., & Lin, C. J. (2010). *A practical guide to support vector classification*. Technical report, Department of Computer Science and Information Engineering, National Taiwan University.
- Hsu, C. W. & Lin, C. J. (2002). A comparison of methods for multi-class support vector machines. *IEEE Transactions on Neural Networks*, **13**, 415-425.
- Hu, X., Wang, Z. Z., & Ren, X. M. (2005). Classification of surface EMG signal using relative wavelet packet energy. *Computer Methods and Programs in Biomedicine*, **79**(3), 189-195.
- Hu, Y. & Loizou, P. C. (2007). Subjective comparison and evaluation of speech enhancement algorithms. *Speech Communication*, **49**, 588-601.
- Jamaludin, N., Mba, D., & Bannister, R. H. (2001). Condition monitoring of slow-speed rolling element bearings using stress waves. *Proceedings of the Institution of Mechanical Engineers: Part E: Journal of Process Mechanical Engineering*, 245-271.
- Kaiser, J. (1950). *Untersuchungenuber das Aufireten Gerguschenbeim Zugversuch*. Dr.-Ing. Dissertation, Technische Hochschule Munchen, Germany (in German), translation UCRL-Trans-1 082(L). Translated into English for Lawrence Radiation Laboratory, Livermore, California in June 1964.
- Kim, E., Tan, A., Mathew, J., & Yang, B. S. (2009). Development of an online condition monitoring system for slow speed machinery. *Proceedings of the 4th*

World Congress of Engineering Assets Management (WCEAM 2009), Ledra Marriott Hotel, Athens.

- Kim, E. Y., Tan, A. C. C., Yang, B. S. & Kosse, V. (2007). Experimental study on condition monitoring of low speed bearings: Time domain analysis. *Proceedings of the 5th Australasian Congress on Applied Mechanics (ACAM 2007)*, Brisbane, Australia.
- Koo, I. S., & Kim, W. W. (2000). The development of reactor coolant pump vibration monitoring and a diagnostic system in the nuclear power plant, *ISA Transactions*, **39**(3), 309-316.
- Kuboyama, K. (1997). *Development of low speed bearing diagnosis technique*. NKK Fukuyama Works, Fukuyama City, Hiroshima, Japan.
- Leahy, M., Mba, D., Cooper, P., Montgomery, A., & Owen, D. (2006). Detecting shaft-to-seal rubbing in power generation turbines with the acoustic emission technology. *Journal of Vibration and Acoustics*, **128**, 798 – 800.
- Leonard, S. M. (1997). Increasing the reliability of reciprocating compressors on hydrogen services. *National Petroleum Refiners Association Maintenance Conference*, New Orleans, LA.
- Lin, C. J. (2006). *Support vector machines*. Slides at Machine Learning Summer School, National Taiwan University, Taipei.
- Lin, J. & Qu, L. S. (2000). Feature extraction based on Morlet wavelet and its application for mechanical fault diagnostics. *Journal of Sound and Vibration*, **234**(1), 135-148.
- Lin, Y. H., Wu, H. C. & Wu, C. Y. (2006). Automated condition classification of a reciprocating compressor using time–frequency analysis and an artificial neural network. *Smart Materials and Structures*, **15**(6), 1576-1584.
- Lin, Y. H., Liu, H. S & Wu, C. Y. (2009). Automated valve condition classification of a reciprocating compressor with seeded faults: experimentation and validation of classification strategy. *Smart Materials and Structures*, **18**, 095020, 1-19.
- Liptai, R. G., Harris, D. O., & Tatro, C. A. (1972). An introduction to acoustic emission. *Acoustic Emission*. ASTM STP 505, American Society for Testing and Materials, 3-10.
- Lu, C. J. & Hsu, Y. T. (2000). Application of wavelet transform to structural damage detection. *Shock and Vibration Digest*, **32**, 50.
- MacLaren, J. F. T. & Kerr, S. V. (1969). An analytical and experimental study of self-acting valves in a reciprocating air compressor. *Proceedings of the Institution of Mechanical Engineers*, **184**, 24-33.
- Mallat, S. G. (1989). A theory for multi-resolution signal decomposition: The wavelet representation. *IEEE Transactions on pattern analysis and machine intelligence*, **11**(7), 674-693.
- Mba, D. & Rao, R. B. K. N. (2006). Development of acoustic emission technology for condition monitoring and diagnosis of rotating machines; bearings, pumps,

- gearboxes, engines, and rotating structures. *The Shock and Vibration Digest*, **38**(1), 3-16.
- McElroy, J. W. (1975). Development of acoustic emission testing for the inspection of gas distribution pipelines. *Monitoring Structural Integrity by Acoustic Emission*, ASTM STP 571, American Society for Testing and Materials, 59-79.
- McFadden, P. D., & Smith, J. D. (1983). Acoustic emission transducers for the vibration monitoring of bearings at low speeds. *Report no. CUED/ CMech/ TR29*.
- Miyachika, K., Oda, S & Koide, T. (1995). Acoustic emission of bending fatigue process of spur gear teeth. *Journal of Acoustic Emission*, **13**(1/2), S47-S53.
- Momoh, J. A. & Dias, L. G. (1996). Solar dynamic power system fault diagnostics. *NASA Conference Publication 10189*, 19.
- Muravin, B. (2009). Acoustic emission science and technology. *Journal of Building and Infrastructure Engineering of the Israeli Association of Engineers and Architects*.
- Paya, B. A. & Esat, I. I. (1997). Artificial neural network based fault diagnosis of rotating machinery using wavelet transforms as a pre-processor. *Mechanical Systems and Signal Processing*, **11**(5), 751-765.
- Peng, Z. K., & Chu, F. L. (2004). Application of the wavelet transform in machine condition monitoring and fault diagnostics: a review with bibliography. *Mechanical Systems and Signal Processing*, **18**(2), 199-221.
- Phinyomark, A., Limsakul, C., & Phukpattaranont, P. (2011). Application of wavelet analysis in EMG feature extraction for pattern classification, *Measurement Science Review*, **11**(2), 45-52.
- Qin, Q., Jiang, Z.-N., Feng, K., & He, W. (2012). A novel scheme for fault detection of reciprocating compressor valves based on basis pursuit, wave matching and support vector machine. *Measurement*, **45**(5), 897-908.
- Rafiee, J., Rafiee, M. A., & Tse, P. W. (2010). Application of mother wavelet functions for automatic gear and bearing fault diagnosis. *Expert Systems with Applications*, **37**(6), 4568-4579.
- Rahman, A. G. A., Ong, Z. C., & Ismail, Z. (2010). Effectiveness of impact-synchronous time averaging in determination of dynamic characteristics of a rotor dynamic system. *Measurement*, **44**(1), 34-45.
- Ramesh, R. P. (2007). *Compressor valve failure detection and prognostics*, Master of Science Thesis, University of Missouri-Rolla.
- Ren, Q., Ma, X., & Miao, G. (2005). Application of Support Vector Machines in reciprocating compressor valve fault diagnosis, *Advances in Natural Computation*, **3611**, 81-84, Heidelberg: Springer Berlin.
- Rogers, L. M. (1979). The application of vibration analysis and acoustic emission source location to on-line condition monitoring of anti-friction bearings. *Tribology International*, **12**(2), 51-59.

- Ross, S. M. (2004). *Introduction to probability and statistics for engineers and scientist*. California, USA: Elsevier Academic Press.
- Saravanan, N., Siddabattuni, V. N. S. K., & Ramachandran, K. I. (2010). Fault diagnosis of spur bevel gear box using artificial neural network (ANN), and proximal support vector machine (PSVM). *Applied Soft Computing*, **10**(1), 344-360.
- Schirmer, A. G. F., Fernandes, N. F. & De Caux, J. E. (2004). On-line monitoring of reciprocating compressors, *NPRA Maintenance Conference*, San Antonio, 1-20.
- Schultheis, S. M., Lickteig, C. A., & Parchewsky, R. (2007). Reciprocating compressor condition monitoring. *Proceedings of the Thirthy-Sixth Turbomachinery Symposium*.
- Scruby, C. B. (1987). An introduction to acoustic emission. *Journal of Physics E: Scientific Instruments*, **20**(8), 946-953.
- Shin, K. & Hammond, J. K. (2008). *Fundamentals of signal processing for sound and vibration engineers*. England: John Wiley & Sons Ltd.
- Sikorska, J. Z. & Pan, J. (2003). A review of acoustic emission techniques for the diagnosis of faults in rotating machinery. *Proceedings of the 7th International Conference of Maintenance Societies (ICOMS)*, Perth, Australia.
- Sikorska, J. Z. & Mba, D. (2006). AE Condition Monitoring: Challenges and Opportunities. *Proceedings of World Congress of Engineering Asset Management (WCEAM)*, Australia.
- Sikorska, J. Z. (2006). *The application of acoustic emission monitoring to the detection of flow conditions in centrifugal pumps*. PhD Thesis, University of Western Australia.
- Sikorska, J. Z. & Mba, D. (2008). Challenges and obstacles in the application of acoustic emission to process machinery. *Proceedings of the Institutions of Mechanical Engineers Part E : Journal of Process Mechanical Engineering*, **222**, 1-19.
- Sim., H. Y., Ramli, R., & Abdullah, M. A. K. (2012). Implementing wavelet packet transform for valve failure detection using vibration and acoustic emission signals. *Journal of Physics: Conference Series*, **364**, 012086, 1-14.
- Singh, A., Houser, D. R., & Vijayakar, S. (1996). Early detection of gear pitting. *Power Transmission and Gearing Conference, ASME, DE*, **88**, 673-678.
- Singh, A., Houser, D. R., & Vijayakar, S. (1999). Detecting gear tooth breakage using acoustic emission: A feasibility and sensor placement study. *Journal of Mechanical Design*, **121**, 587-593.
- Singla, R., Chambayil, B., Khosla, A. & Santosh, J. (2011). Comparison of SVM and ANN for classification of eye events in EEG. *Journal of Biomedical Science and Engineering*, **4**(1), 62-69.
- Smith, T. J., Schultheis, S. M. & Hanifan, M. (1997). *Millennium Petrochemicals Inc. Morris Plant improves compressor reliability and onstream time using*

- reciprocating compressor monitoring*, National Petroleum Refiners Association, MC-97-86.
- Tan, C. K. & Mba, D. (2005a). Identification of the acoustic emission source during a comparative study on diagnosis of a spur gearbox. *Tribology International*, **38**, 469-480.
- Tan, C. K. & Mba, D. (2005b). Limitation of acoustic emission for identifying seeded defects in gearboxes. *Journal of Nondestructive Evaluation*, **24**(1), 11-28.
- Tan, C. K., Irving, P., & Mba, D. (2007). A comparative experimental study on the diagnostic and prognostic capabilities of acoustic emission, vibration, and spectrometric oil analysis for spur gears. *Mechanical Systems and Signal Processing*, **21**, 208-233.
- Tandon, N. & Choudhury, A. (1999). A review of vibration and acoustic measurement methods for the detection of defects in rolling element bearings. *Tribology International*, **32**, 469-480.
- Tandon, N. & Mata, S. (1999). Detection of defects in gears by acoustic emission measurements. *Journal of Acoustic Emission*, **17**(1-2), 23-27.
- Toutountzakis, T. & Mba, D. (2003). Observations of acoustic emission activity during gear defect diagnosis. *NDT & E International*, **36**, 471-477.
- Toutountzakis, T., Tan, C. K. & Mba, D. (2005). Application of acoustic emission to seeded gear fault detection, *NDT & E International*, **38**, 27-36.
- Tyagi, C. S. (2008). A comparative study of SVM classifiers and artificial neural networks application for rolling element bearing fault diagnosis using wavelet transform preprocessing. *Proceedings of World Academy of Science, Engineering and Technology*, **43**, 309-317.
- Unser, M. (1999). Ten good reasons for using spline wavelets. *IEEE Signal Processing Magazine*, **16**, 22-38.
- Valens. C. (1999). *A really friendly guide to wavelets*. Internet sources, <http://perso.wanadoo.fr/polyvalens/clemens/wavelets/wavelets.html>. Retrieved Feb 2011.
- Vapnik, V. (1995). *The Nature of Statistical Learning Theory*. New York: Springer-Verlag.
- Vapnik, V. (1999). An overview of statistical learning theory. *IEEE Transactions on Neural Networks*, **10**(5), 988-999.
- Vetterli, M. & Kovačević, J. (1995). *Wavelets and subband coding*. Prentice Hall.
- Wang, J., Lu, H. P., Plataniotis, K. N., & Lu, J. W. (2009). Gaussian kernel optimization for pattern classification. *Pattern Recognition*, **42**(7), 1237-1247.
- Wickerhauser, M. V. (1994). *Adapted Wavelet Analysis from Theory to Software*, Natick, MA: Wellesley.

- Widodo, A., & Yang, B. S. (2007). Support vector machine in machine condition monitoring and fault diagnosis. *Mechanical Systems and Signal Processing*, **21**(6), 2560-2574.
- Williams, R. V. (1980). *Acoustic Emission*. Bristol: Adam Hilger Ltd.
- Williams, T., Ribadeneira, X., Billington, S., & Kurfess, T. (2001). Rolling element bearing diagnostics in run-to-failure lifetime testing. *Mechanical Systems and Signal Processing*, **15**(5), 979-993.
- Wu, J. D. & Liu, C. H. (2009). An expert system for fault diagnosis in internal combustion engine using wavelet packet transform and neural network. *Expert Systems with Applications*, **36**, 4278-4286.
- Yang, B. S., Han, T., An, J. L., Kim, H. C., Ahn, B. H. (2004). Technical note: A condition classification system for reciprocating compressors. *Structural Health Monitoring*, **3**(3), 277-284.
- Yang, B. S., Hwang, W. W., Kim, D. J., & Tan, A. C. (2005). Condition classification of small reciprocating compressor for refrigerators using artificial neural networks and support vector machines. *Mechanical Systems and Signal Processing*, **19**(2), 371-390.
- Yang, H. Y. (2004). *Automatic fault diagnosis of rolling element bearings using wavelet based pursuit features*, PhD thesis, Queensland University of Technology, Australia.
- Yen, G. G & Lin, K. C. (2000). Wavelet packet feature extraction for vibration monitoring. *IEEE Transactions on Industrial Electronics*, **47**(3), 650-667.
- Zarei, J., & Poshtan, J. (2007). Bearing fault detection using wavelet packet transform of induction motor stator current. *Tribology International*, **40**(5), 763-769.